CHALMERS
UNIVERSITY OF TECHNOLOGY

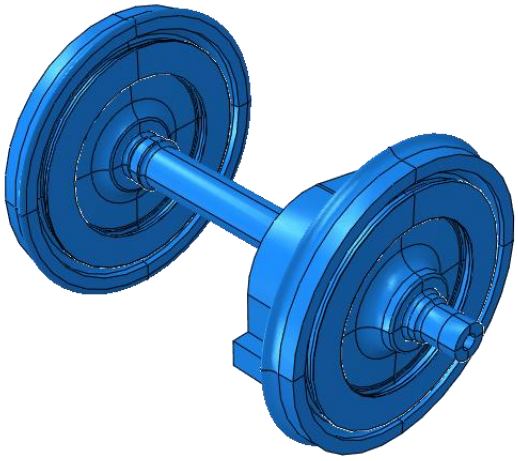

Railway wheel tread damage: Detection and consequences of wheel-rail impact loading

Master's thesis in Mechanics and Maritime Sciences

DAVIDE DELLA VALLE

Department of Mechanics and Maritime Sciences
CHALMERS UNIVERSITY OF TECHNOLOGY
Gothenburg, Sweden 2019

MASTER'S THESIS IN MECHANICS AND MARITIME SCIENCES

Railway wheel tread damage: Detection and consequences of wheel-rail impact loading

DAVIDE DELLA VALLE

Department of Mechanics and Maritime Sciences
Division of Dynamics
CHARMEC
CHALMERS UNIVERSITY OF TECHNOLOGY
Göteborg, Sweden 2019

Railway wheel tread damage:
Detection and consequences of wheel-rail impact loading

DAVIDE DELLA VALLE

Supervisors: Tore Vernersson, Michele Maglio
Examiner: Jens Nielsen

Master's Thesis 2019:34
Department of Mechanics and Maritime Sciences
Division of Dynamics
CHARMEC
Chalmers University of Technology
SE-412 96 Göteborg
Sweden
Telephone: + 46 (0)31-772 1000

Cover:
Snap shot of the modelled wheelset in Abaqus CAD interface.

Department of Mechanics and Maritime Sciences
Göteborg, Sweden 2019-06-11

Railway wheel tread damage:
Detection and consequences of wheel-rail impact loading

Master's thesis in Master's Mechanical Engineering
DAVIDE DELLA VALLE
Department of Mechanics and Maritime Sciences
Division of Dynamics
CHARMEC
Chalmers University of Technology

Abstract

Swedish transport authorities are investing large amounts of capital in technologies aimed at detecting railway wheel tread damage to reduce the costs for maintenance and repair of wheelsets and railway infrastructure. Wheel impact load detectors (WILDs) based on load cells and accelerometers is one such type of technology currently in use by Trafikverket (the Swedish Transport Administration).

This thesis consists of two related parts. The first part is a statistical analysis of data collected by WILDs to assess accuracy and increase confidence in their performance. The statistical tool used to fit the measured data is a multiple linear regression model. For a few selected wheels with evolving rolling contact fatigue damage, data collected over a one-year period have been analysed. At the early stages of wheel tread degradation, it is shown that the measured dynamic loads are considerably influenced by the train speed. For wheels with severe tread damage, the loads are also significantly influenced by the time since the previous wheel maintenance or replacement (probably related to the increasing wheel tread degradation rate over time). It is observed that the accuracy of the detectors cannot be firmly checked since the data are shown to be influenced by train speed and the time of measurement, and because of lack of measured data within a short time window where the tread damage is close to constant. However, a few observations indicating a need for detector calibration are given by comparing the results from different detectors when based on data registered for the same set of wheels.

In the second part of the thesis, a Python script for the Abaqus software has been written to automatically generate a parameterized wheelset model. The Python script allows to easily alter the geometrical features of the wheel design, such as the rim thickness. A non-powered wheelset model is used to evaluate the fatigue resistance of the hollow wheelset axle. A case of warning alarm values registered by a WILD is used to define the periodic loads acting on the rolling contact circle of the wheels. It is shown that the Sines' criterion is the most suitable to calculate the equivalent stress of the most stressed section. For the given set of applied loads, the calculated stress state in the hollow axle does not induce a fatigue damage to the axle.

Key words: wheel impact load detectors, multiple linear regression model, parameterized wheelset model, dynamic analysis.

Acknowledgements

I would like to thank my supervisors Jens Nielsen, Tore Vernersson and Michele Maglio for all the support and help they have given to me during these months. I have deeply appreciated their careful revision of all my work.

A huge gratitude goes to all my friends who have always encouraged and cheered me up in all the moments of my studies.

I would like to thank my girlfriend Luisa because she never made me feel completely far from her despite the distance.

I would like to thank my grandmother Maria whose '*malocchi*' were necessary to pass every single exam.

I would like to thank my brothers and my sweet sister who represented my role model. I am the way I am because of them.

I would like to thank my parents who have always made me feel their love.

Last but not the least, a special thought goes to my grandfather Enrico, my uncle Giancarlo, my aunts Teresa and Nunziata who passed away during my university studies, but they would be happy for this important moment.

DAVIDE DELLA VALLE

Contents

Preface

The present Master's thesis was carried out between December 2018 and June 2019 at the Division of Dynamics at the Department of Mechanics and Maritime Sciences, Chalmers University of Technology, Sweden. The work is part of the EU project *In2Track2*, which is one of the many ongoing projects within the National Center of Excellence in Railway Mechanics, CHARMEC. Further, the project was carried out in collaboration with Trafikverket and Green Cargo AB.

The accomplishment of this project would not have been possible without the help of the following people:

Mr Lars Fehrlund, from Green Cargo AB, who handed over the data registered by the wheel impact load detectors.

Dr Matthias Asplund, from Trafikverket, who shared information regarding the wheel impact load detectors (WILDs) and provided feedback on the first part of this project regarding the analysis of WILDs data.

I want to particularly thank my supervisors, Prof. Jens Nielsen and Dr Tore Vernersson, whose insights and guidance were fundamental for the completion of my thesis. A special thanks to my youngest supervisor, Mr Michele Maglio, who was my firm reference point during the development of my work.

Finally, it is worth mentioning that this MSc thesis was produced within the Erasmus+ bilateral agreement between Chalmers University of Technology and Politecnico di Torino.

DAVIDE DELLA VALLE

Nomenclature

Abbreviations

FE	Finite element
PRESS	Predicted error sum of squares
RCF	Rolling contact fatigue
WILD	Wheel impact load detector

Symbols

F_{dyn}	Dynamic wheel impact load
F_l	Mean wheel load
F_P	Peak wheel impact load
I_m	First invariant of the mean stress tensor
M	Mean stress sensitivity
MS_{res}	Mean sum of residual squares
R^2	Coefficient of determination
SSE	Sum of squares explained
SSR	Sum of the residuals squared
SST	Sum of the total squares
$\sigma_{a,i}$	Alternate component of the *i*th principal stress
σ_i	*i*th principal stress
$\sigma_{m,i}$	Mean component of the *i*th principal stress

1 Introduction

For the dynamics of a railway vehicle, the interaction between wheel and rail is by far the most important aspect. Keeping the wheels and vehicles in an acceptable condition is a major concern for both railway operators and infrastructure owners [1]. Since damage induced on the wheel tread might be detrimental for both track and vehicle components, infrastructure owners have adopted several countermeasures in order to reduce costs for repair and maintenance. To this aim, criteria for determining when a railway wheel should be replaced or reprofiled have been debated and updated over time. For instance, in the last decades Swedish criteria were based on identifying only a critical length of the wheelflat, whereas recent studies have shown that the depth of the flat may have a more considerable influence than the length [2]. Severe wheel-rail impact loads are also generated by other discrete wheel tread defects, such as clusters of rolling contact fatigue (RCF) damage leading to pieces of material breaking out from the tread.

Wheel flats and severe RCF damage, apart from having a large impact on noise generation, might also cause safety problems. Moreover, they induce large impact forces, see Figure 1.1.

The wheel-rail impact forces occur whenever a wheel flat on the wheel tread meets the rail. The wheel flat results in a transient and periodic loading due to an impact for each revolution of the wheel. During this phase, the wheel moves downwards to compensate for the missing wheel material and at the same time the rail moves upwards. Since the wheel and rail cannot utterly compensate for the irregularity due to their inertia, there is a reduction in the contact force. After passing the centre of the flat, the wheel continues downwards because of its higher inertia. This results in a peak in the contact force, which is followed by a damped transient response [3].

These impact forces aggravate damage on the wheel tread. Damage on the railway wheels occur due to mainly two phenomena, fatigue and wear, and their synergetic effects.

Before introducing what countermeasures have been adopted by infrastructure owners to reduce costs for repair and maintenance of track infrastructure, it is worthwhile to give a brief introduction regarding the most common types of damage of railway wheels.

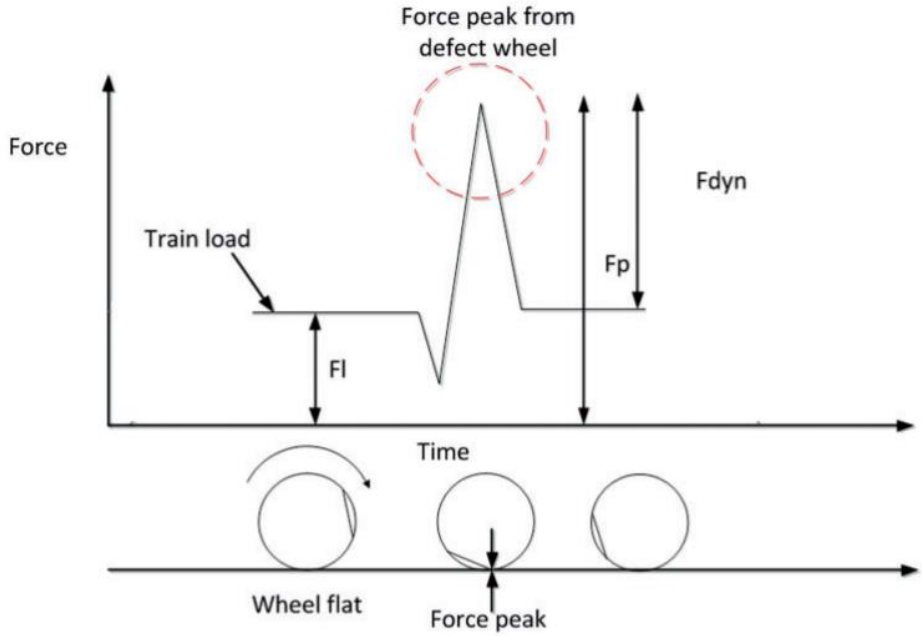

Figure 1.1: Theoretical description of an impact force acting on the wheel of a railway vehicle [4].

2 Wheel tread damage

2.1 Rolling contact fatigue of railway wheels

The development of rolling contact fatigue damage (RCF) can in general be divided into four phases. The first phase involves the crack initiation. Then follows a second phase during which an early crack propagation occurs. The third phase refers instead to an extended crack propagation, whereas the last phase is the one responsible for the final fracture [5].

Surface-initiated RCF cracks occur when a railway component in rolling contact is subjected to cyclic tangential wheel-rail contact loads of high magnitude due to braking and curving. Under these conditions, the contact surface deforms plastically. Consequently, the accumulated plastic strains lead to crack formation as the fracture strain is exceeded [6].

RCF cracks are commonly classified based on their appearance and location on the wheel. As a matter of fact, the lateral and longitudinal (tangential) forces that occur within the wheel tread may lead to damage in four specific zones.

The most common form of RCF cracks are located on the field side of the tread (Zone 1, see Figure 2.2). These cracks are mainly due to the interaction between the wheel and the lower inner rail during curving and their orientation depends on the loading. The cracks are commonly oriented perpendicularly to the direction of the resulting tangential contact force during curving, which is usually around 30°-45° with respect to the wheel axis [7]. The same mechanism and forces, but acting during the interaction between the wheel and the higher outer rail during curving are responsible for damage occurrence in Zone 2. Cracks affecting Zone 2 are typically oriented by 30°-60° with respect to the wheel axis, see picture on the left in Figure 2.2. Zone 3 RCF occurs far less frequently than in Zone 1 or Zone 2. Fatigue cracks occurring in Zone 3 are located in the centre of the tread and they arise from repeated application of high longitudinal tractive forces which in turn result from an increase in the longitudinal creep. On the contrary, cracks occurring in Zone 4 have a significant longitudinal orientation of around 60°-80° to the wheel axis, which indicates that they have been induced by a resultant lateral creep force [8]. Lastly, RCF clusters arising from mainly braking operations appear at the centre of tread. They are in general oriented parallel to the wheel axis, see Figure 2.2.

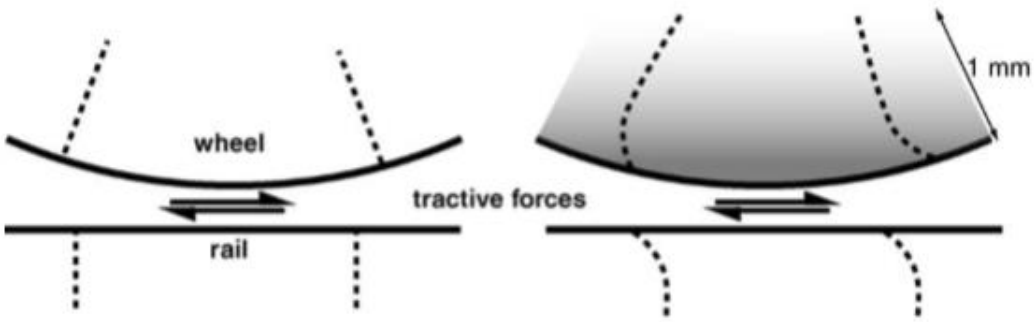

Figure 2.1: Schematic sketch regarding plastic deformation of the surface material in a railway wheel due to tangential loading. The dashed lines indicate material planes before and after deformation [6].

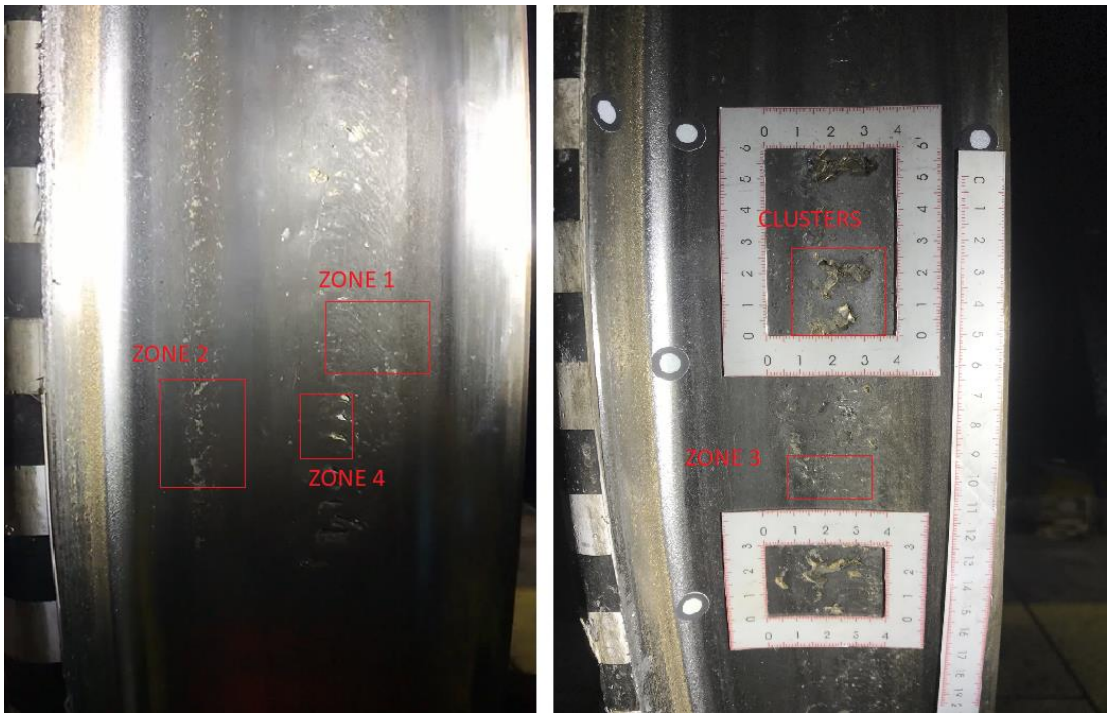

Figure 2.2: RCF damage on a locomotive wheel. [Picture courtesy Michele Maria Maglio].

2.2 Wheel flat

Wheel flats are the most common form of wheel tread damage. Wheel flats are caused by the sliding of the wheel along the rail that occurs as a consequence of a blockage or partial blockage of the wheelset. The reason for the sliding may be either a fault in the brake system or an excessive applied braking force [8, 9]. Consequently, the dissipated friction energy turns into heat and makes the tread surface locally flat. This local flat defect is designated as wheel flat, see Figure 2.3.

However, under the significantly high temperatures (e.g. 800˚) reached during the generation of the flat, the pearlitic microstructure of the wheel steel transforms into martensite. Martensite is a very hard and brittle form of steel microstructure. As a consequence of further cyclic loads arising from the wheel-rail contact, cracks can develop in the brittle material and grow considerably until the brittle surface starts to spall out from the wheel tread [8, 9].

The cavities on the tread surface, such as RCF clusters and wheel flats with spalling, produce a local deviation from the nominal wheel radius. This deviation may generate impact loads in the wheel-rail contact that further aggravate the irregularity [9].

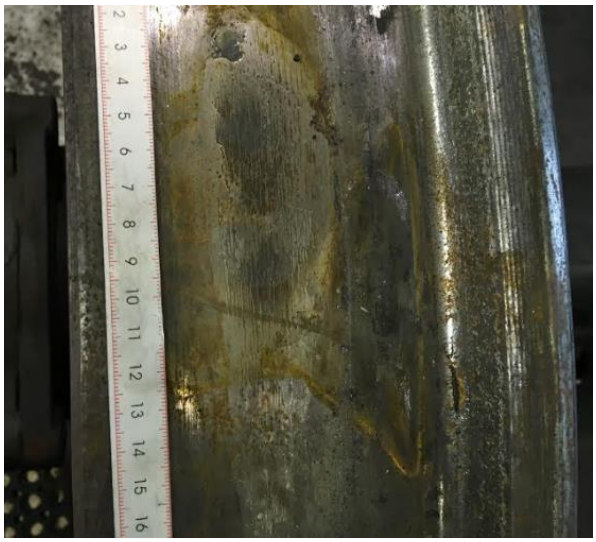

Figure 2.3: Wheel flat on the tread surface. [Picture courtesy Michele Maria Maglio].

2.3 Wear of railway wheels

The broadest definition of "wheel wear" includes any kind of damage occurring on the running surface that involves loss of material. Wheel wear can be categorized into three main classes, deeply described in [10]:

- Flange wear, involving the reduction of the flange thickness that leads to a reduction in the strength and a worsening in wheel-rail contact, see Figure 2.4;
- Wheel tread wear, involving an increase in the flange height and an increase in the flange thickness which in turn might cause severe problems in turnouts or crossings;
- Out-of-round wheel is often caused by the presence of a mixed microstructure within the wheel tread as a result of heat treatments issues during wheel manufacturing [8].

All of these phenomena lead to a significant change in the shape of the wheel profile, which in turn could severely affect the dynamics of the vehicle and the safety against derailment. These modifications may be recovered by reprofiling the wheel, i.e. turning it to its original shape. However, a limited number of reprofiling operations may be carried out before the height and thickness of the rim do not comply anymore with the mechanical resistance of the wheel. As this limit is reached, the wheel must be replaced [12].

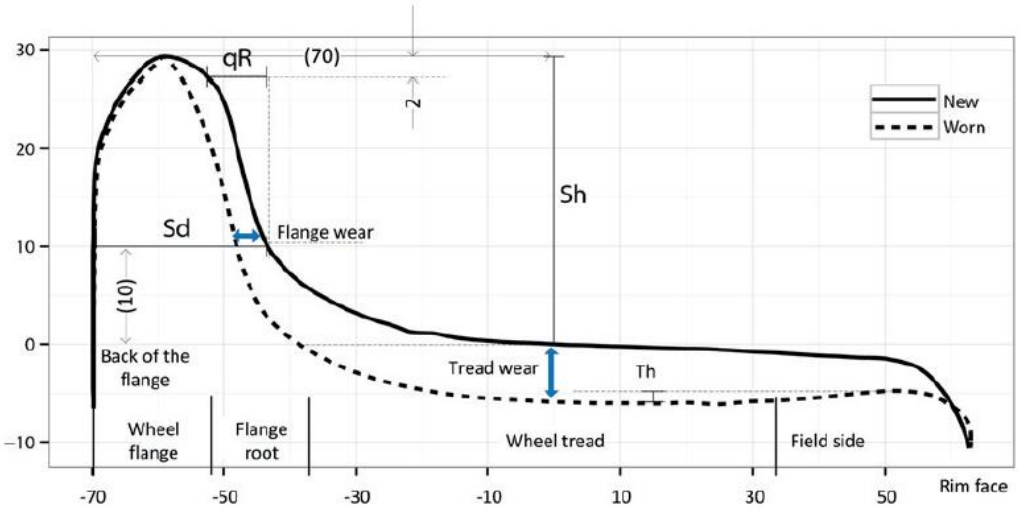

Figure 2.4: Typical railway wheel profile. The picture shows also flange and tread wear phenomena [11].

3 Statistical analysis of wheel impact load detector data

The first goal of the present thesis project has been to analyse data detected by wheel impact load detectors located in Sweden in order to draw some conclusions from the arising trends and to increase the confidence in the performance of the detectors.

3.1 Wheel impact load detectors

A significant amount of capital is being invested by the Swedish transport authorities in technologies aimed at detecting railway wheel damage on time to reduce costs deriving from maintenance and repair and to meet noise legislation. One countermeasure that has been adopted is represented by wheel impact load detectors (WILDs). A WILD system consists of sensors set along the sleepers connecting the two rails. The system makes use of a combination of vertical load receptors, lateral receptors and accelerometers. These sensors collectively provide coverage for approximatively five meters of tangent track, which becomes the detection zone as shown in Figure 3.1.

This system is equipped with an automatic vehicle identification (AVI) system that detects the unique vehicle number characterizing each passing wagon, regardless of the travel direction, through the detection zone [14].

The WILD system provides the following information:

- Train speed;
- Direction of travel;
- Mean wheel load (F_l) on left and right rails;
- Peak wheel impact load (F_P) on left and right rails;
- Dynamic wheel impact load ($F_{dyn} = F_P - F_l$) on left and right rails;

In addition, the WILDs generate alarms when any of the above-mentioned loads exceeds a threshold value configured by the operators or set by the regulations. These output data are then saved in a file, which is stored on disk and is available to the operators. These results can be used for statistical analyses as has been done in the present thesis work.

Figure 3.1: Wheel impact load detector (WILD) installed in track [13].

3.2 Preface to the analysis

3.2.1 Introductory notes

The analysed data have been provided in different Microsoft Excel files by Mr Lars Fehrlund, vehicle engineer at Green Cargo AB. More specifically, each Excel file refers to a specific axle of one specific locomotive. Each file contains information about the dates and time instants at which the data were registered, the name of the detector station, the travel direction of the train, the train speed, and the mean and peak impact loads registered for both wheels.

Based on additional information provided by Lars Fehrlund, data detected at Mellansjö USP MJ MDS and Mellansjö NSP HJ MDS stations have been excluded from the analysis because these detectors have not yet been calibrated. In addition, data detected for low train speeds (lower than 40 km/h) have been excluded because of a relatively high risk that the WILD is not able to identify the locomotive correctly.

3.2.2 Aims

As far as the aims are concerned, the first goal has been to create a unique Matlab code that reads any Excel file having the same format as the ones provided by Lars Fehrlund. Its functionalities are explained in Appendix A.

Then, several analyses have been carried out using statistical tools. More specifically, the influence of the train speed on the mean wheel loads has been investigated first, and then the dependence on dynamic impact loads of the train speed and the time instants at which data have been registered has been studied.

Lastly, the performance of different detectors has been evaluated by comparing measured dynamic loads when subjected to the same wheel tread defect. More specifically, the analysis focused on sequences of data where, according to detector data, the degradation rate of the RCF defects led to a slow increase in dynamic load over time.

3.2.3 Theoretical background to the statistical analysis

3.2.3.1 Simple linear regression model

The statistical technique that has been used for investigating different relationships between the data registered by the wheel impact load detectors is the regression analysis. Reference [15] has been taken into account to provide a theoretical background allowing for carrying out a simple but solid statistical analysis.

Regardless of the selected pair of variables to be analysed, it is possible to display any couple of data registered by WILDs in a scatter diagram. A scatter plot, as the one shown in Figure 3.2, might suggest a possible relationship between the two variables.

Based on a first impression given by the scatter plot in Figure 3.2, the two variables can be related by a linear relationship. The straight line obtained by linear interpolation can be described by Eq. (3.1):

$$y = \beta_0 + \beta_1 x \qquad (3.1)$$

where y represents the dependent variable, x represents the independent variable, β_0 is the intercept and β_1 accounts for the slope. These two latter coefficients are also known as regression coefficients and are statistically computed based on the sample data.

However, since the data points do not lie exactly on the straight line, the difference between the observed data (y) and the straight line $(\beta_0 + \beta_1 x)$, namely the statistical error (e) or residual, should be considered. Hence, a more plausible model is represented by the following equation.

$$y = \beta_0 + \beta_1 x + e \qquad (3.2)$$

Equation (3.2) is called a linear regression model. The independent variable x is usually denoted as the predictor or regressor variable, whereas the dependent variable y is the response variable. The linear regression model described by Eq. (3.2) is referred to as a simple linear regression model because it involves only a single regressor variable. Moreover, the mean value of the errors is assumed to be zero, their variance is unknown and they are supposed to be uncorrelated, that means that the value of one error does not depend on the value of any other error.

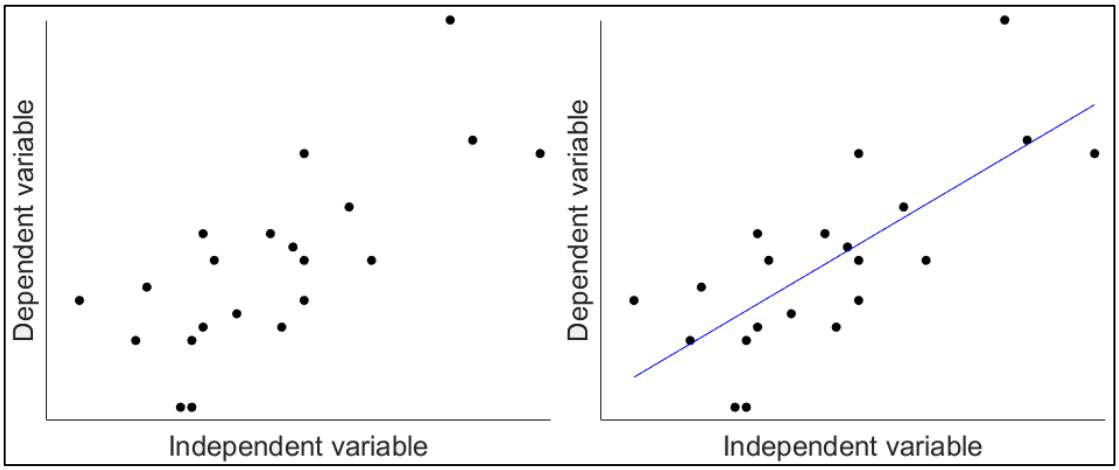

Figure 3.2: (a) Example of a typical scatter plot. (b) Linear interpolation between independent and dependent variable.

A simple linear regression model has been used to study the influence of the train speed and the time instants at which data have been registered on the mean loads measured by the detectors. Simple linear regression models have been generated in Matlab using the function *fitlm* [16], see Appendix A. This function saves any statistical parameters of interest in a nested structure. These parameters include the regression coefficients, which in turn are estimated through the method of least squares, meaning that the sum of the squares of the differences between the observations y_i and the straight line has a minimum. The sum of squared errors *S* is written as:

$$S(\beta_0, \beta_1) = \sum_{i=1}^{n}(y_i - \beta_0 - \beta_1 x_i)^2 \qquad (3.3)$$

Therefore, the least-squares estimators of β_0 and β_1 must satisfy

$$\frac{\partial S}{\partial \beta_1} = -2 \sum_{i=1}^{n}(y_i - \beta_0 - \beta_1 x_i)x_i = 0 \qquad (3.4)$$

and

$$\frac{\partial S}{\partial \beta_0} = -2 \sum_{i=1}^{n}(y_i - \beta_0 - \beta_1 x_i) = 0 \qquad (3.5)$$

By simplifying Eq. (3.4) and Eq. (3.5) and solving for β_0 and β_1, it is possible to deduce the equation representing the simple linear regression model.

Before applying the fitted model, the significance of the regression model has to be checked along with the accuracy of the basic assumptions. One statistical tool used to check if the data agree with certain predictions is the hypothesis test. This procedure requires the additional assumption that the errors e_i are normally distributed. It considers two hypotheses: the null hypothesis and the alternative hypothesis. The null hypothesis (H_0) is the hypothesis that is directly tested, for instance the assumption that no regression relationship exists between the response (y) and the predictor variable (x). As opposite to the null hypothesis, the alternative hypothesis (H_1) will consequently indicate that there is instead a regression relationship between the response and the predictor variable.

The P-value approach is usually used to check the validity of the null hypothesis. After having assumed the null hypothesis as true, the hypothesis testing procedure involves subsequently the calculation of *t*-statistics. The *t*-statistics is defined as the ratio between the estimated value of a parameter ($\widehat{\beta}$) from its hypothesized value (β_0) and its standard error [15] .

$$t_{\widehat{\beta}} = \frac{\widehat{\beta} - \beta_0}{se(\widehat{\beta})} \qquad (3.6)$$

According to the aim of the statistical analysis, the estimated parameter involved in Eq. (3.6) might be either the intercept or the slope of the regression model. Both these parameters are determined through the method of least squares. Moreover, the *t*-statistics follows a *t*-distribution with *n*-1 degrees of freedom, where *n* accounts for the number of observed values. Hence, using the known distribution of the *t*-statistics,

it is possible to compute the P-value. The latter then has to be compared to a significance level α, which in this study has been set to 0.05 and assumed as default in the regression models generated by the *fitlm* function in Matlab. If the P-value is less than α, the null hypothesis will be rejected in favour of the alternative. On the contrary, if the P-value is larger than α, the null hypothesis should not be rejected [17].

Another way to assess the goodness of the fit is through the evaluation of the coefficient of determination R^2. The coefficient of determination, customarily also denoted as R-squared, is defined according to Eq. (3.7):

$$R^2 = \frac{SSE}{SST} = 1 - \frac{SSR}{SST} \tag{3.7}$$

where:

- SST is the sum of the quadratic deviations of the observed values (y_i) from their average;
- SSE is the sum of the quadratic deviations of the response values from their average;
- SSR is the sum of the squares of the residuals deduced from the fitted model.

Since SST is a measure of the variability in y without considering the effect of the regressor variable x, and SSR is a measure of the variability in y remaining after x has been considered, R-squared accounts for the proportion of variation in y explained by the regressor x. It ranges between 0 and 1 and the larger its value is, the better the variability in y is explained by the adopted regression model [18].

3.2.3.2 Multiple linear regression model

Multiple linear regression models have been used to analyse the correlation between the measured dynamic impact loads, the time at which the data have been registered and the train speed. A multiple linear regression model relates the response variable (y) to *k* regressor variables. The model is described by Eq. (3.8):

$$y = \beta_0 + \beta_1 x_1 + \beta_2 x_2 + \cdots + \beta_k x_k + e \tag{3.8}$$

or equivalently in matrix form by Eq. (3.9):

$$\boldsymbol{y} = \boldsymbol{\beta X} + \boldsymbol{e} \tag{3.9}$$

where each regression coefficient β_k indicates the expected change in the response variable per unit of change in x_k when all the other regressor variables are held constant. It is worth underlining that the term linear refers to a response variable expressed as a linear function of the unknown regression coefficients and not of the regressor variables.

As already explained in Section 3.2.3.1, the first step is to calculate the regression coefficients through the method of least squares. For the sake of brevity, the mathematical passages used to compute the regression coefficients that minimize the sum of squared errors are here omitted but their final expression is reported in Eq. (3.10).

$$\boldsymbol{\beta} = (\boldsymbol{X}'\boldsymbol{X})^{-1}\boldsymbol{X}'\boldsymbol{y} \tag{3.10}$$

Consequently, the vector of the fitted values $\hat{\boldsymbol{y}}$ turns out to be:

$$\hat{\boldsymbol{y}} = \boldsymbol{X}\boldsymbol{\beta} = \boldsymbol{X}(\boldsymbol{X}'\boldsymbol{X})^{-1}\boldsymbol{X}'\boldsymbol{y} \quad = \boldsymbol{H}\boldsymbol{y} \tag{3.11}$$

The $n\ x\ n$ matrix $\mathbf{H} = \mathbf{X}(\mathbf{X}'\mathbf{X})^{-1}\mathbf{X}'$is known as "hat matrix" and allows to correlate the vector of observed values to the vector of fitted values. This matrix has particular properties and plays a relevant role in multiple regression analyses [15].

As far as the test for significance of the adopted regression model is concerned, a very close procedure to what has been presented in Section 3.2.3.1 is usually performed. This test still involves the definition of two hyphotheses: the null hypothesis that implies that no regressor variables influence the response variable ($H_0: \beta_0 = \beta_1 = \cdots = \beta_k = 0$), and the alternative hypothesis that implies that at least one regressor variable affects significantly the response variable ($H_1: \beta_k \neq 0$ for at least one *k*-variable). The rejection of the null hypothesis can be checked by looking at *F*-statistics or the P-value. Once having created a multiple regression model in Matlab through the *fitlm* function, all these parameters of interest may be accessed through the *anova* function [16], see Appendix A.

After having verified that the response variable is significantly influenced by at least one regressor variable, it is worth figuring out which multiple regression model best fits the observed data. This cannot be achieved by looking at the R-squared value because its value cannot decrease by adding regressor variables to the model [17]. Instead, this may be achieved by looking at the adjusted R-squared that is defined as:

$$R^2_{Adj} = 1 - \left[\frac{SSR}{n-p-1}\ \frac{n-1}{SST}\right] \tag{3.12}$$

where *n* accounts for the number of observed data and p is the number of regressor variables used in the regression model. Since $SST/(n-1)$ is constant regardless of how many variables have been introduced in the model and $SSR/(n-p-1)$ is the residual mean square, R^2_{Adj} will only increase if the addition of the regressor variable reduces the residual mean square [18]. This statistical tool allows therefore to evaluate and compare regression models.

Another useful statistical tool in comparing regression models is the PRESS statistics. Reference [15] defines the predicted residual sum of squares (PRESS) as the difference between the *i*th observed value and the predicted value of the *i*th observed response by fitting a model that excludes the *i*th observation. This definition of the PRESS residual or predicted error is outlined by Eq. (3.13)

$$e_{(i)} = y_i - \widehat{y_{(i)}} \tag{3.13}$$

According to the definition given above, it would seem that to calculate all PRESS residuals requires to fit *n* regression models. However, it is possible to deduce the PRESS residuals from the results of the least squares fit. As a matter of fact, the *i*th PRESS residual may be calculated according to Eq. (3.14):

$$e_{(i)} = \frac{e_i}{1-h_{ii}} \tag{3.14}$$

Eq. (3.13) defines the PRESS residual as the ordinary residual, weighted according to the diagonal elements of the hat matrix h_{ii}. Consequently, from the definition of the PRESS residual it is possible to define the predicted error sum of squares, commonly known as PRESS statistics, that is defined according to Eq. (3.15):

$$PRESS = \sum_{i=1}^{n}(y_i - \widehat{y_{(i)}})^2 \ = \sum_{i=1}^{n}\left[\frac{e_i}{1-h_{ii}}\right]^2 \tag{3.15}$$

Both the adjusted R-squared and PRESS statistics approaches suggest the model that best fits the data. Generally, the PRESS statistics tend to recommend smaller models than the adjusted R-squared. However, the regression model that does not exhibit large gaps in the PRESS statistics and the adjusted R-squared values with respect to higher order polynomials is commonly the one that is chosen.

3.2.3.3 Model adequacy checking

As mentioned in the previous sections, the regression models and the significance tests are based on some assumptions. In fact, it has been assumed that the error term *e* has constant variance and is uncorrelated. Additionally, the hypothesis testing procedure requires an additional assumption, namely that the errors are normally distributed. All these assumptions must be checked before the fitted model can be applied. The detection of any violations of these assumptions, along with the detection of any model inadequacy, is generally carried out through the study of residual plots. These plots usually involve scaled residuals.

The first category refers to standardized residuals that use the approximate average variance of residuals, that in turns is represented by the mean sum of squares (MS_{res}), as scaling factors. The definition of a standardized residual is herein reported as

$$d_i = \frac{e_i}{\sqrt{MS_{res}}} \tag{3.16}$$

However, using MS_{res} as the variance of the *i*th residual is just an approximation. This approximation may be improved by using as scaling factor the exact standard deviation of the *i*th residual. This is considered in the definition of studentized residuals, whose expression is proposed by Eq. (3.14):

$$r_i = \frac{e_i}{\sqrt{MS_{res}(1-h_{ii})}}, \quad i = 1,2,\dots,n \tag{3.17}$$

Studentized residuals are usually preferred in the graphical analysis [15]. The graphical analysis involves the study of different residual plots. The first one is the plot of residuals versus the corresponding fitted values. This plot allows to detect model inadequacies and, for the sake of clarity, a typical one is proposed in Figure 3.3.

If the residuals can be contained within two horizontal bands, the model has no obvious deficiencies. Patterns that deviate from this one might instead indicate a non-constant variance or nonlinearity and therefore the models should be corrected by other statistical procedures [15].

Especially if the hypothesis testing that is based on the normal distribution assumption of residuals has been carried out, the normality must be checked. This property is usually checked through a normal probability plot of residuals. This graph is constructed in such a way that the cumulative of the normal distribution will appear as a straight line. Consequently, if the residuals, commonly the studentized residuals, are plotted against the cumulative probability on the normal probability plot, they should lie approximatively on the straight line as shown in Figure 3.4 for the case in which the normal distribution assumption holds. Any eventual strong deviation from the straight line will therefore indicate that the distribution is not normal and consequently the hypothesis testing procedure cannot be considered as reliable.

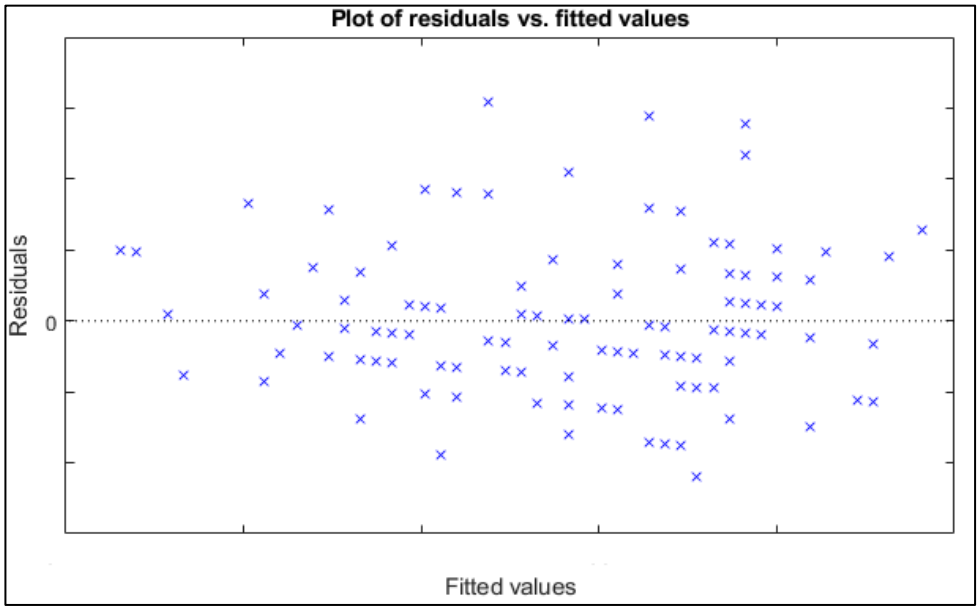

Figure 3.3: Typical plot of residuals versus corresponding fitted values.

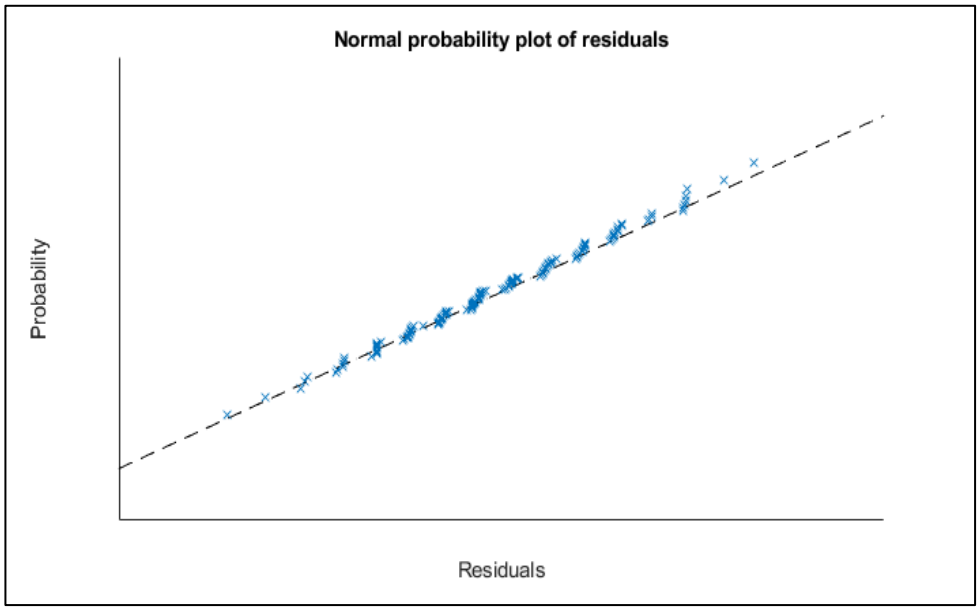

Figure 3.4: Typical normal probability plot of studentized residuals.

3.3 Influence of train speed on mean wheel load

In the following section, the influence of train speed on the mean wheel load has been investigated for several detector stations. The mean wheel loads measured by the WILDs should correspond to the static wheel loads that are merely depending on the weight of the vehicle and any possible external static load acting on it (for example snow and ice). Hence, the registered mean loads are expected to be independent of train speed. Further, for a given wheel on a given vehicle, it is expected that the different detectors should measure the same mean load.

Nonetheless, the mean loads on the left and right wheels become quasistatic and slightly dependent on the train speed during curving because of several factors, such as curve radius and cant deficiency. This may lead to a re-distribution of wheel loads between the left and right rails [10].

However, because of lack of information regarding the exact track geometry at the WILDs, it has not been possible to consider this relevant aspect in the statistical analysis.

Simple linear regression models, described by Eq. (3.2), involving data registered by each detector station have been determined to investigate the dependence of the train speed (regressor variable) on the mean wheel load (response variable). The analysis has been carried out for loads measured on both wheels of the first axle of three different freight locomotives, each of them identified by a vehicle number. These vehicle numbers are 917400014341, 917400014234 and 917400014325. The analysis involved data collected between March 18th 2018 and January 29th 2019 during which maintenance interventions took place. The same analysis was carried out also by considering restricted time intervals in order to reduce the amount of scattered data. First the period from May 1st to October 18th was considered, and secondly October 18th to December 18th. For these cases, similar results were achieved that led to the same conclusions.

Detector stations at which less than thirty passages were registered during this time interval were excluded from the analysis.

An example of results arising from this analysis is reported in Figure 3.5. The fitted linear model suggests that the mean loads do not depend on train speed (because the slope of the regression line given by the regression coefficient β_1 is close to zero). Along with the linear model, the plot of residuals against fitted values must be analysed to prove that the model does not suffer any significant deficiency, see Figure 3.6.

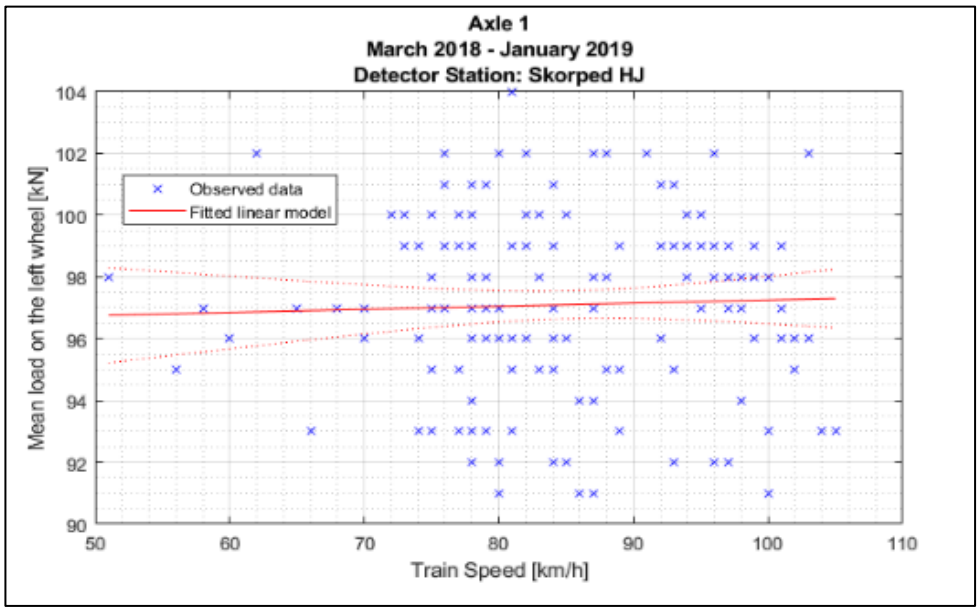

*Figure 3.5: Simple linear regression model between train speed and mean wheel loads detected for the **left** wheel of the first axle of locomotive **917400014325** between March 18th 2018 and January 29th 2019 at **Skorped** detector station. Red dashed lines account for the confidence bounds.*

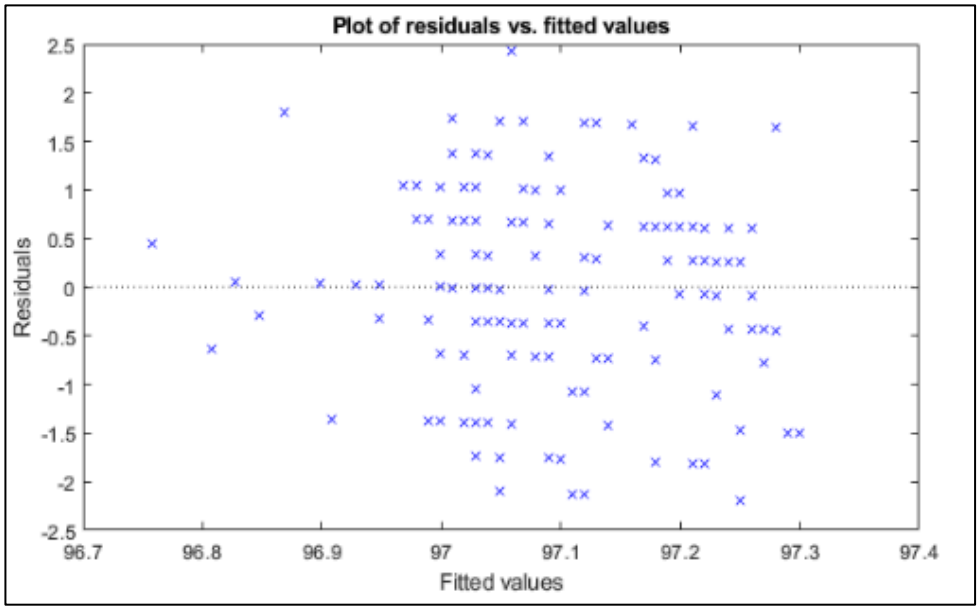

*Figure 3.6: Plot of studentized residuals versus fitted values derived from the simple linear regression model between train speed and mean wheel loads detected for the **left** wheel of the first axle of locomotive **917400014325** between March 18th 2018 and January 29th 2019 at **Skorped** detector station.*

Since Figure 3.6 shows that the studentized residuals are randomly distributed around zero, it is possible to state that the adopted linear regression model has no obvious deficiency. Graphs showing linear regression models for other detector stations and for all the considered locomotives are reported in Appendix B. However, for some models the plot of the studentized residuals against the fitted values shows a double-row pattern indicating a non-constant variance. In those cases, reference [15] suggests to perform a transformation to either the response variable or regression variable in order to stabilize the variance.

However, in order to prove that the mean loads may be considered as independent of train speed at a given confidence level, hypothesis testing has been performed according to the procedure described in Section 3.2.3.1. In such a case, the null hypothesis states that no linear relationship exists between the regressor and the response variable ($H_0: \beta_1 = 0$). Failing to reject the null hypothesis by the P-value approach will therefore imply that there is no linear relationship between train speed and mean loads.

The results arising from the hypothesis testing with a 95 % confidence interval care listed in the following tables. Each table provides information regarding the estimate of the regression coefficients, the number of observed data *n*, the P-value and the coefficient of determination. Furthermore, the statement concerning whether the null hypothesis is rejected or not is included in the rightmost cell of the table.

By looking at the results listed in the tables, it is observed that the null hypothesis stating no linear relationship exists between mean loads and train speed has not been rejected for all models. Therefore, based on the data measured by the detectors, the results do not completely rule out that the mean wheel loads may be seen as independent of the train speed. On the other hand, a further insight helping in stating that the mean loads do not depend on the train speed may be obtained by looking at the R-squared values. Due to their low values in all models, it is possible to confirm that the used linear regression model does not indicate that the variance in the response variable is expressed to a large extent by the regressor variable. Therefore, the train speed does not exhibit a high influence on the mean loads.

*Table 3.1: Results arising from the hypothesis testing for each detector station. Regression analysis involved mean loads registered by WILDs for the **left** wheel of the first axle of locomotive **917400014314** between March 18th 2018 and January 29th 2019.*

Locomotive 1 RFID: 917400014341						
Detector Station	Estimate		n	P-value	R^2	Rejected Null hypothesis
	β_0	β_1		β_1		
Bodsjön	90.47	0.040	118	0.070	0.028	No
Degerbäcken	92.03	-0.057	94	0.018	0.059	Yes
Jörn	97.88	-0.089	120	0.001	0.089	Yes
Koler	104.17	-0.136	96	0.000	0.192	Yes
Skorped	94.78	0.022	107	0.338	0.008	No
Sunderbyns Sjukhus	95.75	-0.019	121	0.465	0.004	No

*Table 3.2: Results arising from the hypothesis testing for each detector station. Regression analysis involved mean loads registered by WILDs for the **right** wheel of the first axle of locomotive **917400014314** between March 18th 2018 and January 29th 2019.*

Locomotive 1 RFID: 917400014341						
Detector Station	Estimate		n	P-value	R^2	Rejected Null hypothesis
	β_0	β_1		β_1		
Bodsjön	91.56	0.100	118	0.000	0.111	Yes
Degerbäcken	93.45	0.012	94	0.637	0.002	No
Jörn	105.35	-0.132	120	0.000	0.126	Yes
Koler	94.247	0.051	96	0.039	0.044	Yes
Skorped	98.676	0.001	107	0.780	0.000	No
Sunderbyns Sjukhus	94.39	0.040	121	0.077	0.026	No

*Table 3.3: Results arising from the hypothesis testing for each detector station. Regression analysis involved mean loads registered by WILDs for the **left** wheel of the first axle of locomotive **917400014234** between March 18th 2018 and January 29th 2019.*

Locomotive 2 RFID: 917400014234						
Detector Station	Estimate		n	P-value	R^2	Rejected Null hypothesis
	β_0	β_1		β_1		
Bodsjön	90.07	0.070	176	0.000	0.079	Yes
Degerbäcken	90.17	-0.004	90	0.806	0.001	No
Jörn	93.69	-0.010	184	0.655	0.001	No
Koler	93.19	0.002	158	0.884	0.000	No
Skorped	90.04	0.082	170	0.000	0.078	Yes
Sunderbyns Sjukhus	97.21	-0.001	179	0.877	0.001	No

*Table 3.4: Results arising from the hypothesis testing for each detector station. Regression analysis involved mean loads registered by WILDs for the **right** wheel of the first axle of locomotive **917400014234** between March 18th 2018 and January 29th 2019.*

Locomotive 2 RFID: 917400014234						
Detector Station	Estimate		n	P-value	R^2	Rejected Null hypothesis
	β_0	β_1		β_1		
Bodsjön	86.92	0.095	176	0.000	0.094	Yes
Degerbäcken	92.88	-0.009	90	0.726	0.001	No
Jörn	93.67	-0.039	184	0.124	0.013	No
Koler	99.66	-0.058	158	0.016	0.036	Yes
Skorped	97.27	-0.024	170	0.172	0.011	No
Sunderbyns Sjukhus	94.03	0.008	179	0.829	0.001	No

*Table 3.5: Results arising from the hypothesis testing for each detector station. Regression analysis involved mean loads registered by WILDs for the **left** wheel of the first axle of locomotive **917400014325** between March 18th 2018 and January 29th 2019.*

Locomotive 3 RFID: 917400014325						
Detector Station	Estimate		n	P-value	R^2	Rejected Null hypothesis
	β_0	β_1		β_1		
Bodsjön	90.40	0.061	175	0.001	0.061	Yes
Degerbäcken	87.73	0.005	59	0.847	0.001	No
Hållsta	100.13	-0.040	39	0.123	0.063	No
Jörn	95.06	-0.034	174	0.163	0.011	No
Koler	88.20	0.048	157	0.023	0.033	Yes
Skorped	96.24	0.010	164	0.643	0.001	No
Sunderbyns Sjukhus	101.22	-0.055	166	0.055	0.022	No

*Table 3.6: Results arising from the hypothesis testing for each detector station. Regression analysis involved mean impact loads registered by WILDs for the **right** wheel of the first axle of locomotive **917400014325** between March 18th 2018 and January 29th 2019.*

Locomotive 3 RFID: 917400014325						
Detector Station	Estimate		n	P-value	R^2	Rejected Null hypothesis
	β_0	β_1		β_1		
Bodsjön	91.91	0.053	175	0.007	0.041	Yes
Degerbäcken	94.53	-0.028	59	0.470	0.009	No
Hållsta	82.33	0.217	39	0.000	0.452	Yes
Jörn	96.02	-0.061	174	0.006	0.042	Yes
Koler	95.54	-0.009	157	0.614	0.002	No
Skorped	94.55	0.012	164	0.527	0.002	No
Sunderbyns Sjukhus	91.71	0.038	166	0.224	0.009	No

For those models where the null hypothesis was rejected, the normal distribution assumption has been checked via a graphical approach and reported in Appendix B, see Section B1. According to the graphs, the normal distribution assumption is conserved for all models. As a matter of fact, the graphs do not show substantial deviations from the straight line. Nonetheless, some of them show a typical defect, that is the occurrence of a few residuals exhibiting low offset from the straight line. This phenomenon is usually an indication that the corresponding observations are outliers [15].

Lastly, a brief comparison between the detectors is proposed in terms of the average value of the mean loads registered over time. The comparison was made by taking into account data registered during the summer time to exclude any influence of snow and ice packed in the bogies.

In addition, because of limited amount of data registered during this time period for the locomotive identified by vehicle number 917400014341, the analysis focused on data measured for the first axle of the locomotive identified by vehicle number 917400014234. The average values of the mean loads measured for both wheels at each detector station in the period of time May 1st to November 1st 2018 is shown in Figure 3.7 and Figure 3.8.

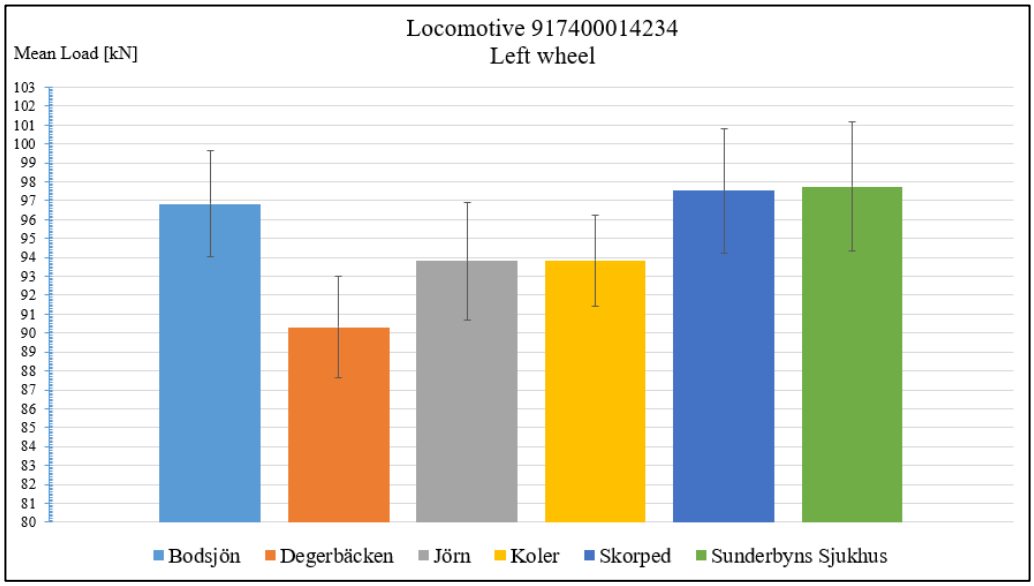

*Figure 3.7: 2D-Bar plot showing the average value of mean loads registered for the **left** wheel of the first axle of locomotive **917400014234** at each detector station in the period of time **May 1st 2018 to November 1st 2019** . The vertical axis shows the average of the mean load. The thin vertical line for each bar allows to identify the upper and lower bounds for the sample data standard deviation.*

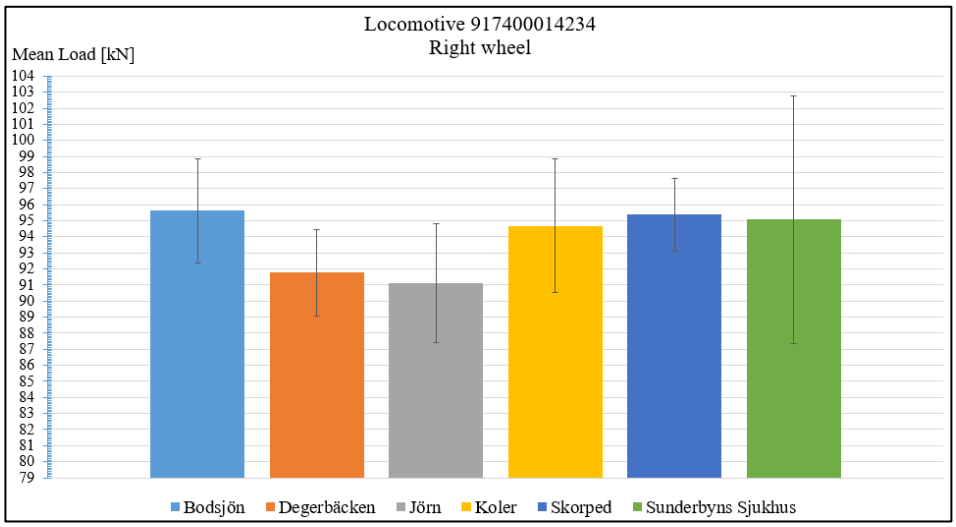

*Figure 3.8: 2D-Bar plot showing the average value of mean loads registered for the **right** wheel of the first axle of locomotive **917400014234** at each detector station in the period of time **May 1st 2018 to November 1st 2019** . The vertical axis shows the average of the mean load. The thin vertical line for each bar allows to identify the upper and lower bounds for the sample data standard deviation.*

By looking at the Figure 3.7 and Figure 3.8, it is observed that not all the wheel impact load detectors exhibit the same performance in registering the mean loads. This aspect may be evidenced by looking at the average values of the mean loads registered at each detector station. The average value (estimated around 97 kN) of mean loads registered for the left wheel is rather similar at the Bodsjön, Skorped and Sunderbyns Sjukhus detector stations, but evident differences from these values can be observed at the Degerbäcken, Jörn and Koler detector stations. The same differences, but slightly lower, may be observed for the loads registered for the right wheel.

As far as the standard deviation is concerned, it generally ranges between 2.5 kN and 3.5 kN. However, a larger value is derived for data registered at the Sunderbyns Sjukhus detectors station which is estimated 7.7 kN. Since the standard deviation accounts for the variability in the measured data, it is possible to state that there are some other hidden factors related to the registered mean load that make the statistical results not completely reliable.

3.4 Investigation on dynamic load

The dynamic loads due to wheel-rail impact caused by severe wheel tread damage are of major interest because they are responsible for wheelset and track damage occurrence and growth. Their values in turn depend on the extent of the damage on the wheel tread; larger defects on the wheel tread are responsible for the occurrence of higher dynamic loads [11]. In addition, for a specific type of damage on the wheel tread, a linear increase in dynamic load with increasing speed was shown in [13]. Based on these expectations, the analysis proposed in this section aims at finding any possible correlation between dynamic load, train speed and the time since initiation of the wheel tread defect in order to increase the confidence in WILDs detection ability.

Among the three locomotives considered in the analysis proposed in the previous section, Lars Fehrlund also provided additional information regarding the maintenance of one of the locomotives, the one identified by the vehicle number 917400014341. According to this information, the wheelset corresponding to the first axle has undergone maintenance more than once during the time period in which data have been measured. More specifically, on April 9th and May 23rd both wheels were replaced, whereas on October 18th 2018 the wheels were reprofiled. The match of this information may be found by looking at the variation in dynamic loads over time for the right wheel that is shown in Figure 3.9. The corresponding impact load distribution for the left wheel may be found in Appendix B, see Figure B1.45.

As is possible to notice from Figure 3.9, the dynamic loads show increasing trends corresponding to a deteriorating state of the wheel tread. Moreover, the sudden reduction in F_{dyn} values occurs at specific time instants which perfectly match the dates provided by Lars Fehrlund at which the wheelset was maintained. Another decrease in F_{dyn} occurs in the middle of February. Another maintenance action may be expected to have taken place in this period, but no information about this has been received. Thus, having confirmed that the registered dynamic impact loads depend on the time since the initiation of the wheel damage, the analysis was focused on restricted time intervals.

More specifically, the influence of the train speed on the dynamic impact loads over a time period with low wheel tread damage has been investigated first. Secondly, the same investigation has been repeated during a time interval where the damage on the wheel tread is more significant.

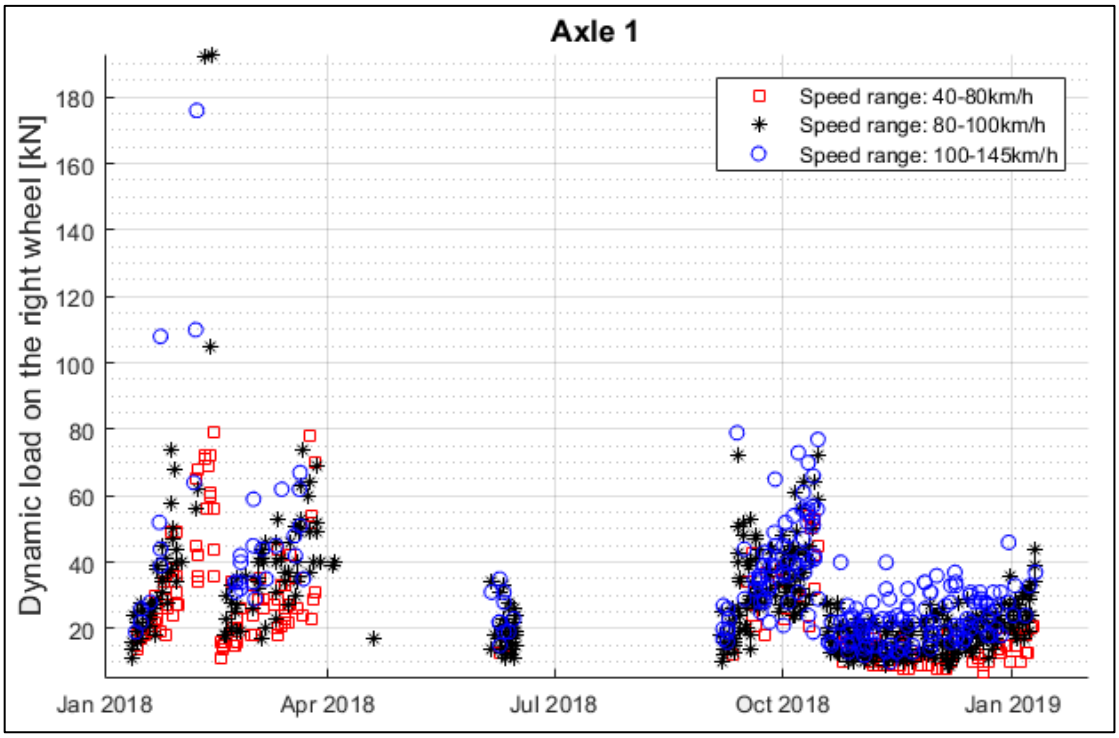

*Figure 3.9: Scattered data of dynamic impact loads generated by the **right** wheel of the first axle of locomotive **917400014341** and registered by all WILDs over one year period. The data have been plotted for three different train speed ranges.*

3.4.1 Influence of train speed on dynamic load: low wheel tread damage

In this section, the influence of train speed on the dynamic impact loads measured shortly after the wheelset was maintained on October 18th is investigated. More specifically, the time period between October 18th and December 18th has been considered.

To this aim, an insight helping for the understanding of what can be expected from the influence of train speed on dynamic loads is provided by a 3D-bar plot illustrating the mean (average value) of the dynamic loads registered during different time intervals and for different speed ranges. A typical trend can be seen in Figure 3.10.

By looking at the trends shown in Figure 3.10, it is possible to notice that the dynamic impact loads tend to increase with increasing train speed. As expected, the trend shows also an increase of the dynamic impact loads over time. This is an expected result because of continuous growth of the RCF damage. Hence, not only the time instants at which data were registered but also the train speed influence somehow the dynamic loads.

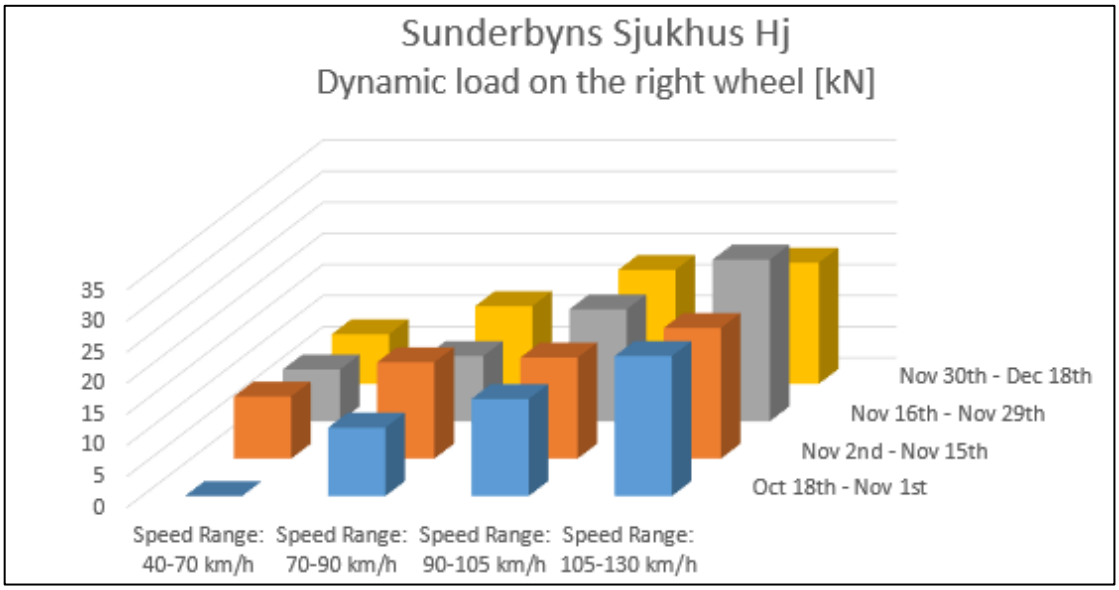

*Figure 3.10: 3D-Bar plot showing the mean of dynamic loads registered for the **right** wheel of the first axle of locomotive **917400014341** at the Sunderbyns Sjukhus detector station during specific time intervals and for specific train speed ranges. The vertical axis shows the dynamic load values. The Y-axis shows the time intervals at which data have been registered, while the X-axis shows the considered speed ranges.*

3.4.1.1 Results from a multiple regression analysis

The next step has been to determine the polynomial that best fits the measured data. To this aim, multiple linear regression models described by Eq. (3.8) have been generated.

Data subject of the following statistical analysis refer to dynamic impact loads on both wheels of the first axle of the locomotives identified respectively by vehicle numbers 917400014341and 917400014234 and registered between October 18th and December 18th 2018 by the detector stations located at Sunderbyns Sjukhus and Bodsjön. Similar results were achieved for all the other detectors. However for the sake of brevity, only results related to data detected at Sunderbyns Sjukhus detector station are presented here. Results regarding the data measured at the Bodsjön detector station are presented in Appendix B, see Section B2.

Several regression models have been generated. First, only one regressor variable was included, either time or train speed. Then models including a combination of both variables and including higher power exponents have been generated. Then, the models have been compared by looking at PRESS statistics, adjusted R-squared and MS_{res}, whose details are given in Section 3.2.3.2. Lastly, the model characterized by the best results in terms of PRESS statistics and R^2_{Adj} has been chosen as the one that best fits the measured dynamic impact loads.

The results are listed in the following tables. Each table provides information regarding the number and type of regressor variables used in the fitted model.

*Table 3.7: Results in terms of PRESS statistics, R^2_{Adj} and MS_{res} derived by the adoption of different regression models involving the regressor variables indicated in the rightmost cells of the table. The analysis involved dynamic impact loads measured for the **right** wheel of the first axle of locomotive **917400014341** at **Sunderbyns Sjukhus** detector station between October 18th and December 18th.*

LOCOMOTIVE 917400014341 Sunderbyns Sjukhus								
N° of regressor variables	PRESS	R^2_{Adj}	MS_{res}	t	v	t^2	v^2	v^3
1	54.52	-0.007	26.99	x				
1	54.97	0.601	10.69		x			
2	57.38	0.608	10.50	x	x			
2	54.97	0.601	10.69		x	x		
2	54.00	0.622	10.13		x		x	
3	57.31	0.623	10.11	x	x		x	
4	61.11	0.614	10.33	x	x		x	x

*Table 3.8: Results in terms of PRESS statistics, R^2_{Adj} and MS_{res} derived by the adoption of different regression models involving the regressor variables indicated in the rightmost cells of the table. The analysis involved dynamic impact loads measured for the **left** wheel of the first axle of locomotive **917400014341** at **Sunderbyns Sjukhus** detector station between October 18th and December 18th.*

LOCOMOTIVE 917400014341 Sunderbyns Sjukhus								
N° of regressor variables	PRESS	R^2_{Adj}	MS_{res}	t	v	t^2	v^2	v^3
1	56.65	0.057	25.62	x				
1	57.22	0.593	11.05		x			
2	62.27	0.666	9.07	x	x			
2	57.22	0.593	11.05		x	x		
2	60.96	0.637	9.84		x		x	
3	70.31	0.694	8.31	x	x		x	
4	82.81	0.690	8.41	x	x		x	x

*Table 3.9: Results in terms of PRESS statistics, R^2_{Adj} and MS_{res} derived by the adoption of different regression models involving the regressor variables indicated in the rightmost cells of the table. The analysis involved dynamic impact loads measured for the **left** wheel of the first axle of locomotive **917400014234** at **Sunderbyns Sjukhus** detector station between October 18th and December 18th.*

LOCOMOTIVE 917400014234 Sunderbyns Sjukhus								
N° of regressor variables	PRESS	R^2_{Adj}	MS_{res}	t	v	t^2	v^2	v^3
1	41.75	0.175	42.35	x				
1	44.14	0.599	20.58		x			
2	51.82	0.737	13.52	x	x			
2	44.14	0.599	20.58		x	x		
2	55.17	0.612	19.92		x		x	
3	68.99	0.766	11.99	x	x		x	
4	83.45	0.775	11.55	x	x		x	x

*Table 3.10: Results in terms of PRESS statistics, R^2_{Adj} and MS_{res} derived by the adoption of different regression models involving the regressor variables indicated in the rightmost cells of the table. The analysis involved dynamic impact loads measured for the **right** wheel of the first axle of locomotive **917400014234** at **Sunderbyns Sjukhus** detector station between October 18th and December 18th.*

LOCOMOTIVE 917400014234 Sunderbyns Sjukhus								
Number of regressor variables	PRESS	R^2_{Adj}	MS_{res}	t	v	t^2	v^2	v^3
1	45.98	0.089	52.90	x				
1	47.74	0.514	28.24		x			
2	45.78	0.579	24.44	x	x			
2	47.73	0.514	28.24		x	x		
2	44.91	0.585	24.09		x		x	
3	55.3	0.67	19.11	x	x		x	
4	252.72	0.661	19.66	x	x		x	x

By comparing the results reported in the tables above, it is possible to notice that time is not the most relevant regressor variable in the regression model. This can be seen by looking at the adjusted R-squared and the mean of the sum of residual squares values. As a matter of fact, the adjusted R-squared for the regression model involving merely the time as regressor variable turns out to have a very low value. This means that the variability in the dynamic loads expressed by the time variable accounts for a small fraction. In reality this indicates that over a two-month period, namely between October 18th and December 18th 2018, the damage on the wheel treads did not grow enough to lead to a drastic increase in the dynamic load values. The opposite conclusion may be derived for the train speed. In fact, due to the large adjusted R-squared values, the train speed is confirmed to have a high influence on the dynamic impact loads.

Additionally, the regression model that best fits the measured data turns out to be the one expressing the dynamic impact load values as a linear function of time and including both linear and quadratic terms of train speed. This can be deduced because the regression model leads to a slight improvement in the R-squared value with respect to the ones derived for lower-order polynomials and at the same time it does not show huge differences in the PRESS-statistics value. The outcome slightly contradicts the experimental results demonstrated in [13], where the dynamic loads exhibited an linear increase with the train speed for the same wheel tread damage.

The surface fitting of the observed data by using a multiple regression model expressing the dynamic impact loads as a linear function of time and both linear and quadratic terms of the train speed is presented in Figure 3.11 and Figure 3.12. According to these figures, it is observed that the dynamic impact loads show an increase with train speed and also a slight increase over time.

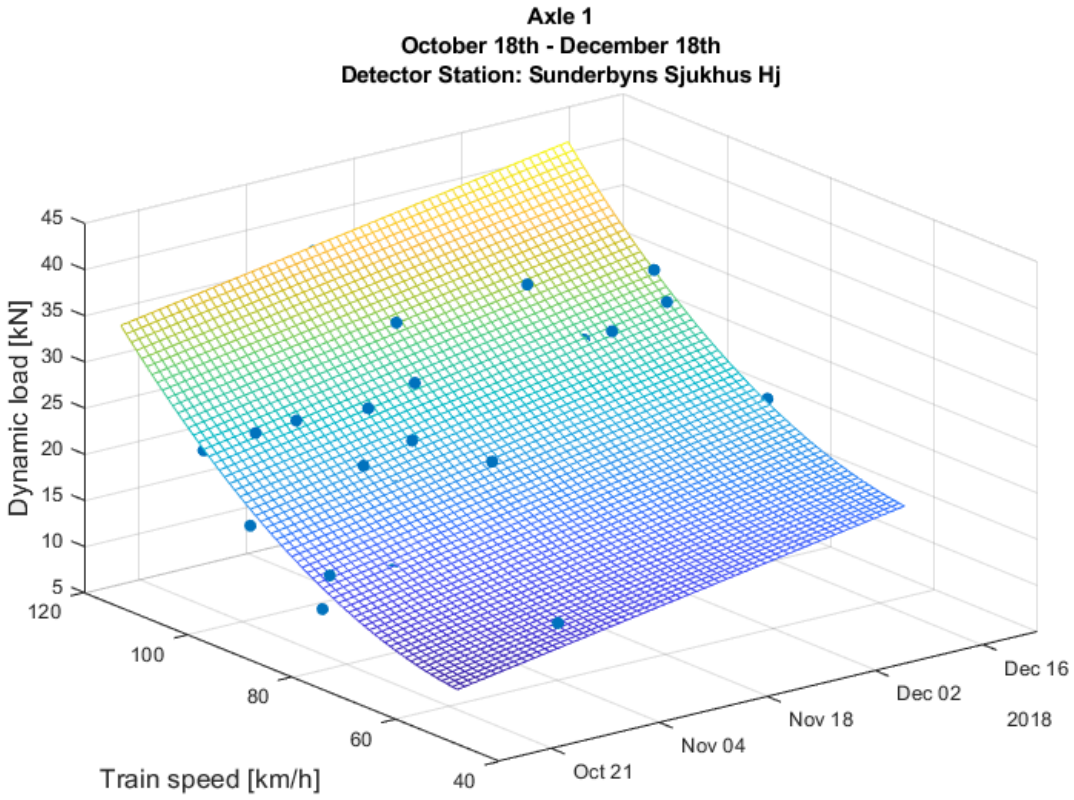

Figure 3.11: Surface fitting of dynamic impact loads expressed as a linear function of time and including both linear and quadratic terms of the train speed. Data have been registered by the ***Sunderbyns Sjukhus*** *detector station and referring to dynamic impact loads measured for the* ***right*** *wheel of the first axle of locomotive* ***917400014341*** *between October 18th and December 18th 2018.*

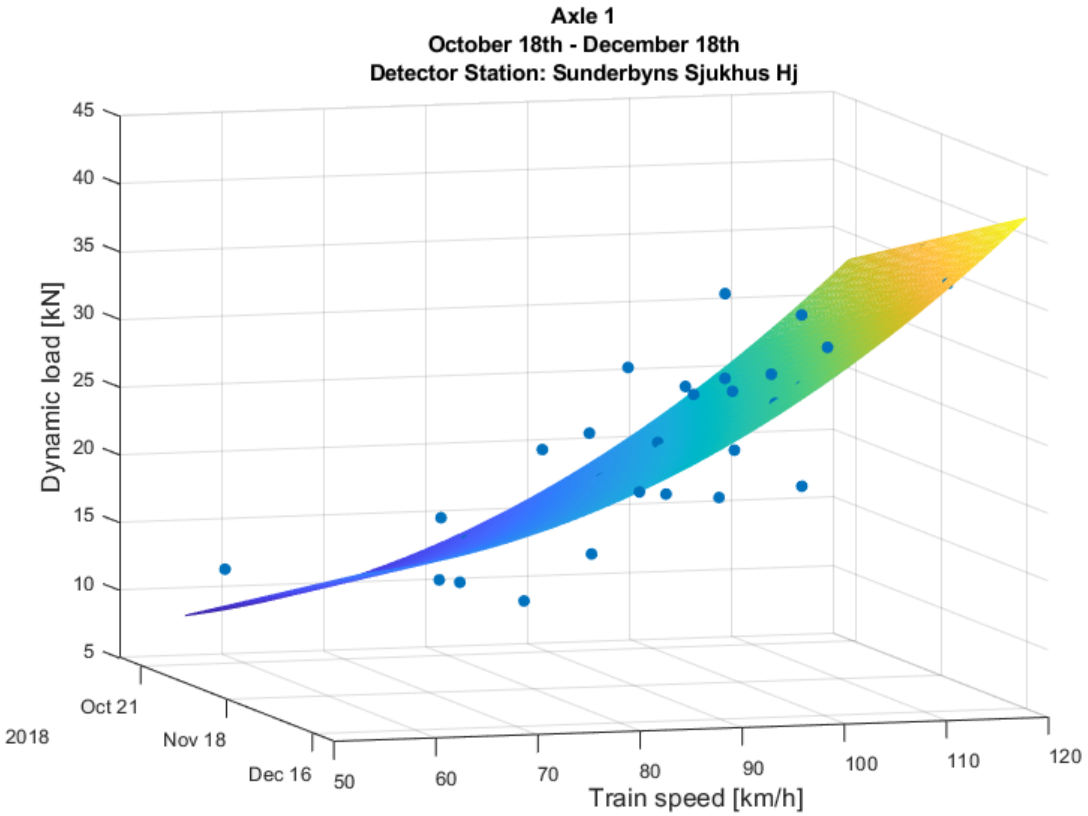

Figure 3.12: Complementary view to Figure 3.11.

3.4.1.2 Low wheel tread damage: comparison between wheel impact load detectors

In the previous section, it was shown that the dynamic loads registered when the wheel tread damage is not severe depend mainly on the train speed. The next step was to use simple linear regression models involving merely the train speed as regressor variable in order to make some comparisons on the data registered by each wheel impact load detector.

Figure 3.13 illustrates observed data and corresponding fitted linear regression models for each detector station over the period October 18th to December 18th. Complementary information to Figure 3.13 are presented in Table 3.11. The table highlights the values of the slope corresponding to each regression model reported in Figure 3.13.

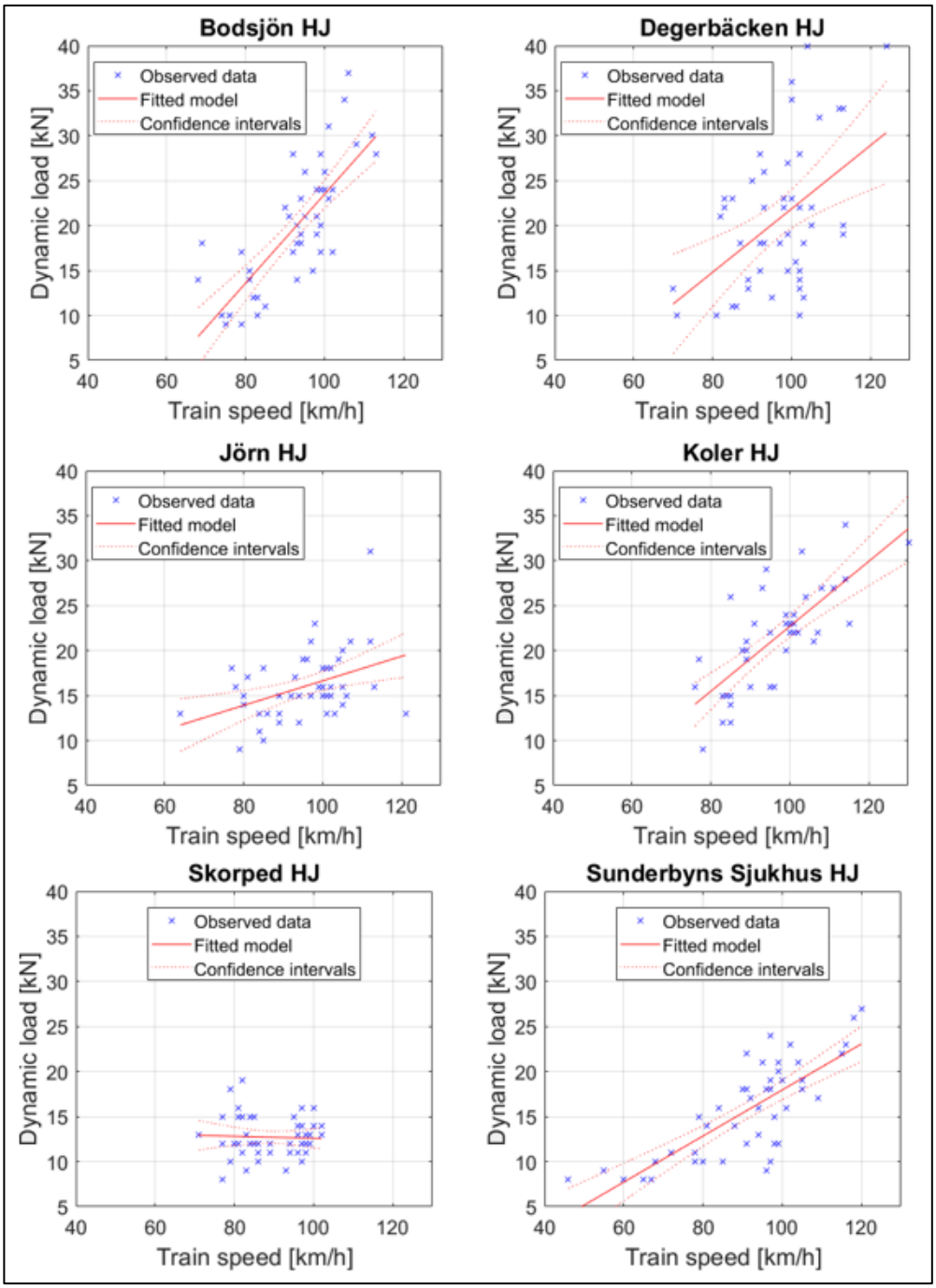

*Figure 3.13: Simple linear regression models between train speed and dynamic loads detected for the **right** wheel of the first axle of locomotive **917400014341** between October 18th 2018 and December 18th for each detector station.*

Table 3.11: Regression coefficient (β_1) values corresponding to the regression models reported in Figure 3.13

Detector station	Regression coefficient β_1
Bodsjön	0.494
Degerbäcken	0.353
Jörn	0.137
Koler	0.361
Skorped	-0.011
Sunderbyns Sjukhus	0.255

By looking at Figure 3.13 it is possible to notice that the linear models derived based on data registered at Bodsjön, Degerbäcken, Koler and Sunderbyns Sjukhus detector stations show a sharp increase in the dynamic loads with increasing train speed. A less steep trend arises from data registered at the Jörn HJ detector station. The slope of the fitted models varies between the detectors. However, for the detectors at Degerbäcken, Koler and Sunderbyns Sjukhus, the slope (β_1) is rather similar and in the order of 0.3 kN/(km/h).

On the contrary, the fitted linear model derived for data collected at the Skorped detector station does not exhibit an increase in dynamic loads with increasing speed. This is also confirmed by the acceptance of the null hypothesis stating that no linear relationship exists between regressor and response variable. A reason for this might be the lack of data measured at higher train speeds which have a high influence in the results for all the other detectors. It could also indicate that the vehicle dynamics at Skorped is different compared to at the other detectors (leading to a different rolling band that may not interact with the position of the tread damage) or that the performance of this detector needs to be calibrated.

Figure 3.13 also illustrates a significant scatter in the data measured for similar train speeds. In particular, this is evident for the Degerbäcken detector station. Based on this observation, the accuracy of each detector in measured dynamic loads in a restricted train speed range is reported in Figure 3.14.

Figure 3.14 shows dynamic loads registered over a two-month period and corresponding to a measured train speed ranging between 95 km/h and 105 km/h. Despite the restricted train speed range, the dynamic loads turn out to be still very scattered. This implies that despite a period of time with low wheel tread damage was considered, a small growth of the damage still occurred. Therefore, based on this consideration, the time interval was reduced even further. Figure 3.15 illustrates the updated information by considering only the dynamic loads measured between October 18th and October 30th and for train speeds ranging between 95 km/h and 105 km/h. Results derived from other time intervals and a more restricted train speed range may be found in the Appendix B, Figure B1.46 and Figure B1.47.

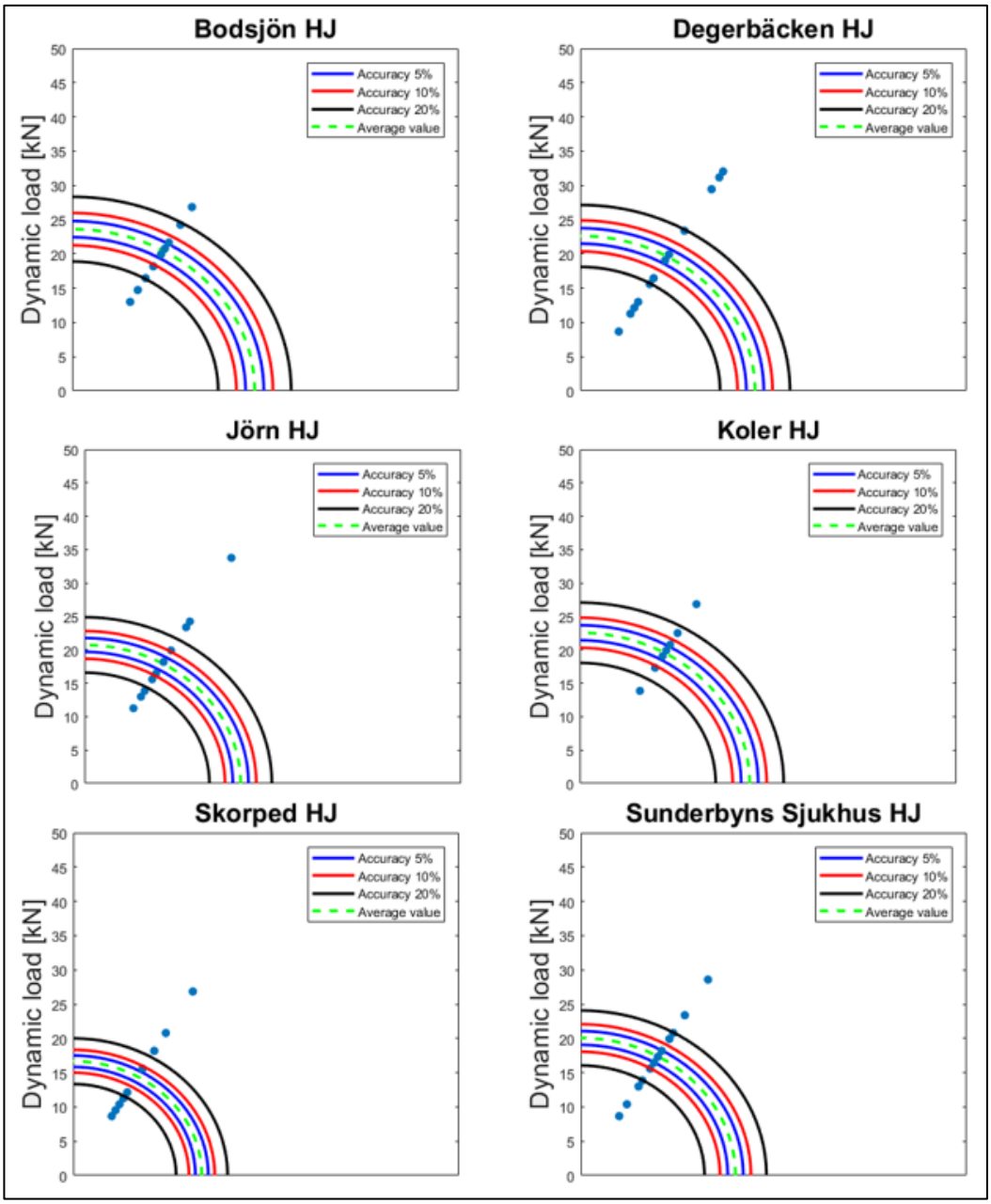

*Figure 3.14: Target diagrams involving dynamic impact loads registered at each detector station and referring to the **right** wheel of the first axle of the locomotive identified by the vehicle number **917400014341**. Data were measured between **October 18th and December 18th 2018** and correspond to measured train speed ranging between **95 km/h and 105 km/h**. The green dashed line indicates the mean value of the dynamic loads. The blue solid lines represent an accuracy of 5%, the red solid lines an accuracy of 10% whereas the black solid lines an accuracy of 20% computed with respect to the mean value.*

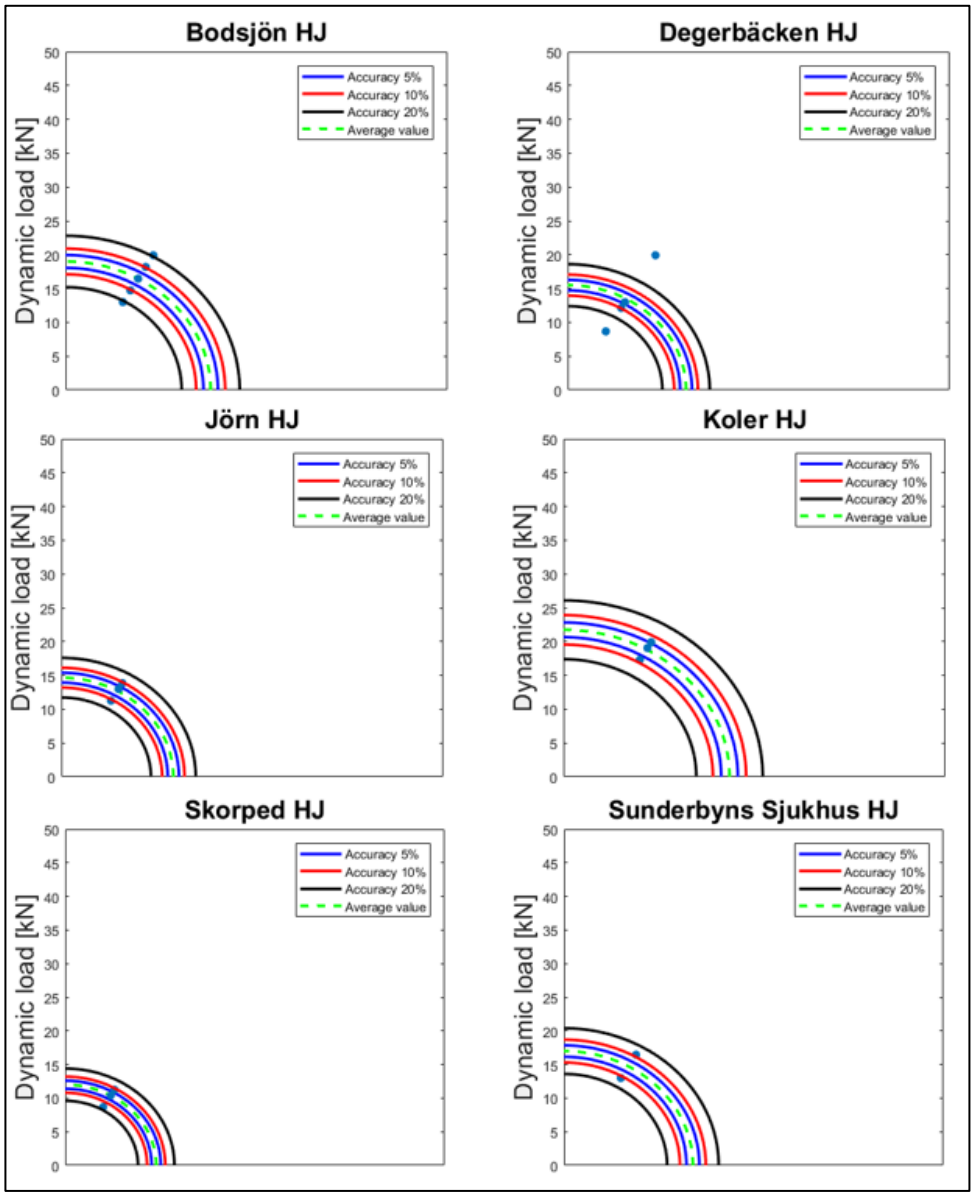

*Figure 3.15: Target diagrams involving dynamic impact loads registered at each detector station and referring to the **right** wheel of the first axle of the locomotive identified by the vehicle number **917400014341**. Data were measured between **October 18th and October 30th 2018** and correspond to a measured train speed ranging between **95 km/h and 105 km/h**. The green dashed line indicates the mean value of dynamic loads. The blue solid lines represent an accuracy of 5%, the red solid lines an accuracy of 10% whereas the black solid lines an accuracy of 20% computed with respect to the mean value.*

By analyzing the information in Figure 3.15, Figure B1.46 and Figure B1.47 the following conclusions can be drawn.

Data registered at Dergebäcken detector station are very scattered, which may indicate that this station has a poor accuracy and needs to be calibrated. A further assessment of the performance of this detector station is recommended.

All the other detectors exhibit a better performance in measuring data because the dynamic loads magnitudes measured for the same wheel over a short period of time and for a limited train speed range are close to each other. The accuracy of each detector may be estimated around 20%. However, an accuracy of 20% does not match the one prescribed by the authorities which is 5%. It is clear that the poor accuracy

can partly be explained by the fact that the data have been measured on different occasions and at slightly different speeds.

Therefore, it is not possible to assess the exact accuracy of each detectors because of the lack of data registered in a very short time interval (implying that the wheel tread damage would be constant) and for the exact same train speed. Further, since the RCF damage has a local appearance on the wheel tread, it is not possible to exclude the possibility that the damage is only partly, or perhaps not at all, interacting with the rolling band when the damaged wheel is passing a given detector.

3.4.2 Influence of train speed on dynamic loads: severe wheel tread damage

Contrary to the analysis proposed in the previous section, the following analysis focuses on a time interval where the damage on the wheel tread is more significant leading to higher dynamic loads. Such a time interval may be deduced from the variation in dynamic loads over time, as the one proposed in Figure 3.9. As a matter of fact, a sharp increase in the dynamic impact load values over time marks the presence and evolution of severe RCF damage on the wheel treads.

The same type of analysis as in the previous section has been repeated for the different time interval. The analysis whose results are presented below is based on data collected by the detector stations at Sunderbyns Sjukhus and Bodsjön and referring to both wheels of the first axle of the locomotive identified by vehicle number 917400014341.
Particularly, dynamic impact loads registered from January 14th to February 14th 2018 have been considered because of their abnormal trend shown in Figure 3.9 and Figure B1.45, available in Appendix B. As it has been proposed in the previous section, an insight helping for the understanding of the expected trends may be obtained by looking at Figure 3.16. According to the figure, the dynamic loads exhibit a sharp increase over time.

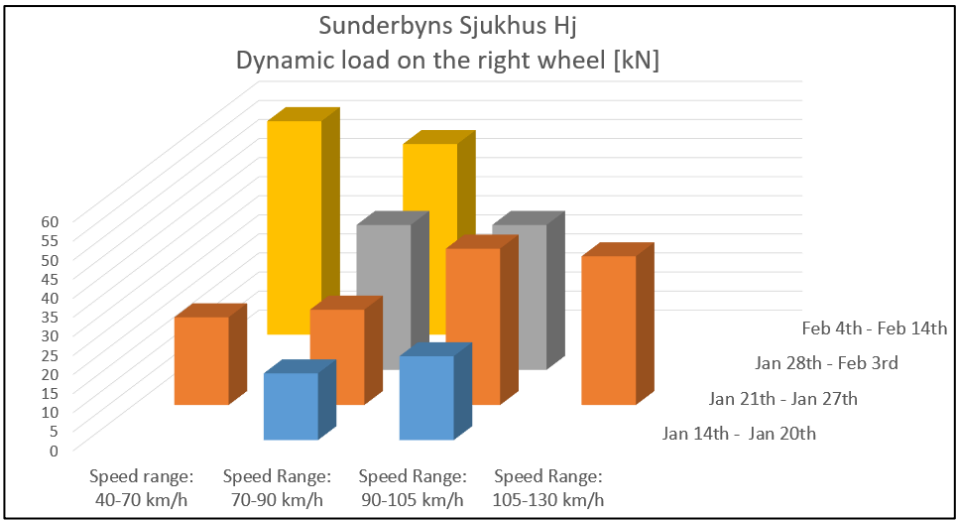

*Figure 3.16: 3D-Bar plot showing the mean of dynamic loads registered for the **right** wheel of the first axle of locomotive **917400014341** at the Sunderbyns Sjukhus detector station during specific time intervals and for specific train speed ranges. The vertical axis shows the dynamic load values. The Y-axis shows the time intervals at which data have been registered, while the X-axis shows the considered speed ranges.*

*Table 3.12: Results in terms of PRESS statistics, R^2_{Adj} and MS_{res} derived by the adoption of different regression models involving the regressor variables indicated in the rightmost cells of the table. Analysis involved dynamic impact loads measured for the **left** wheel of the first axle of locomotive **917400014341** at **Sunderbyns Sjukhus** detector station between January 14th and February 14th.*

LOCOMOTIVE 917400014341 Sunderbyns Sjukhus								
N° of regressor variables	PRESS	R^2_{Adj}	MS_{res}	t	v	t^2	v^2	v^3
1	27.41	0.637	45.92	x				
1	29.44	-0.025	129.56		x			
2	35.07	0.762	30.02	x	x			
2	29.44	-0.025	129.56		x	x		
2	45.40	0.008	125.34		x		x	
3	56.83	0.796	25.65	x	x		x	
4	150.87	0.795	25.89	x	x		x	x

*Table 3.13: Results in terms of PRESS statistics, R^2_{Adj} and MS_{res} derived by the adoption of different regression models involving the regressor variables indicated in the rightmost cells of the table. Analysis involved dynamic impact loads measured for the **right** wheel of the first axle of locomotive **917400014341** at **Sunderbyns Sjukhus** detector station between January 14th and February 14th.*

LOCOMOTIVE 917400014341 Sunderbyns Sjukhus								
N° of regressor variables	PRESS	R^2_{Adj}	MS_{res}	t	v	t^2	v^2	v^3
1	32.46	0.781	44.17	x				
1	28.34	-0.051	212.32		x			
2	40.28	0.849	30.50	x	x			
2	28.34	-0.051	212.32		x	x		
2	40.84	-0.092	220.51		x		x	
3	47.48	0.842	31.90	x	x		x	
4	93.73	0.835	33.28	x	x		x	x

*Table 3.14: Results in terms of PRESS statistics, R^2_{Adj} and MS_{res} derived by the adoption of different regression models involving the regressor variables indicated in the rightmost cells of the table. Analysis involved dynamic impact loads measured for the **left** wheel of the first axle of locomotive **917400014341** at **Bodsjön** detector station between January 14th and February 14th.*

LOCOMOTIVE 917400014341 Bodsjön								
N° of regressor variables	PRESS	R^2_{Adj}	MS_{res}	t	v	t^2	v^2	v^3
1	29.45	0.695	42.25	x				
1	32.65	-0.046	144.87		x			
2	34.19	0.683	43.89	x	x			
2	32.65	-0.046	144.87		x	x		
2	37.13	-0.103	152.79		x		x	
3	36.13	0.684	43.73	x	x		x	
4	41.28	0.681	44.13	x	x		x	x

*Table 3.15: Results in terms of PRESS statistics, R^2_{Adj} and MS_{res} derived by the adoption of different regression models involving the regressor variables indicated in the rightmost cells of the table. Analysis involved dynamic impact loads measured for the **right** wheel of the first axle of locomotive **917400014341** at **Bodsjön** detector station between January 14th and February 14th.*

LOCOMOTIVE 917400014341 Bodsjön								
N° of regressor variables	PRESS	R^2_{Adj}	MS_{res}	t	v	t^2	v^2	v^3
1	80.21	0.468	856.58	x				
1	61.87	0.074	1491.3		x			
2	143.74	0.689	501.71	x	x			
2	61.87	0.074	1491.3		x	x		
2	67.43	0.028	1564.7		x		x	
3	163.97	0.676	521.34	x	x		x	
4	176.81	0.696	488.97	x	x		x	x

By looking at the results listed in the tables above, it is possible to notice that the train speed is no longer the most influencing regressor variable. This is evidenced by the results arising from the adoption of multiple linear regression models involving merely the train speed as variable. Instead, the regression models involving the presence of time as a regressor variable provides a better fit to the observed data.

A typical surface fitting arising from the adoption of a multiple linear regression model involving both train speed and time as regressor variables is shown in Figure 3.17. As it is possible to notice from Figure 3.17, in this time interval the dynamic loads exhibit a (in relation to the time dependence) low increase with train speed but instead a sharp increase over time.

These results might be related to a fast wheel tread damage growth over time. This implies that the contribution to the increase in the dynamic loads registered by the detector stations due to the fast deterioration of the wheel tread is much more

significant than the increase induced by higher train speeds. This conjecture will therefore result in regression models that suffer the train speed dependence. Further, it is even more difficult to compare the performance of the different detectors since the measured dynamic loads are not stable over time.

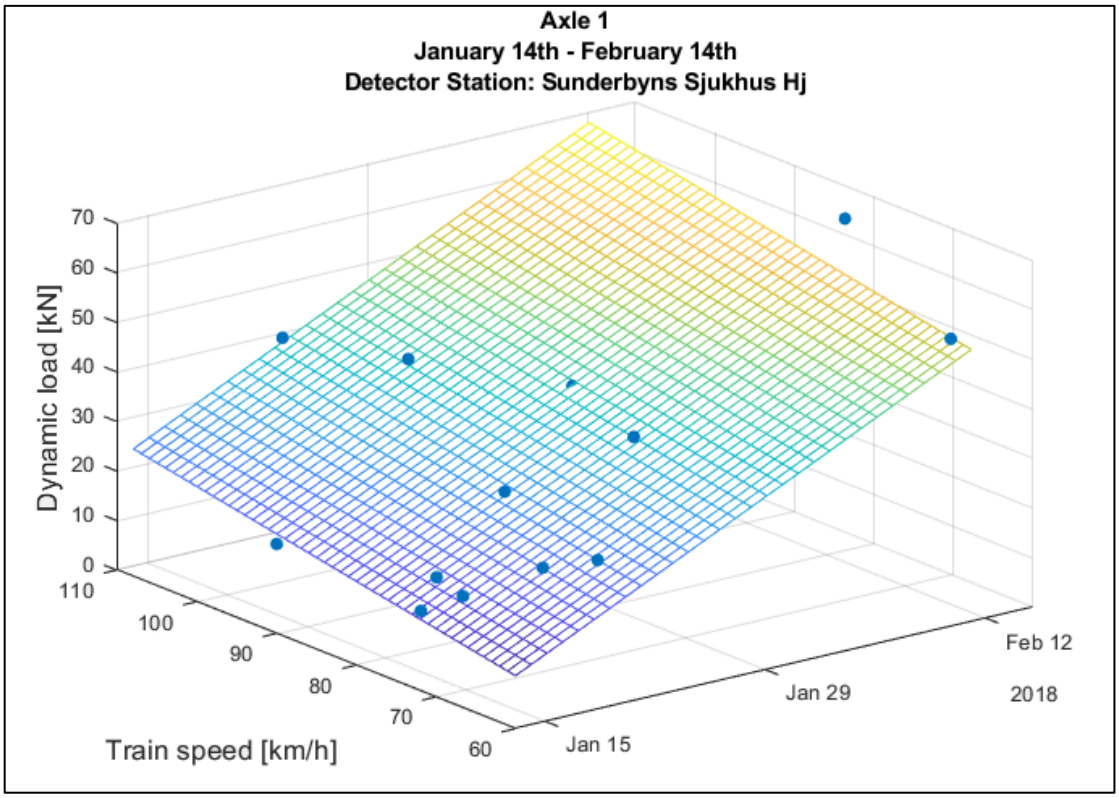

*Figure 3.17: Surface fitting of dynamic impact loads expressed as a linear function of time and train speed. Data have been registered at the Sunderbyns Sjukhus detector station and referring to dynamic impact loads detected for the **right** wheel of the first axle of locomotive **917400014341** between January 14th and February 14th 2018.*

3.4.3 Concluding comments

In conclusion, from the results achieved in Chapter 3 the following key points may be highlighted:

- The mean loads registered by the WILDs cannot be considered as completely independent of train speed. The linear simple regression model between mean load and train speed does not allow to properly correlate these two variables.
- The dynamic loads registered by WILDs exhibit an increase with increasing train speed and over time.
- For low wheel tread damage, the measured dynamic loads depend mainly on the train speed. This confirms the results presented in [13], where a linear increase in the dynamic loads with increasing train speed for the same wheel tread damage (rolling contact fatigue) was shown.
- For severe wheel tread damage, the progressive growth over time of the wheel tread damage leads to an increase in the loads acting on the wheels that is much more significant than the increase induced by higher train speed.

- For both above-mentioned cases, the multiple linear regression model between dynamic load, train speed and time instants at which data were measured provides a good fit to the registered data.
- It is not possible to firmly assess the accuracy of the wheel impact load detectors because of the lack of data registered in a very short time and for the same train speed. However, indications for necessary calibration of a wheel impact load detector may be given by comparing data registered by each device for a given wheel in a very short time period and for a restricted range of train speeds.

4 Parameterized finite element model

4.1 Implementation phase

The second part of the present thesis project aimed at generating a parameterized three-dimensional wheelset model that will be used for further analyses in the EU project In2Track2.

For this purpose, Python scripts have been used to generate FE models in Abaqus. Abaqus is a commercial software package for finite element analysis developed by Dassault Systèmes Simulia Corp [19].

The Abaqus scripting procedure is summarized in Figure 4.1. The Abaqus/CAE graphical user interface (GUI) was used to create the wheelset model. The GUI generates all command functions accounting for each performed operation and saves them in a journal-file whose extention is *.jnl* [20]. The journal-file is written in object-oriented programming language and therefore it can be saved as a Python-file. Subsequently, the Python script may be edited to add parameterization of some geometrical features. In addition, it allows to easily alter the model properties such as materials, mesh size and element type. The Python code may then be run in Abaqus/CAE. The Abaqus kernel interprets the commands to generate the modified model [21].

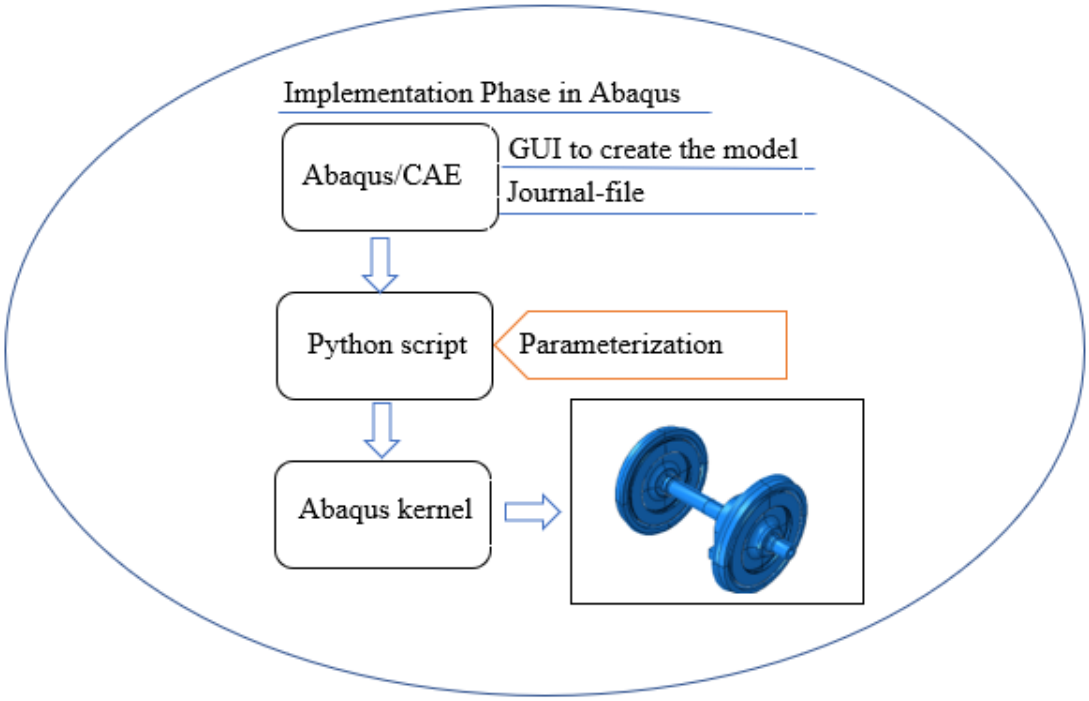

Figure 4.1: Block diagram summarizing the implementation procedure in Abaqus.

4.2 Wheelset model

A conventional wheelset consists of two coned wheels rigidly connected to the axle so that both wheels exhibit the same angular velocity and the distance between the wheels is preserved.

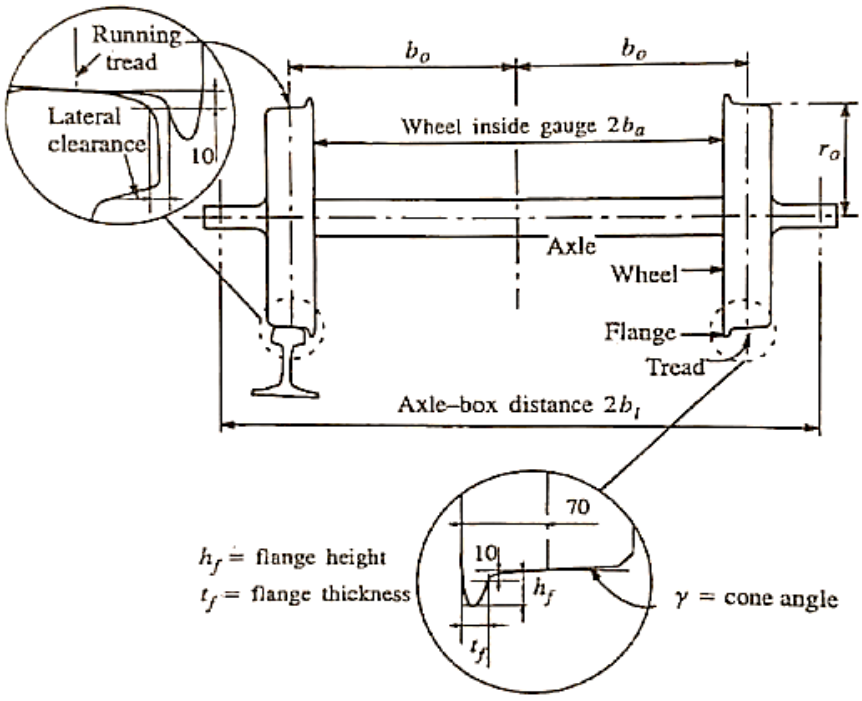

Figure 4.2:Schematic of a conventional wheelset. Measures in mm. [22]

The surface of the wheel where contact with the rail occurs is characterized by two parts: the flange and the wheel tread. The flange is located at the inner side of the wheel and aims to provide lateral guidance especially in curves. The wheel tread is the conical running surface that meets the rail [22]. Additionally, the wheelset involves the presence of brake discs that are mounted on the wheels (or on the axle). A powered wheelset also includes a traction gear box which is mounted on the axle of the wheelset.

The modelled wheelset refers to a powered wheelset of a freight locomotive whose drawings were provided by the Bombardier Transportation company. The drawings included a detailed sketch of the wheel and the assembly drawing of the whole wheelset. However, because of the lack of detailed sketches regarding the gear box housing, gear wheel and brake discs, some simplifications in their modelling were made. Reference [23] was used as a guideline to perform these simplifications. As a matter of fact, in reference [23], the FE model of a powered railway wheelset is characterized by similar geometry and characteristics as the one analysed in this thesis project. Hence, components for which detailed information were missing have been modelled in such a way that their characteristics were similar to the corresponding ones reported in [23].

The main assumptions and simplifications adopted in the model are:

- The wheels are rigidly connected to the wheelset axle.
- The brake discs are rigidly connected to the wheels.
- The gear wheel has been modelled as a hollow cylinder rigidly connected to the axle.
- The gear housing is rigidly connected to the gear wheel.

- The roller bearings ensuring the interface between axle and gear box were modelled by springs applied in lateral and radial directions. More specifically, a 500 MN/m spring stiffness was assumed in the longitudinal (k_L) and radial vertical directions (k_{RV}), whereas a 1 MN/m spring stiffness was used to model the interaction in the radial horizontal direction (k_{RH}), [23]. An illustration showing the mentioned interaction is presented in Figure 4.3.

The CAD model of the wheelset is shown in Figure 4.4.

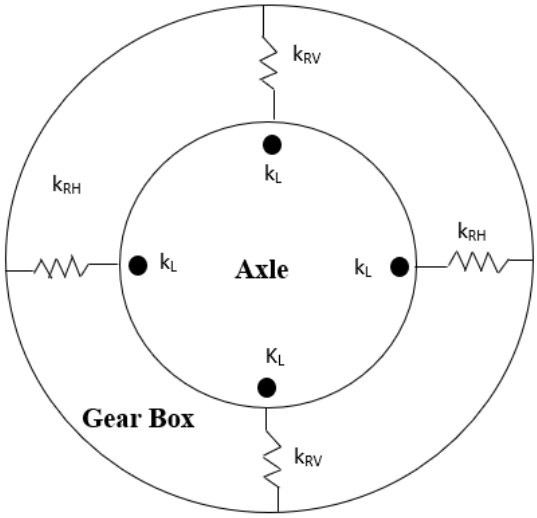

Figure 4.3: Schematic illustrating the modelled interaction between axle and gear box.

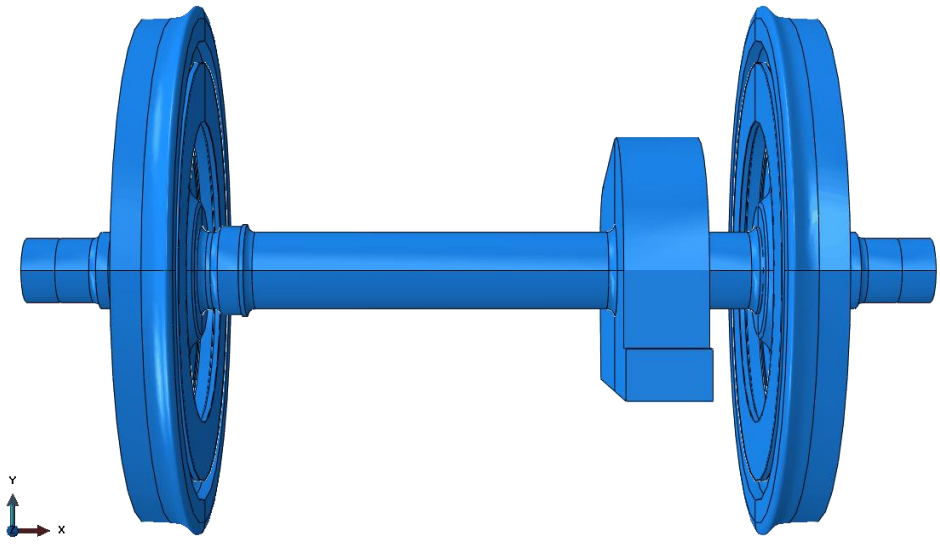

Figure 4.4: Frontal view of the wheelset model in Abaqus CAD interface.

4.2.1 Material properties

Three different materials were used to assign the mechanical properties to each component of the wheelset.

Common steel was used to assign the mechanical properties to the brake discs, gear wheel and gear housing. A slightly lower density steel was assigned to the wheels to match the wheel mass prescribed by the drawing provided by Bombardier Transportation. Lastly, EA1N steel was assigned to the axle [24]. The mechanical properties defined for each component of the wheelset and the corresponding mass are presented in the following tables.

Table 4.1: Mechanical properties for each modelled component

Component	**Material**	**Young Modulus [GPa]**	**Density [$\frac{kg}{m^3}$]**	**Poisson coefficient [-]**
Axle (hollow)	EA1N	210	7500	0.26
Wheel	Steel	210	7700	0.3
Brake disc	Steel	210	7800	0.3
Gear wheel	Steel	210	7800	0.3
Gear housing	Steel	210	7800	0.3

Table 4.2: Mass of each component of the wheelset and overall mass of the wheelset.

Component	**Quantity**	**Total Mass [kg]**
Axle	1	430
Wheel	2	1222
Brake disc	4	528
Gear wheel	1	241
Gear housing	1	642
		$\sum$ 3063

4.2.2 Python code and modal analysis

The Python script allows to create railway wheelset models that differ in terms of geometrical features of the wheel, such as the rim thickness. The goal was to create a parameterized wheelset model that enables to generate automatically different models characterized by railway wheels with varying external diameter, thus considering the wear of the tread. The use of the Python script is to easily make available different wheelset models to reduce the time demanded to create each of them directly in the Abaqus GUI.

The following section presents a description of the Python script and results arising from a modal analysis of the wheelset for two different thicknesses of the wheel rim. Finally, a few suggestions for further analyses are proposed.

4.2.2.1 Description of the Python code

As mentioned in Section 4.1, the modelling process has been carried out in the Abaqus graphical user interface (GUI). By saving the model and converting the journal-file into a Python file it was possible to get access to information regarding all the operations executed. However, this information appears in the form of numbered

entities, thus not allowing to modify the code. Therefore, the first action was to type the instruction "*session.journaloptions.setvalues(replaygeometry = coordinate, recovergeometry = coordinate)"* into the command line interface [20]. By applying this instruction, the information available in the Python code appears as function of the coordinates of each selected entity. Consequently, it was possible to parameterize each entity belonging to the rim of the wheel as a function of the rim thickness.

The Python script takes only the external diameter of the wheel as input. The modelled wheel has a nominal external diameter of 1.25 m. Nevertheless, the rim thickness of the wheel diminishes gradually due to wear of the tread until it reaches a critical value. For this wheel type, the prescribed threshold diameter beyond which the wheel must be replaced is 1.17 m.
An idea about the maximum allowable range of wheels due to the reduction of the rim is given in Figure 4.5.

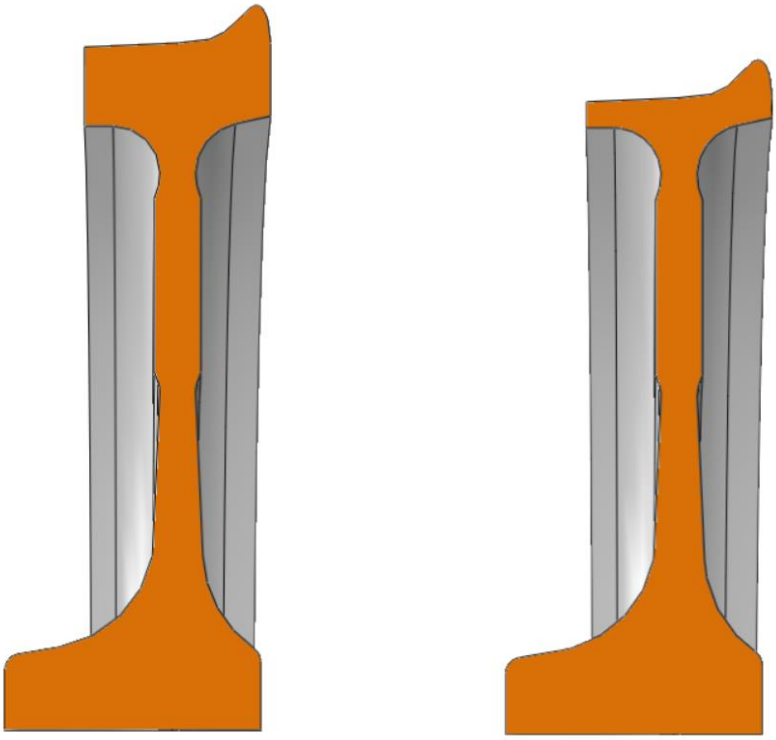

Figure 4.5: Cross section view of the modelled railway wheel: the wheel having nominal external diameter is shown on the left , whereas critical prescribed external diameter thereof is shown on the right.

4.2.2.2 Modal analysis of free wheelset

This section proposes the numerical results arising from a modal analysis of the wheelset for two different cases: the first case was derived by the adoption of the wheelset model characterized by the wheel having nominal external diameter, whereas the second one considered a wheel having the limit prescribed external diameter.

The analysis may be seen as starting point of further analyses aimed at studying the dynamic response of the wheelset for different wear conditions of the railway wheel. The analysis was carried out in Abaqus CAE/Standard. The elastic modes of the wheelset in the frequency range 0 - 1000 Hz were calculated. Solid 8-node linear

hexahedral elements were used to mesh all the components of the wheelset except the gear housing. The latter was instead meshed with 10-node quadratic tetrahedral elements. A convergence study revealed that a 50 mm element size was appropriate. Finally, free boundary conditions were assumed and the Lanczos solver was adopted to run the analysis.

Table 4.3 shows some of the significant modes and the corresponding eigenfrequencies for both analysed cases. The table also provides the percentage of the difference between the eigenfrequencies derived for the two mentioned cases.

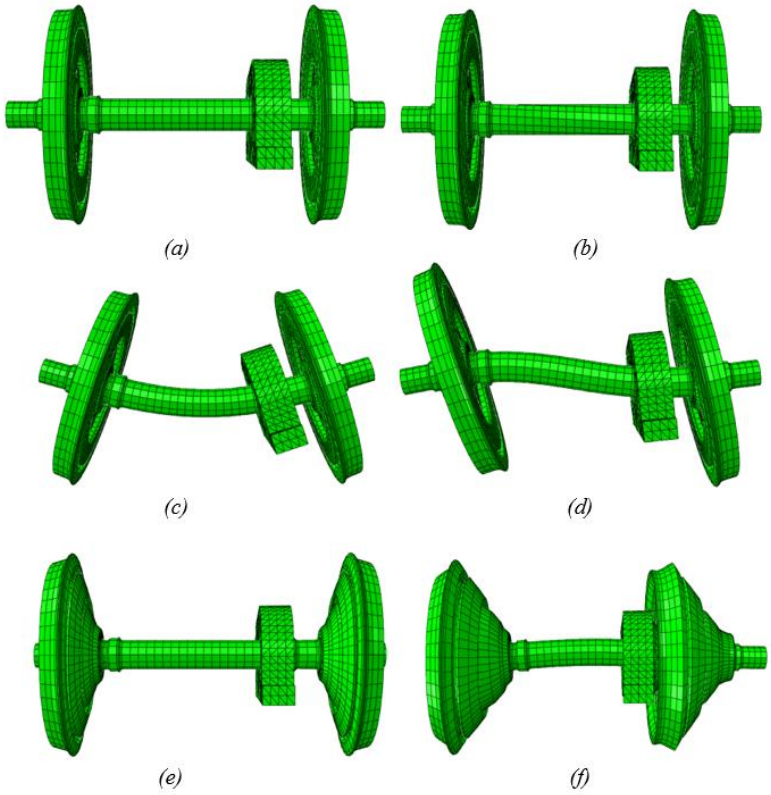

Figure 4.6: Elastic modes of the wheelset: (a) Undeformed wheelset. (b) Mode 3. (c) Mode 4. (d) Mode 7. (e) Mode 11. (f) Mode 17.

Table 4.3: Eigenmodes and corresponding eigenfrequencies of the wheelset for two different cases: wheelset characterized by a wheel with nominal dimensions and wheelset characterized by a wheel having critical external diameter. Percentage increase in terms of eigenfrequencies is shown in the rightmost column.

		Frequency [Hz]		
Mode	Type	Nominal	Limit	Limit - nominal difference [%]
1 - 2	Rigid body	0	0	-
3	First torsion mode	42.7	51.5	17.0
4	First bending mode	53.3	60.3	11.6
7	Second bending mode	96.2	113.7	15.4
11	First umbrella mode	194.9	227.3	14.2
17	Second umbrella mode	363.9	399.3	8.9

By comparing the results listed in Table 4.3, an increase in the eigenfrequency values with reduced external diameter of the wheel is observed. This is an expected and reasonable result. As a matter of fact, a reduction in the rim thickness results in a decrease in the overall mass of the system that leads consequently to an increase in the eigenfrequency values since the eigenfrequencies are inversely proportional to the mass. Further, it is possible to observe that the percentage increase in the eigenfrequency values due to the reduction of the rim thickness of the wheel tends to decrease for higher modes of the wheelset.

The parameterized wheelset model might be used for innumerable purposes. Many current researches in the railway sector focus on the wheel–rail interaction. For instance in [25], a three dimensional wheel–rail model was object of study to predict the occurrence of defects on both rail and wheel surfaces. In this context, a useful means of the parameterized wheelset model might be to go into more specific issues and investigate how the reduction of the rim thickness due to the wear may affect the interaction between wheel and rail trying to predict how the damage occurrence might be influenced. Additionally, the study of the wheelset flexibility might be another interesting lead to be undertaken. For this purpose, the deformation of the axle and wheels through the receptance method might be investigated for different wheel geometries and for different train speeds [26].

In conclusion, the Python scripting for finite element analysis (FEA) softwares is a suggested tool to create parameterized models because it allows to generate different models automatically, and moreover it opens up many avenues for further analyses.

5 Fatigue analysis: non-powered wheelset

5.1 Aims and background

In the last chapter, a dynamic analysis aimed at checking the fatigue resistance of the axle of a non-powered wheelset while subject to periodic sinusoidal loads acting on the wheels is performed. The intent of this analysis is to increase the confidence in the alarm limits currently set for the wheel impact load detectors, but at the same time also to encourage other studies and research for improved wheel design and for defining a precise timeframe within which the maintenance of the wheels must be carried out to prevent any consequent and serious damage to the railway axles.

The fatigue phenomenon is a well understood type of damage which is triggered by variable loading conditions on a mechanical component that might lead to a sudden failure thereof. Railway axles are designed for infinite life which means that the time-varying stress state is below the limit (endurance limit) that causes crack initiation. This cautionary condition is ensured by generous safety factors applied to the material fatigue properties [27].

Railway axles undergo a complex and three-dimensional state of stress. Therefore, multiaxial fatigue criteria must be used to determine a scalar quantity (equivalent stress) that equivalently describes the stress state of the component. Subsequently, the equivalent stress must be compared to the fatigue limit prescribed by the regulations.

Multiaxial fatigue criteria can be categorised in several typologies, see [28]. The use of the most suitable criterion depends on the case being analysed. The main distinction between different multiaxial fatigue criteria entails the type of loading. Multiaxial loadings can be classified into two categories: proportional and non-proportional loading. The difference refers to the direction of the principal stresses over time. For the first category, the direction of the principal stresses does not change over time, whereas multiaxial non-proportional loadings lead to the change in principal stresses directions instant by instant [29].

In section 5.3 a proportional loading condition is proven to reflect the stress state in the wheelset axle caused by first order sinusoidal loads applied on the rolling circle of the wheels. Based on this outcome, the multiaxial fatigue criterion that best suits the proportional loading condition turned out to be the Sines' criterion.

The Sines' criterion is an invariant based criterion; the term invariant is used because the first invariant of the mean stress tensor appears in the formulation of the equivalent stress [30]. The definition of the equivalent stress is described by Eq. (5.1):

$$\sigma_{a,eq} = \sigma_{vM,a} + M \cdot I_m \qquad (5.1)$$

where:

- $\sigma_{vM,a}$ is the von Mises equivalent alternating stress which is described by Eq. (5.2):

$$\sigma_{vM,a} = \frac{1}{\sqrt{2}} \sqrt{\left(\sigma_{a,1} - \sigma_{a,2}\right)^2 + \left(\sigma_{a,2} - \sigma_{a,3}\right)^2 + \left(\sigma_{a,3} - \sigma_{a,1}\right)^2} \quad (5.2)$$

where $\sigma_{a,i}$ accounts for the alternate component of the *i*th principal stress;

- I_m is the first invariant of the mean stress tensor, as described by Eq. (5.3):

$$I_m = \sigma_{m,1} + \sigma_{m,2} + \sigma_{m,3} \quad (5.3)$$

where $\sigma_{m,i}$ accounts for the mean component of the *i*th principal stress;

- M is the mean stress sensitivity and depends on the material properties.

  FKM-Richtline provides an estimate of the mean stress sensitivity based on experimental results [31]. This factor can be calculated according to Eq. (5.4):

$$M = a \cdot 10^{-3} R_m + b \quad (5.4)$$

where R_m (expressed in MPa) is the ultimate strength of the material, whereas a and b are coefficients depending on the material. The coefficients are estimated to 0.35 and -0.1 for different steel alloys.

According to Sines' criterion, the equivalent stress described by Eq. (5.1) must be lower than the fatigue limit prescribed by the technical standards to prevent any initiation and propagation of cracks.

5.2 Dynamic analysis

The fatigue resistance of a hollow wheelset axle has been assessed via local approach. This is the opposite to the global approach where the fatigue resistance of a mechanical component is evaluated via hand calculations and by using tables to estimate the influence of several effects such as the notch. The local approach uses the numerical results arising from a finite element simulation where such effects are embedded in the FE model.

A non-powered wheelset was object of the analysis. Furthermore, for the sake of simplicity, the same wheelset model generated by the Python code described in Section 4.2.2 was considered. However, since the analysis focused on a non-powered wheelset, the gear box was omitted from the model. The deletion of the gearbox was needed because of the lack of data regarding gearbox characteristics such as power, gear ratio and geometric dimensions that would have allowed for modelling the forces and moments exchanged between the gear wheel and the axle.
Therefore, the analysis of the examined axle reflects approximatively the reality, but it might still be considered fair because there are just a few other differences in the geometry between powered and non-powered railway wheelset axles which do not significantly affect the dynamic response.

The analysis was carried out in the Abaqus software. The stress state of the hollow axle was derived from a finite element simulation. After identifying the most stressed section and verifying the proportional loading assumption, the equivalent stress according Sines' criterion was determined and compared to the fatigue limit prescribed in the technical standard [32]. For this purpose, the stress-time history of the most critical section was saved in an Abaqus report-file (extension *.rpt*) and imported in Matlab. Finally, the principal stress-time histories were plotted in Matlab and used to calculate the alternate and mean components that appear in the formulation of the Sines' equivalent stress.

5.2.1 Loads and boundary conditions

As mentioned in Section 5.1, one of the aims of such an analysis is to increase the reliability of the current alarm limits set for the wheel impact load detectors. The current peak load alarm for freight locomotives set by the regulations in Sweden is 320 kN. However, a precautionary warning alarm is set at 250 kN [33].

Hence, one case of warning alarm highlighted in the data sheets provided by Lars Fehrlund has been considered to define the loads on the railway wheels. The warning alarm refers to the one registered at the Bodsjön detector station on February 13th 2018 for the first axle of the locomotive 917400014431. The data measured are reported in Table 5.1.

*Table 5.1: Data registered by the wheel impact load detector at the **Bodsjön** station on **February 13th 2018** for the first axle of locomotive **917400014341**.*

	Mean load [kN]		**Peak load [kN]**	
Train speed [km/h]	Left wheel	Right wheel	Left wheel	Right wheel
96	94	98	143	291

The data reported in Table 5.1 were used to define two sinusoidal loads acting respectively on the left and right wheels. The definition of first-order sinusoidal loads is a fair approximation for loads acting on the wheels when the wheel radius is not perfectly circular but eccentric.

The two sinusoidal loads were applied at the rolling contact point of each wheel and defined in such a way that the means and the peaks correspond to the measured ones. Furthermore, the circular frequency (ω) of the two sinusoidals was defined from the value of the measured train speed (v). Subsequently, the time (T) employed by the wheel to perform one revolution was derived from the circular frequency. The mentioned quantities are correlated to each other by Eq. (5.5).

$$\omega = \frac{v}{r} = \frac{2\pi}{T} \tag{5.5}$$

where r is the nominal wheel radius (half the nominal diameter of the wheel mentioned in Section 4.2.2.1).

Figure 5.1 shows the load applied at each wheel in one revolution. Lastly, it is worth mentioning that each load was associated to a dynamic implicit step in Abaqus. This a suitable choice when dynamic analyses must be carried out.

As far as the boundary conditions are concerned, the primary suspensions were modelled by a spring-damper system. The spring was modelled by a stiffness (k) of 10.5 MN/m, whereas the damper by a viscous damping coefficient (c) of 50 kNs/m. These values are typical values for the design of the primary suspension system of railway wheelset of freight locomotives. Figure 5.2 shows the location where the spring-damper system modelling the primary suspension was applied.

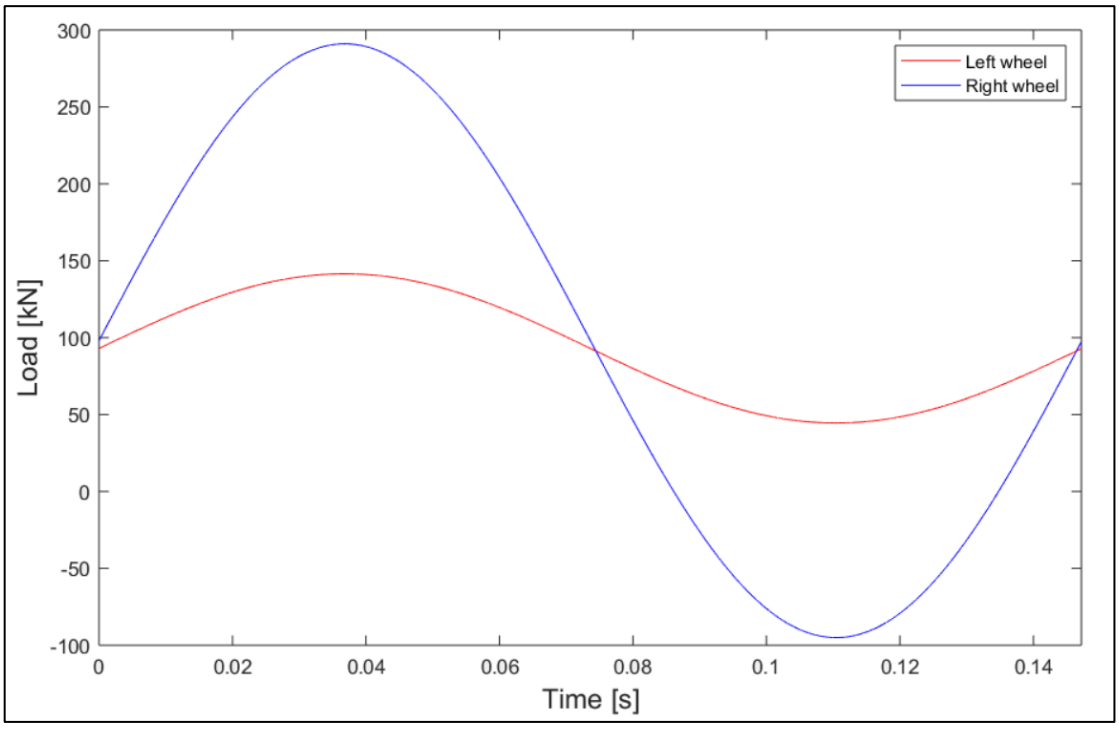

Figure 5.1: Load time history in one revolution of the wheel.

Figure 5.2: Schematic showing the location and the modelling of the primary suspension system.

5.2.2 Mesh

The definition of the mesh when performing stress analysis is critical. The mesh is required to be well-defined and fine enough to ensure the reliability of the numerical results. Since the aim was to evaluate the stress state in the hollow axle, a fine mesh was used there, whereas the wheels and brake discs were meshed rather coarsely to reduce the computational time needed to run the finite element simulation. The axle

was meshed with 20-node quadratic hexahedral (brick) elements, whereas the wheels and brake discs were meshed with 8 node linear hexahedral elements, see Figure 5.3.

The first adopted mesh was relatively fine and was used to identify the most stressed section. The latter coincides with the axle section on the left of the fillet located next to the right wheel seating. Subsequently, the axle model was partitioned in the proximity of the most stressed section to allow for a further refinement of the mesh in that specific area.

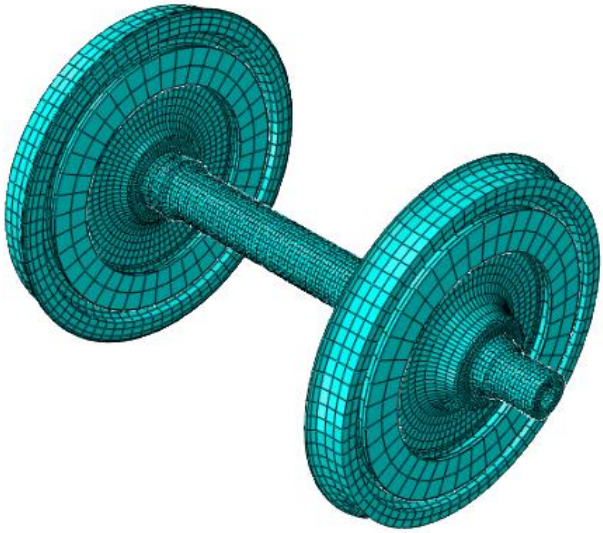

Figure 5.3: Mesh of the wheelset model. The figure refers to the final mesh adopted for extracting the numerical results.

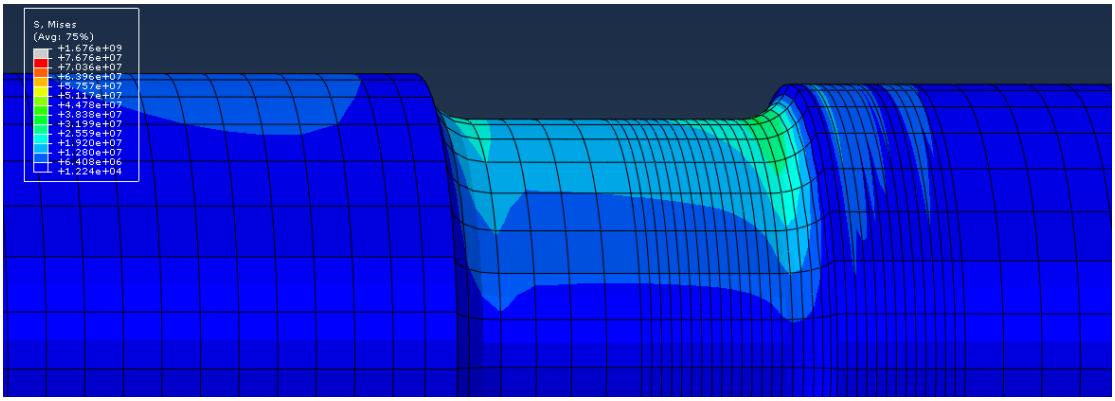

Figure 5.4: Snap shot of the numerical results in terms of Von Mises equivalent stress aimed to visualize the most critical section. The figure refers to the numerical results arisen from the adoption of the "medium" mesh.

5.2.2.1 Sensitivity analysis

A convergence study was performed to evaluate the robustness of the mesh. A node located on the most stressed section was chosen for the sensitivity analysis. However, the convergence study was not focused on the whole stress history, but on the maximum principal stresses detected at the time instant for which the peak loads occur on the rolling contact circle of the wheels.

Table 5.2: Characteristics of the coarse, medium and fine mesh of the axle.

	Approximative global element size [cm]	**Element size in the refined area [cm]**	**Number of nodes**
Coarse	2	0.8	72768
Medium	1.5	0.6	120813
Fine	1.5	0.4	129987

Three similar meshes were adopted for this analysis. The meshes are respectively designated as coarse, medium and fine mesh. A *h*-refinement of the coarse mesh was carried out to search for a suitable mesh whose use would have not resulted in large differences in the stress values arising from the FE simulation with respect to the results derived from the adoption of the previous mesh. Figure 5.5 illustrates the different global element size and the different local refinement between the three meshes of the axle. The characteristics of the three different meshes used for the axle are proposed in Table 5.2.

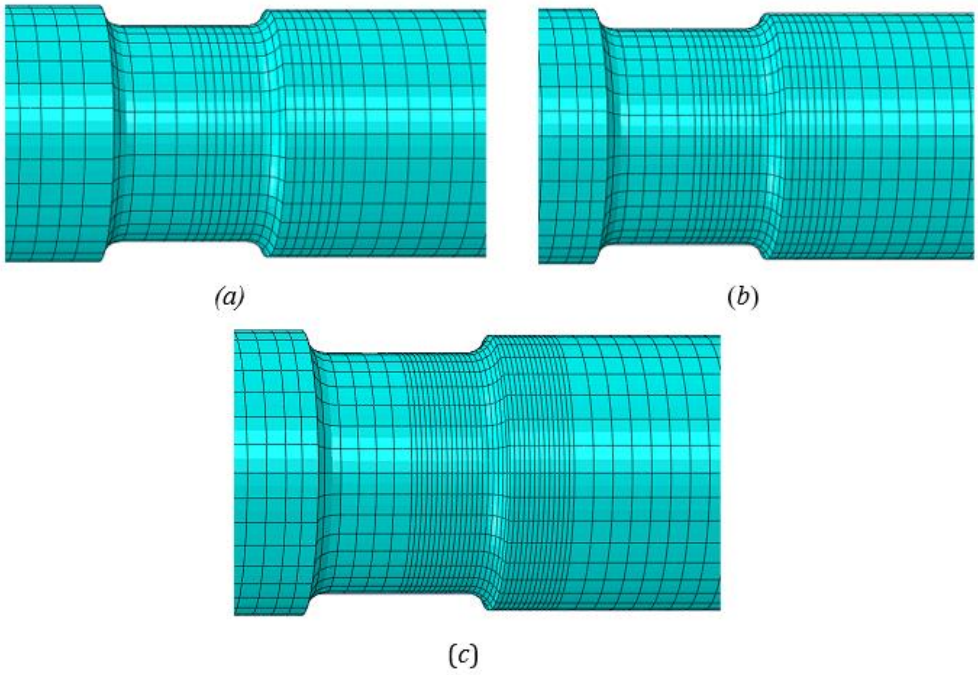

Figure 5.5: Axle mesh. (a) coarse mesh (b) medium mesh (c) fine mesh

Table 5.3: Number of nodes of the full wheelset model for the three different meshes.

	Total number of nodes
Coarse	84636
Medium	132681
Fine	141855

Table 5.4: Principal stress values for the node located on the most stressed section for the three different meshes.

	Coarse	**Medium**	**Fine**	**Coarse-medium difference [%]**	**Medium-fine difference [%]**
σ_1 **[MPa]**	196,64	210,03	210,79	6.3	0.36

The wheels and brake discs were meshed with 8-node linear hexahedral elements. A global element size of 3 cm was chosen for the wheel, whereas a global element size of 7cm was chosen for the brake discs. The number of nodes of the full wheelset model for the three different meshes of the axle is reported in Table 5.3.

The maximum principal stress ($\sigma_1(t)$) evaluated at the node located on the most stressed section and at the time instant when both wheels undergo the peak loads are presented in

Table 5.4.

The difference in results between the medium and fine meshes is 0.36%. This is confirmed by the full principal stress history in one-wheel revolution where no evident differences can be noticed from the adoption of the fine and medium meshes, see Figure 5.6. The same results are observed by looking at the minimum and mid principal stresses.

Consequently, the medium mesh was considered robust enough to perform the dynamic analysis.

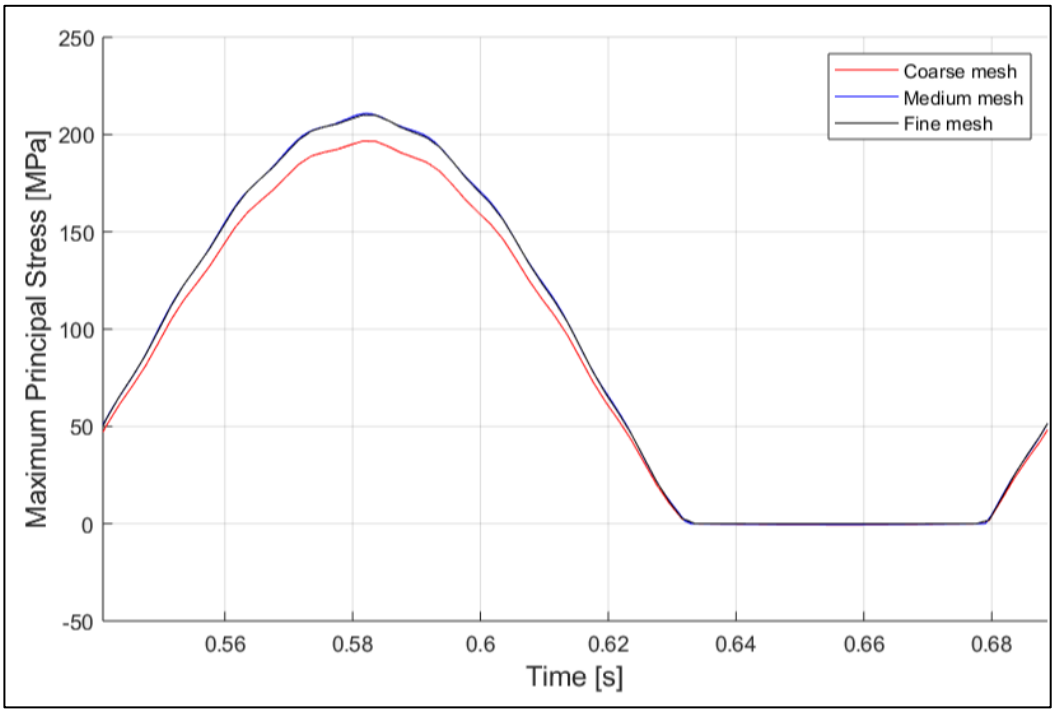

Figure 5.6: Comparison of the maximum principal stress time histories in one revolution of the wheel using the three different meshes.

5.3 Results

The stress-time histories of the node of interest (see Figure 5.7) elaborated by the finite element simulation were saved in the Abaqus report file and imported in Matlab software.

By looking at the stress state in the hollow axle generated by the periodic loads applied to the rolling contact circle of the wheels, it is observed that the loading condition is proportional in each revolution of the wheel. A proportional load condition results in a constant principal stress direction over time and therefore the Sines´criterion can be used to evaluate the equivalent stress state in the axle. The proportional loading can be confirmed by looking at the stress state for each revolution of the wheel which is presented in Figure 5.8.

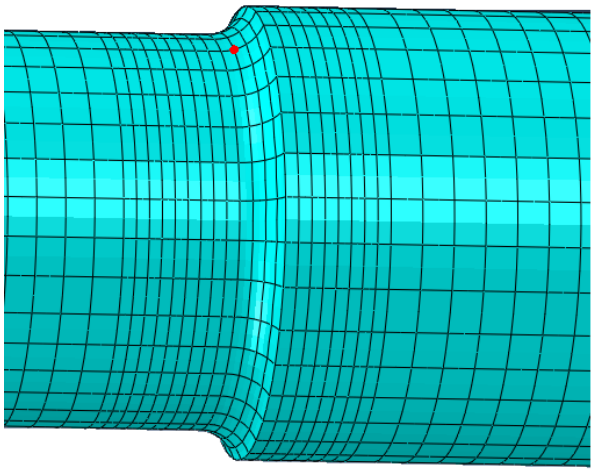

Figure 5.7: Position of the node used to extract the numerical results.

It can be noticed that the stresses are in-phase and therefore the principal stress direction does not change over time. Furthermore, the point of interest is very close to be parallel to the axial direction and therefore the maximum principal stress should be very similar to the normal stress due to the bending when in tension. A proof can be given by looking at Figure 5.9 where a maximum difference 8.5% in tension can be observed. This confirms that the orientation of the surface where the node of interest is located is not completely parallel to the axial direction (x-direction).
Based on the principal, mid and minimum principal stress-time histories (reported respectively in Figure 5.10,Figure 5.11 and Figure 5.12) the alternate and mean components appearing in the formulation of the equivalent stress according to Sines' criterion were derived. The values of the alternate and mean components of the principal stresses are presented in Table 5.5.

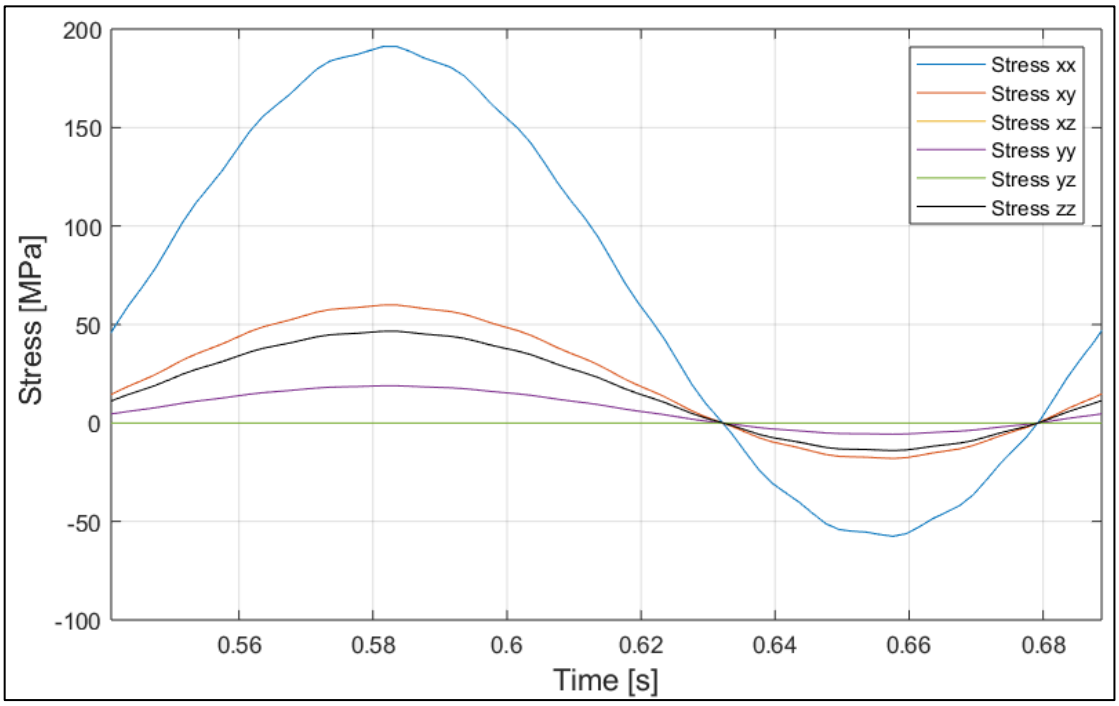

Figure 5.8: Normal and tangential stress of the point of interest in one revolution of the wheel.

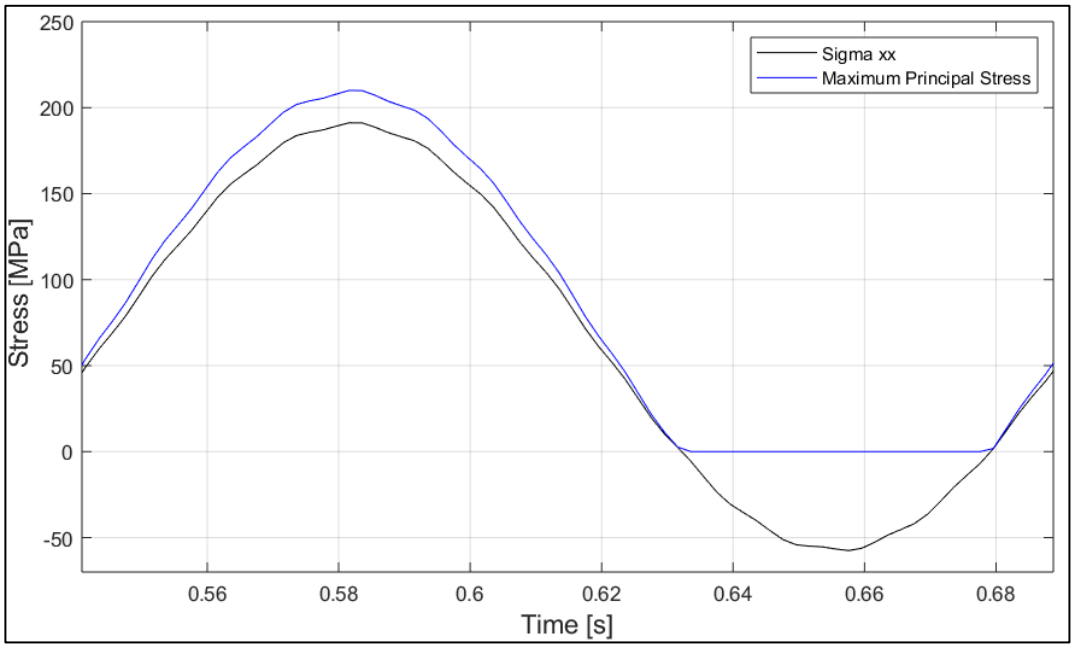

Figure 5.9: Time history in one revolution of the wheels of the maximum principal stress and normal stress due to the bending.

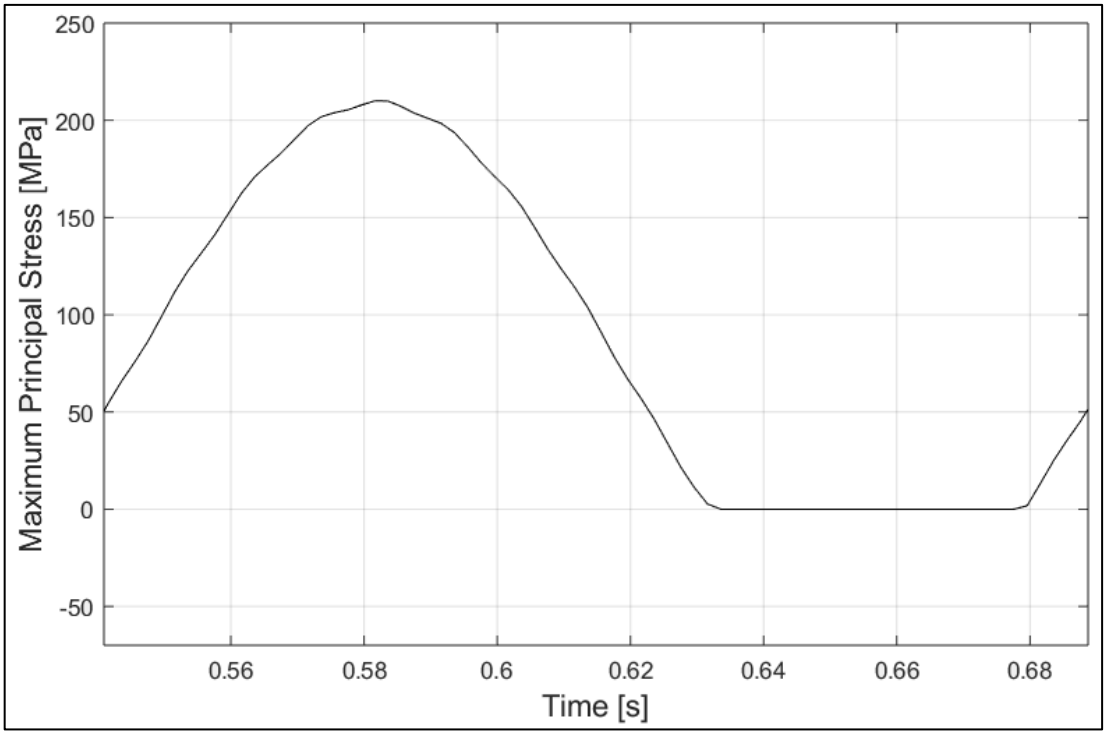

Figure 5.10: Time history of the maximum principal stress evaluated at the node of interest during one revolution of the wheels.

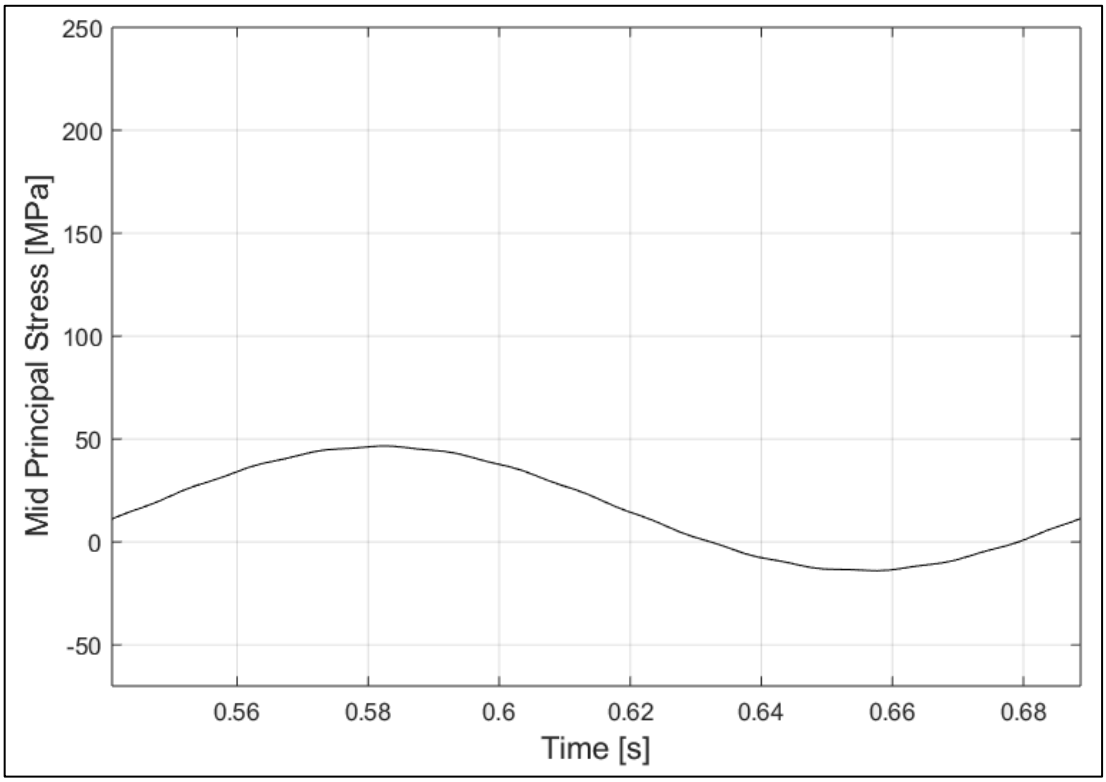

Figure 5.11: Time history of the mid principal stress evaluated at the node of interest during one revolution of the wheels.

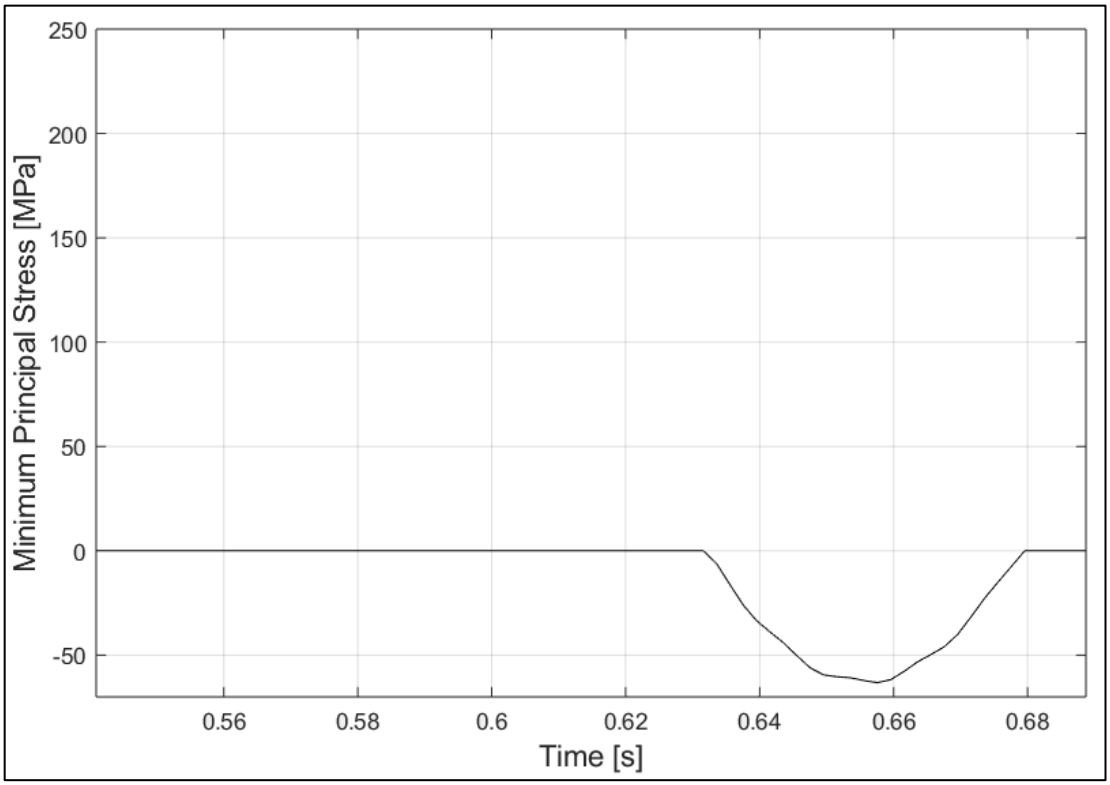

Figure 5.12: Time history of the minimum principal stress evaluated at the node of interest during one revolution of the wheels.

Table 5.5: Alternate ($\sigma_{a,i}$) and mean ($\sigma_{m,i}$) component of the ith principal stress.

	Mean component ($\sigma_{m,i}$) [MPa]	**Alternate component ($\sigma_{a,i}$) [MPa]**
Maximum principal stress (σ_1)	105.0	105.0
Mid principal stress (σ_2)	16.3	30.3
Minimum principal stress (σ_3)	-31.6	31.6

The values reported in Table 5.5, along with the mean sensitivity (M) of EA1N steel which was calculated and estimated as 0.11 by Eq. (5.4) and by using 600 MPa as ultimate strength of the material [24], have been used to deduce the equivalent stress in the most stressed section of the axle through Eq. (5.1). The equivalent stress value turns out to be 84.7 MPa.

Finally, the equivalent stress is compared to the fatigue limit value prescribed by the technical standard. Reference [32] prescribes 110 MPa as the fatigue limit value for the hollow axle beneath the fitting.

In conclusion, since the equivalent stress is lower than the fatigue limit prescribed by the technical standard, it is possible to state that the case of warning alarm values registered by the WILD does not induce fatigue damage to the hollow non-powered wheelset axle of this study. This should be verified in future work where the dynamic load is applied as an impact load instead of as a low-frequency sinusoidal load.

6 Conclusions and future work

6.1 Summary

In conclusion, this thesis has dealt with two different parts that have a common denominator: wheel impact load detectors.

In the first part, the performance of the wheel impact load detectors has been evaluated through a statistical analysis of the data provided by Lars Fehrlund. More specifically, the analysis focused on mean loads and dynamic loads registered by the wheel impact load detectors.

The results from the hypothesis testing show that the mean loads cannot be considered as completely independent of train speed, despite the mean load generated by the wheels is expected not to change over time.

Secondly, the performance of the detectors was evaluated by generating multiple linear regression models involving measured dynamic loads, train speed and the time when the measurement was performed. The models were compared with the results measured for a similar type of wheel tread damage presented in [13]. For a given wheel tread damage, reference [13] demonstrated that the dynamic impact load increases linearly with train speed. In principle, this outcome complies with the results arising from the statistical analysis carried out in this thesis when a lower magnitude of the wheel tread damage was considered.

On the contrary, for a more severe form of the wheel tread damage, the dynamic loads show a considerable increase over time due to the fast deterioration of the wheel tread. Because of the fast deterioration of the tread surface, the influence of the train speed on the dynamic load values becomes secondary.

Having proven that the dynamic loads depend significantly on train speed and the time of the detection, a comparison of the accuracy of each detector has been investigated via a graphical approach. In essence, the dynamic impact loads registered for a given wheel within a restricted time window and for a reduced speed interval have been plotted in target diagrams. The comparison shows that the dynamic loads registered at the Degerbäcken detector station are much more scattered than the dynamic loads measured at all other detector stations. Therefore, it is recommended to perform a calibration of the wheel impact load detector at Degerbäcken.

The second part of the thesis aimed at developing a parameterized wheelset model. For this purpose, a Python script for the Abaqus software has been written. The Python script allows to easily alter the rim thickness of the railway wheels. The Python script can be extended to include also other wheelset design parameters.

The fatigue resistance of the hollow axle of a non-powered wheelset has been assessed. To this aim, a case of warning alarm values registered by a WILD was used to define the periodic loads acting on the contact rolling circle of the wheels. It was shown that the periodic loads resulted in a proportional loading condition and therefore the multiaxial Sines´criterion turned out to be a suitable approach to calculate the equivalent stress in the most stressed section. The results showed that the selected case of warning alarm values did not induce fatigue damage to the axle.

6.2 Future work

Many different analyses have been left for future work due to lack of time (e.g. the finite element simulations were very time consuming and required even days to finish a single simulation) and the need of further information (e.g. information concerning the gearbox of the modelled wheelset that would have allowed a fatigue analysis of a powered wheelset axle). However, in this last chapter new proposals for further analyses are presented.

As far as the statistical analysis of the data measured by the WILDs is concerned, data registered for different axles of the same locomotive might be analysed and compared. For example, it would be of interest to investigate whether certain axles in the trainset are more prone to rolling contact fatigue damage than others, and in that case whether the degradation rate differs between these axles. Such information might suggest a change in maintenance intervals set by the transport authorities.

Further, it might be interesting to dig deeper into the numerous provided Excel files with data registered by the wheel impact load detectors to find a time period within which different detectors detected dynamic impact loads at the same train speed and within a restricted time window (order of a few days). This would allow for a better comparison between the performance of different detectors.

The Python code might be used to estimate to which extent the dynamic flexibility and fatigue resistance of the wheelset is influenced after reprofiling the railway wheels.

The fatigue analysis performed in Section 5 should be repeated for a time history of the wheel load corresponding to a wheel-rail impact. The impact loading will include a wide range of excitation frequencies that may affect the stresses in the axle in a different way than the harmonic load applied in this thesis. The fatigue resistance of a powered wheelset axle might be evaluated for warning alarm values of the wheel impact load detectors. Eventual fatigue damage induced to the axle might encourage further studies aimed at assessing a precise time window (dependent on the measured loads) within which the authorities should take action and make maintenance of the wheels.

References

1. Palo M., Schunnesson H., Kumar U. (2012): Condition monitoring of rolling stock using wheel/rail forces. *The Ninth International Conference on Condition Monitoring and Machinery Failure Prevention Technologies*, vol. 1, pp. 560-568.
2. Nielsen J. C. O., Johansson A., (2000): Out-of-round railway wheels - A literature survey. *Proceedings of the Institution of Mechanical Engineers, Journal of Rail and Rapid Transit*, vol. 214, pp. 79-91.
3. Bian J., Gu Y., Murray M., (2013): Numerical study of impact forces on railway sleepers under wheel flat. *Advances in Structural Enginering*, vol. 16, pp. 127-134.
4. Asplund M., Palo M., Famurewa S. M., Rantatalo M., (2016): A study of railway wheel profile parameters used as indicators of an increased risk of wheel defects. *Proceedings of the Institution of Mechanical Engineers. Part F, Journal of Rail and Rapid Transit*. vol. 230, pp. 323-334.
5. Ringsberg J. W., (2001): Life prediction of rolling contact fatigue crack initiation. *International Journal of Fatigue*, vol 23, pp. 575-586.
6. Ekberg A., Kabo E., (2004): Fatigue of railway wheels and rails under rolling contact and thermal loading –An overview. *Wear*, vol. 258, pp. 1288-1300.
7. Karttunen K.,(2015): Influence of rail, wheel and track geometries on wheel and rail degradation. Ph.D Thesis. Chalmers University of Technology, Gothenburg, Sweden, pp. 8-12.
8. Deuce R., (2007): *Wheel tread damage – An elementary guide*. Bombardier Transportation, pp. 8-28.
9. Nielsen J. C. O., Pieringer A., Thompson D. J., Torstensson P. T., (2019): Wheel-rail impact loads, noise and vibration: A review of excitation mechanisms, prediction methods and mitigation measures, to be presented at the 13th International Workshop on Railway Noise, Ghent, Belgium, 40 p.
10. Railway group KTH (2014): *Rail Vehicle Dynamics*, KTH Vetenskap och Konst, Stockholm, Sweden, pp. 9-1–10-6.
11. Asplund M., (2016): Wayside condition monitoring system for railway wheel profiles: Applications and performance assessment, Ph.D Thesis. Luleå University of Technology, Sweden, p. 18.
12. Iwnicki S. (editor), (2009): *Wheel-rail interface handbook*, CRC Press, Woodheard Publishing Limited, Cambridge, UK, p. 172.
13. Asplund M., (2018): Provkörning med hjulskada över hjulskdedetektor. Technical report, Trafikverket, 18 p.
14. On Track Technology. Section Products: *Wheel Impact Detector*. Online documentation available at: http://binary-technology.com/products/wimwim/, accessed 2019-3-3.
15. Montgomery D. C., Peck E. A., Vining G. G., (2012): Introduction to linear regression analysis. John Wiley & Sons, Hoboken, New Jersey, 385 p.
16. Mathworks, Online documentation available at: https://se.mathworks.com/help/stats/fitlm.html, accessed 2019-03-13.

17. Rice J. A., (2007): Mathematical statistics and data analysis. Books/cole, Belmot, USA, pp. 329-336.
18. Cornell J. A., Berger R. D., (1987): Factors that influence the value of the coefficient of determination in simple linear and nonlinear regression models. *Florida Agricultural Experiment Stations Journal Series*, Paper 6709, pp. 63-68.
19. ABAQUS. Getting Started with ABAQUS: Interactive Edition, version 6.14, Dassault Systèmes Simulia Corp., Providence, USA, 2014.
20. ABAQUS. Abaqus Analysis User's guide: Abaqus/CAE execution. Version 6.14, Dassault Systèmes Simulia Corp., Providence, USA, 2014.
21. ABAQUS. Abaqus Scripting User's Manual: Abaqus/CAE and the Abaqus Scripting Interface. Version 6.10, Dassault Systèmes Simulia Corp., Providence, USA, 2014.
22. Chaar N., (2002): Structural flexibility models of wheelsets for rail vehicle dynamics analysis-A pilot study. Report, Kungl Tekniska Högskolan, Stockholm, Sweden, pp. 1-12.
23. Chaar N., (2007): Wheelset Structural flexibility and track flexibility in vehicle-track dynamic interaction. PhD Thesis. Royal Institute of Technology (KTH), Stockholm, Sweden, pp. A1-A10.
24. Raduta A., Locovei C., Nicoara M., Cucuruz L. R., (2010): On the influence of residual stresses on fatigue fracture of railway axles. *WSEAS Transactions on Applied and Theoretical Mechanics*, vol. 5, p. 199.
25. Andersson C., Johansson A., (2004): Prediction of rail corrugation generated by three dimensional wheel-rail interaction. *Wear*, vol. 257, pp. 423-434.
26. Zonca P., Frigerio M., (2010): Flexible wheeset-track model for numerical estimation of stresses in railway axles. MSc Thesis. Politecnico di Milano, Milano, Italy , pp. 32 -40.
27. Beretta S., Carboni M., Cervello S., (2011): Design review of a freight railway axle: Fatigue damage versus damage tolerance. *Materialwissenschaft und Werkstofftechnik*, vol. 42, p. 1099.
28. Meggiolaro M. A., Pinho de Castro J. T., Wu H., (2015): Invariant-based and critical-plane rainflow approaches for fatigue life prediction under multiaxial variable amplitude loading. *Procedia Engineering*, vol. 101, pp. 69-76.
29. Ion D., Lorand K., Mircea D., Karoly M., (2011): The equivalent stress concept in multiaxial fatigue. *Journal of Engineering Studies and Research*, vol. 17, p. 53.
30. Olofsson N., (2010): Design of experimentts for validation of multiaxial high cycle fatigue criteria. MSc Thesis, Chalmers University of Technology, Gothenburg, Sweden, pp. 8-10.
31. Rechnerischer Festigkeitsnachweis für Machinenbauteile. VDMA-Verlag, 6th edition, 2012.
32. Swedish Standards Institute, (2010): *Railway applications – Wheelsets and bogies – Non powered axles – Design method*. Svensk Standard SS-EN 13103:2009+A1:2010.
33. Asplund M., Palo M., Famurewa S., Rantatalo M., (2014): A study of railway wheel profile parameters used as indicators of an increased risk of wheel defects. *Proceedings of the Institution of Mechanical Engineers, Journal of Rail and Rapid Transit*, vol. 230, pp. 323-334.

Appendix A

As anticipated in Section 3.2, a Matlab code was written to analyse the data registered by WILDs. A detailed description of the Matlab code is reported in this appendix.

A1 General description of the Matlab Code

The Matlab Code consists of several functions and a main body which allows to display pictures and save parameters of interest related to the statistical analysis described in Section 3.3 and Section 3.4. In this section, a description of all functions that have been implemented is presented:

- *import*: this function allows to import data from Excel Format file to Matlab. This function has been implemented in such a way to exclude data detected at Mellansjö USP MJ MDS and Mellansjö NSP HJ MDS detector stations and data registered for low train speed, whose reasons have been mentioned in Section 3.2.1.

  It takes as input the name of Excel file and the rows including the data, whereas it returns the following outputs:

  i. *num_data*: matrix made of seven columns corresponding respectively to train speed, mean load on the left wheel, mean load on the right wheel, peak impact load on the left wheel, peak impact load on the right wheel, dynamic impact load on the left wheel, dynamic impact load on the right wheel.

  ii. *text_data*: cell array containing three columns corresponding respectively to time instants at which data have been registered, detector station name and travelling direction of the locomotive.

  iii. *raw_data*: cell array including both *text_data* and *num_data*.

  iv. *time*: datetime vector containing the time instants at which data have been registered.

- *name*: this function allows to save the name of the different detector stations appearing in the first column of *text_data* in a string vector. It takes as input *text_data*, whereas it returns as output *NameDetectorStation.*

- *data_station*: this function allows to save data and time instants at which they have been registered for each detector station in a cell array. It takes as inputs *NameDetectorStation*, *text_data*, *num_data*, *time*, whereas it returns the following outputs:

  i. *time_stat*: cell array containing time instants at which data have been measured for each detector station;

  ii. *index*: index position in *text_data* of data related to each detector station

  iii. *data*: cell array containing numerical data for each detector station.

- *index_for_speed*: this function allows to store indices corresponding to data detected within three different speed ranges. This function takes as inputs *NameDetectorStation*, *data*, and *time.* It returns two output parameters:

  i. *index_speed*: is a cell array including the indices defining the data detected for each station and within three specified speed ranges;

ii. *overall_index_speed*: is a cell array including the indices defining the data detected within three specified speed ranges.

- *Plot_dyn:* this function allows to plot the dynamic impact loads over time. The scattered distribution is showed for three different speed ranges. It takes as input parameters *time*, *num_data*, *overall_index_speed*, *Axlenumber*.

A2 Matlab Code

```
                                        %FUNCTION IMPORT
1   function [num_data,text_data,raw_data,time]=import(excelFile,raws)
2   [num_data,text_data,raw_data] = xlsread(excelFile,1,raws);
3   %In each excel file there is one empty column between column 'time'
4   %and column 'detector station'.
5   %Goal: delete it.
6   text_data=[text_data(:,1) text_data(:,3) text_data(:,4)];
7   %Delete data corresponding to stations Mellansjö_USP_HJ_MDS & Mellansjö_NSP_HJ_MDS
8   index=find(text_data(:,2)~="Mellansjö_USP_HJ_MDS" &
9   text_data(:,2)~="Mellansjö_NSP_HJ_MDS");
10  text_data = [text_data(index,1) text_data(index,2) text_data(index,3)];
11  Dynamic_load_L=num_data(:,3)-num_data(:,2);
12  Dynamic_load_R=num_data(:,5)-num_data(:,4);
13  num_data=[num_data Dynamic_load_L Dynamic_load_R];
14  num_data=[num_data(index,1) num_data(index,2) num_data(index,3) num_data(index,4)
15  num_data(index,5) num_data(index,6) num_data(index,7)];
16  %Delete data corresponding to a train speed lower than 40km/h
17  index=find(num_data(:,1)>=40);
18  text_data = [text_data(index,1) text_data(index,2) text_data(index,3)];
19  num_data=[num_data(index,1) num_data(index,2) num_data(index,3) num_data(index,4)
20  num_data(index,5) num_data(index,6) num_data(index,7)];
21  %Extract time instants data
22  time = cellfun(@datenum,text_data(:,1));
23  time=datetime(time,'ConvertFrom','datenum');
24  end

                                        %FUNCTION name
25  function [nameDetectorStation]=name(text_data)
26  nameDetectorStation=unique(text_data(:,2));
27  end

                                        %FUNCTION data_station
28  function [time_stat index  data] = data_station(NameDetectorStation,text_data,num_data,time)
29  %1-Save the index corresponding to each detector station in a cell array
30  %2-Save the data corresponding to each station
31  %3-Save time data for each station
32  for j=1:7
33  for i=1:length(NameDetectorStation)
34   index{i} = {DetectorStation(NameDetectorStation(i),text_data)};
35   data{i,j} = num_data(index{1,i}{1,1},j);
36   time_stat{i} = time(index{1,i}{1,1});
37  end
38  end
39  end

                                        %FUNCTION index_for_speed
40  function [index_speed,overall_index_speed] = index_for_speed(NameDetectorStation,data,num_data)
    % set the speed intervals:
    % first interval: 40 km/h - 80 km/h
    % Second interval: 80 km/h - 100 km/h
    % Third interval: 100 km/h - 145 km/h
41  for i = 1:length(NameDetectorStation)
```

```
42  overall_index_speed{1} = find(num_data(:,1)>=40 & num_data(:,1)<=79.5);
43  index_speed{i,1} = find(data{i,1}>=40 & data{i,1}<=79.5);
44  overall_index_speed{2} = find(num_data(:,1)>=80 & num_data(:,1)<=99.5);
45  index_speed{i,2} = find(data{i,1}>=80 & data{i,1}<=99.5);
46  overall_index_speed{3} = find(num_data(:,1)>=100 & num_data(:,1)<=145);
47  index_speed{i,3} = find(data{i,1}>=100 & data{i,1}<=145);
48  end

                                        %FUNCTION Plot_dyn
49  function  Plot_dyn(time, num_data,overall_index_speed,AxleNumber)

50  Max_L=max(num_data(:,6));
51  Max_R=max(num_data(:,7));
52  Max=max(Max_L,Max_R);
53  Min_L=min(num_data(:,6));
54  Min_R=min(num_data(:,7));
55  Min=min(Min_L,Min_R);

56  subplot(1,2,1)
57  scatter(time(overall_index_speed{1,1}),num_data(overall_index_speed{1,1},6),'r','s')
58  hold on
59  scatter(time(overall_index_speed{1,2}),num_data(overall_index_speed{1,2},6),'k','*')
60  hold on
61  scatter(time(overall_index_speed{1,3}),num_data(overall_index_speed{1,3},6),'b')
62  grid on
63  grid minor
64  title({sprintf('Axle %d',AxleNumber)})
65  ylabel('Dynamic load on the left wheel [kN]')
66  legend('Speed range: 40-80km/h','Speed range: 80-100km/h','Speed range: 100-145km/h')
67  ylim([Min Max])

68  subplot(1,2,2)
69  scatter(time(overall_index_speed{1,1}),num_data(overall_index_speed{1,1},7),'r','s')
70  hold on
71  scatter(time(overall_index_speed{1,2}),num_data(overall_index_speed{1,2},7),'k','*')
72  hold on
73  scatter(time(overall_index_speed{1,3}),num_data(overall_index_speed{1,3},7),'b')
74  grid on
75  grid minor
76  title({sprintf('Axle %d',AxleNumber)})
77  ylabel('Dynamic load on the right wheel [kN]')
78  legend('Speed range: 40-80km/h','Speed range: 80-100km/h','Speed range: 100-145km/h')
79  ylim([Min Max])
80  end

                                        %MAIN BODY
    %% AXLE 1
81  clc
82  clear all
83  AxleNumber=1;
    % NOTATION: name_X: X stands for the axle being considered
84  [num_data_1,text_data_1,raw_data_1,time_1] = import('Ax 1','B8:J907');
85  NameDetectorStation_1 = name(text_data_1);
86  NameDetectorStation_1 = string(NameDetectorStation_1);
87  [time_stat_1 index_1  data_1] =
88  data_station(NameDetectorStation_1,text_data_1,num_data_1,time_1);
89  year=2018;

    %PLOT DYNAMIC LOADS OVER TIME
```

```
[index_speed_1,overall_index_speed_1]=
index_for_speed(NameDetectorStation_1,data_1,num_data_1);
figure()
hold on
Plot_dyn(time_1, num_data_1,overall_index_speed_1,AxleNumber)
figure()

                    %% MEAN LOADS AS A FUNCTION OF THE TRAIN SPEED
t_start = datetime(year,3,18,0,0,0);
 t_end = datetime(year+1,1,29,0,0,0);
 discriminating_limit=30;
for i=1:length(NameDetectorStation_1)
    if length(data_1{i,6})>100
    time_stat_1{1,i}=time_stat_1{1,i}(find((time_stat_1{1,i}>t_start) & (time_stat_1{1,i} < t_end)));
        for j=1:7
    data_1{i,j}=data_1{i,j}(find((time_stat_1{1,i}>t_start) & (time_stat_1{1,i} < t_end)));
        end
    end
end
for i=1:length(NameDetectorStation_1)
    if length(data_1{i,1})>discriminating_limit

%SET Y-AXIS LIMITS
Average_L = mean(data_1{i,2})
Min_L=min(data_1{i,2})
Max_L=max(data_1{i,2})
Average_R = mean(data_1{i,4})
Min_R=min(data_1{i,4})
Max_R=max(data_1{i,4})
Min=min(Min_R,Min_L);
Max=max(Max_R,Max_L);

mdl_L = fitlm(data_1{i,1},data_1{i,2})
subplot(1,2,1)
plot(mdl_L)
grid on
grid minor
AxleNumber=1;
title({sprintf('Axle %d',AxleNumber),'March 2018 - January 2019',sprintf('Detector Station:
%s',NameDetectorStation_1(i))})
xlabel('Train Speed [km/h]')
ylabel('Mean load on the left wheel [kN]')
legend('Observed data','Fitted linear model')
ylim([Min Max])
mdl_R = fitlm(data_1{i,1},data_1{i,4})
subplot(1,2,2)
plot(mdl_R)
grid on
grid minor
AxleNumber=1;
title({sprintf('Axle %d',AxleNumber),'March 2018 - January 2019',sprintf('Detector Station:
%s',NameDetectorStation_1(i))})
xlabel('Train Speed [km/h]')
ylabel('Mean Load on the right wheel [kN]')
legend('Observed data','Linear Regression')
ylim([Min Max])
figure()
subplot(2,3,1)
plotResiduals(mdl_L,'fitted','ResidualType','studentized')
xlabel('Fitted values','FontSize',18)
ylabel('Residuals','FontSize',18)
```

```
146     subplot(2,3,4)
147     plotResiduals(mdl_R,'fitted','ResidualType','studentized')
148     xlabel('Fitted values','FontSize',18)
149     ylabel('Residuals','FontSize',18)
150     subplot(2,3,2)
151     plotResiduals(mdl_L,'probability','ResidualType','studentized')
152     xlabel('Residuals','FontSize',18)
153     ylabel('Probability','FontSize',18)
154     subplot(2,3,5)
155     plotResiduals(mdl_R,'probability','ResidualType','studentized')
156     xlabel('Residuals','FontSize',18)
157     ylabel('Probability','FontSize',18)
158     if i~=length(NameDetectorStation_1)
159                 figure()
160        else
161        end
162        end
163     end

            %% DYNAMIC IMPACT LOADS AS A FUNCTION OF THE TRAIN SPEED AND TIME
164     t_start = datetime(year,10,18,0,0,0);
165     t_end = datetime(year,12,18,0,0,0);

166     for i=1:length(NameDetectorStation_1)
167     if length(time_stat_1{1,i}(find((time_stat_1{1,i}>t_start) & (time_stat_1{1,i} < t_end))))>5

168     x=time_stat_1{1,i}(find((time_stat_1{1,i}>t_start) & (time_stat_1{1,i} < t_end)));
169     x1=datenum(time_stat_1{1,i}(find((time_stat_1{1,i}>t_start) & (time_stat_1{1,i} < t_end))));
170     x2=data_1{i,1}(find((time_stat_1{1,i}>t_start) & (time_stat_1{1,i} < t_end)));
171     y=data_1{i,7}(find((time_stat_1{1,i}>t_start) & (time_stat_1{1,i} < t_end)));

172     X=[ones(size(x1)) x1 x2];
173     [b,bint,r,rint,stats]=regress(y,X);
174     scatter3(x,x2,y,'filled')
175     XX = [x1 x2];
176     mdl = fitlm(XX,y)
177     residuals{i} = mdl.RMSE.^2;
178     R_adjusted{i} = mdl.Rsquared.Adjusted;
179     anova(mdl,'summary')
180     PRESS{i} = sum((table2array(mdl.Residuals(:,3))./(1-diag(mdl.Diagnostics.HatMatrix))).^2);
181     hold on
182     x1fit = min(x1):1:max(x1);
183     x2fit = min(x2):1:max(x2);
184     [X1FIT,X2FIT] = meshgrid(x1fit,x2fit);
185     YFIT = b(1)  + b(2)*X1FIT + b(3)*X2FIT;
186     mesh(datetime(X1FIT,'ConvertFrom','datenum'),X2FIT,YFIT)
187     ylabel('Train speed [km/h]','FontSize',13)
188     zlabel('Dynamic load [kN]','FontSize',13)
189     title({sprintf('Axle %d',AxleNumber),'October 18th - December 18th',sprintf('Detector Station:
190     %s',NameDetectorStation_1(i))})
191     figure()
192     subplot(1,2,1)
193     plotResiduals(mdl,'probability','ResidualType','studentized')
194     subplot(1,2,2)
195     plotResiduals(mdl,'fitted','ResidualType','Raw')
196     ylabel('Residuals','FontSize',16)
197     xlabel('Fitted values','FontSize',16)
198     title('Plot of residuals vs. fitted values','FontSize',16)
199     if i~=length(NameDetectorStation_1)
200                 figure()
201        else
```

```
202         end
203     end
204     end
```

Appendix B

Supplementary information about what has been proposed in this thesis project may be found in this appendix.

B1 Complementary information to Section 3.3

Supplementary graphs to the analysis proposed in Section 3.3 are hereunder reported. More specifically, diagrams showing the simple linear fitted model involving train speed and mean wheel loads are reported. Additionally, for each linear model are presented plots of studentized residual against fitted values and normal probability plots of the residuals.
Additional figures helping the readability and the checking of information provided in Table 3.1.

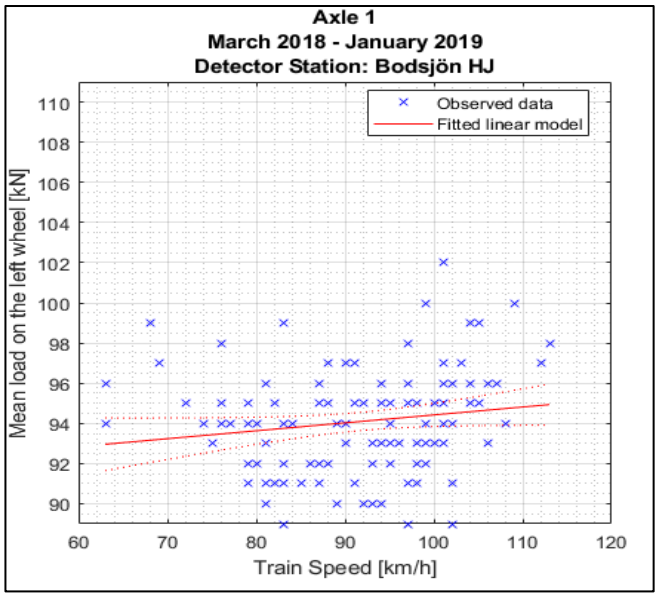

*Figure B1.1: Simple linear regression model between train speed and mean wheel loads detected for the **left** wheel of the first axle of locomotive **917400014341** between March 18th 2018 and January 29th 2019 at **Bodsjön** detector station.*

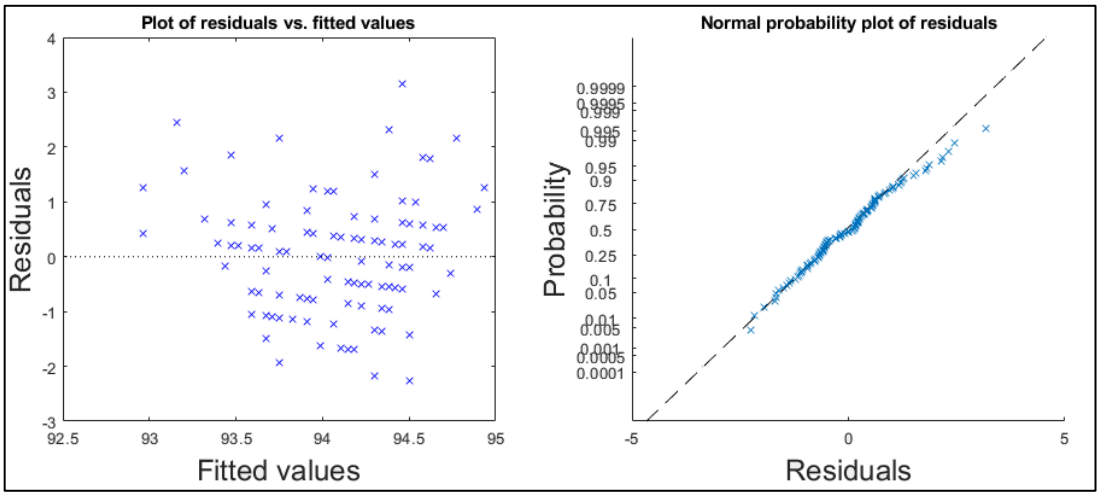

Figure B1.2: Plot of studentized residuals versus fitted values (on the left) and probability plot (on the right) derived from the simple linear regression model between train speed and mean wheel loads

*detected for the **left** wheel of the first axle of locomotive **917400014341** between March 18th 2018 and January 29th 2019 at **Bodsjön** detector station.*

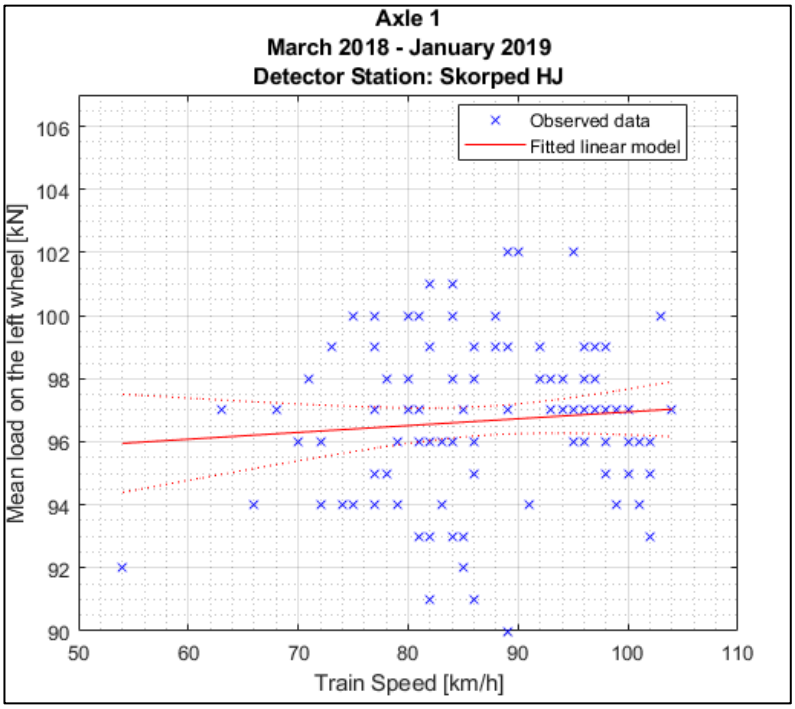

*Figure B1.3: Simple linear regression model between train speed and mean wheel loads detected for the **left** wheel of the first axle of locomotive **917400014341** between March 18th 2018 and January 29th 2019 at **Skorped** detector station.*

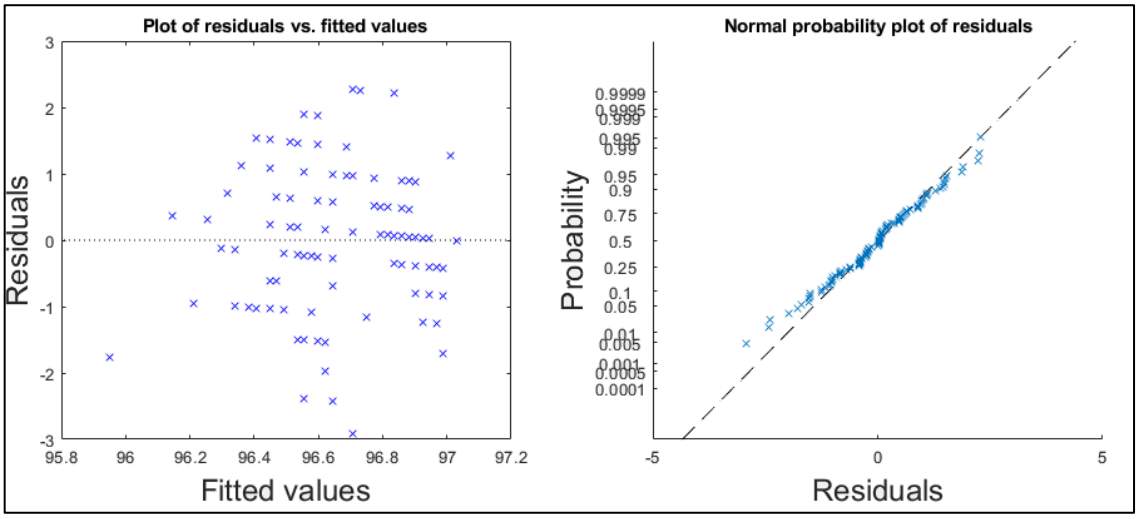

*Figure B1.4: Plot of studentized residuals versus fitted values (on the left) and probability plot (on the right) derived from the simple linear regression model between train speed and mean wheel loads detected for the **left** wheel of the first axle of locomotive **917400014341** between March 18th 2018 and January 29th 2019 at **Skorped** detector station.*

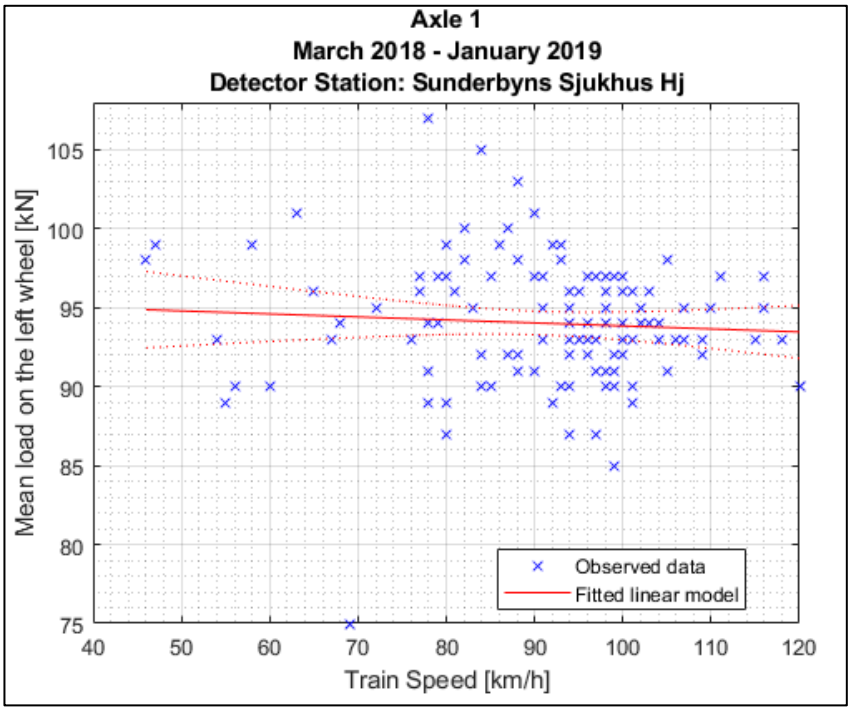

*Figure B1.5: Simple linear regression model between train speed and mean wheel loads detected for the **left** wheel of the first axle of locomotive **917400014341** between March 18th 2018 and January 29th 2019 at **Sunderbyns Sjukhus** detector station.*

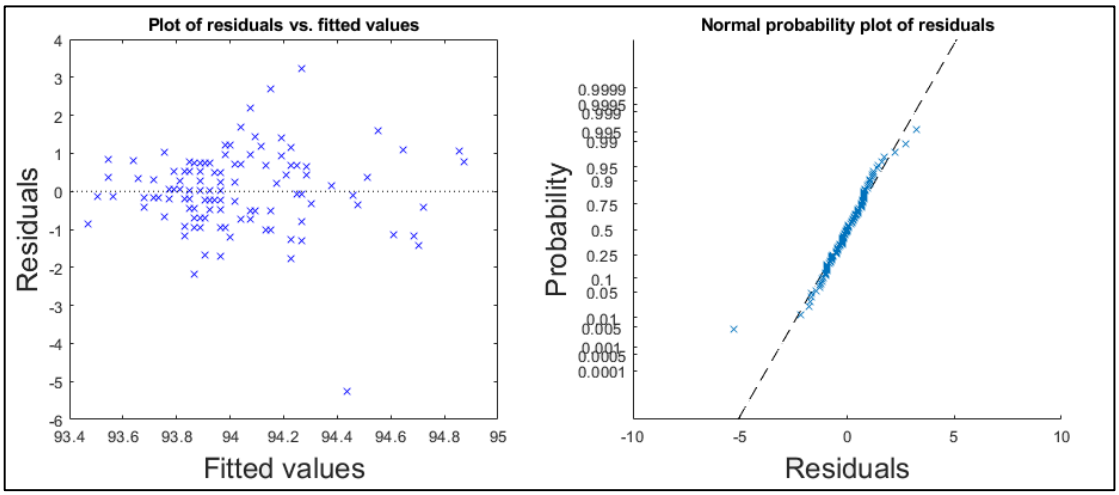

*Figure B1.6: Plot of studentized residuals versus fitted values (on the left) and probability plot (on the right) derived from the simple linear regression model between train speed and mean wheel loads detected for the **left** wheel of the first axle of locomotive **917400014341** between March 18th 2018 and January 29th 2019 at **Sunderbyns Sjukhus** detector station.*

Additional figures helping the readability and the checking of information provided in Table 3.2.

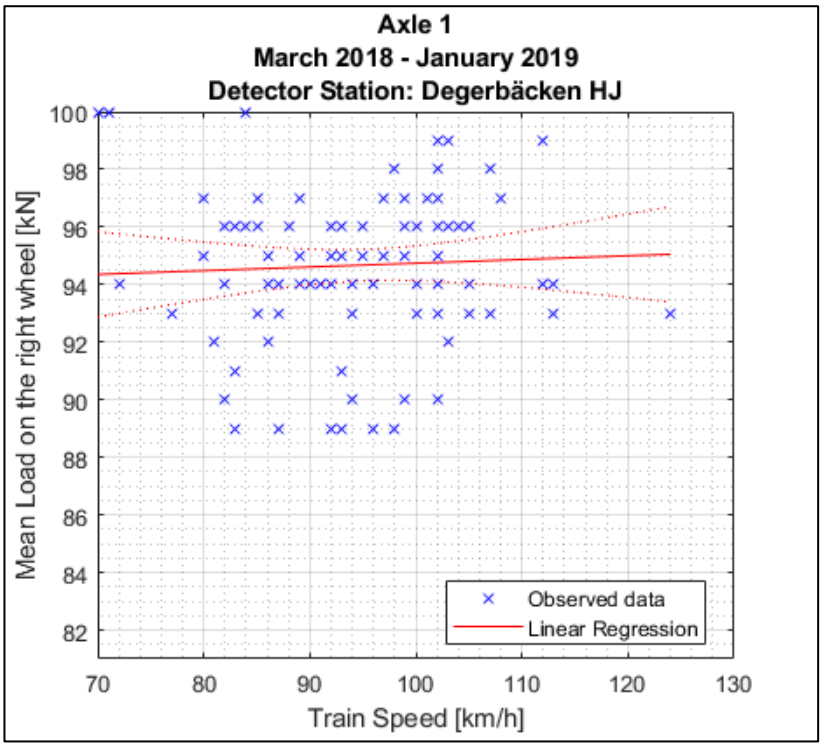

*Figure B1.7: Simple linear regression model between train speed and mean wheel loads detected for the **right** wheel of the first axle of locomotive **917400014341** between March 18th 2018 and January 29th 2019 at **Degerbäcken** detector station.*

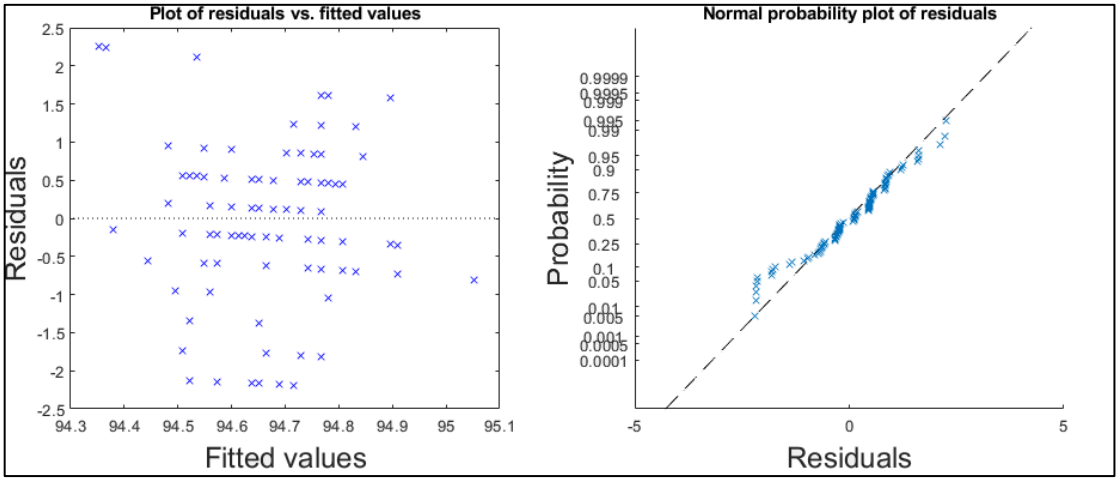

*Figure B1.8: Plot of studentized residuals versus fitted values (on the left) and probability plot (on the right) derived from the simple linear regression model between train speed and mean wheel loads detected for the **right** wheel of the first axle of locomotive **917400014341** between March 18th 2018 and January 29th 2019 at **Degerbäcken** detector station.*

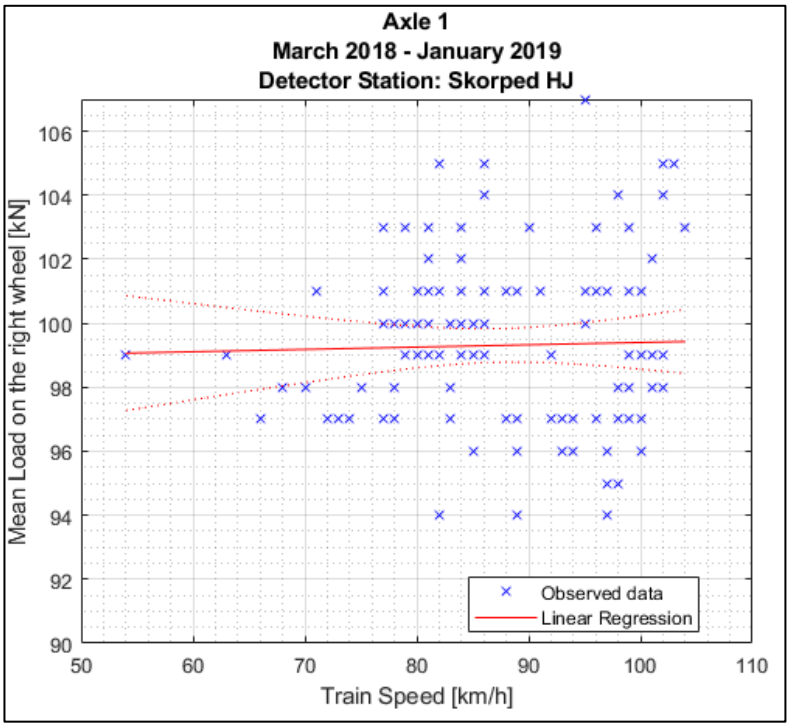

*Figure B1.9: Simple linear regression model between train speed and mean wheel loads detected for the **right** wheel of the first axle of locomotive **917400014341** between March 18th 2018 and January 29th 2019 at **Skorped** detector station.*

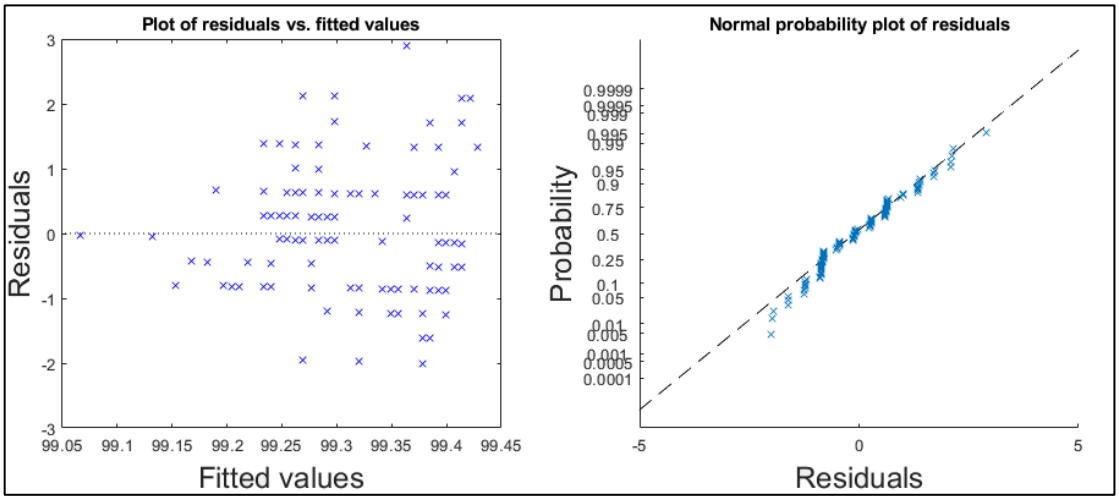

*Figure B1.10: Plot of studentized residuals versus fitted values (on the left) and probability plot (on the right) derived from the simple linear regression model between train speed and mean wheel loads detected for the **right** wheel of the first axle of locomotive **917400014341** between March 18th 2018 and January 29th 2019 at **Skorped** detector station.*

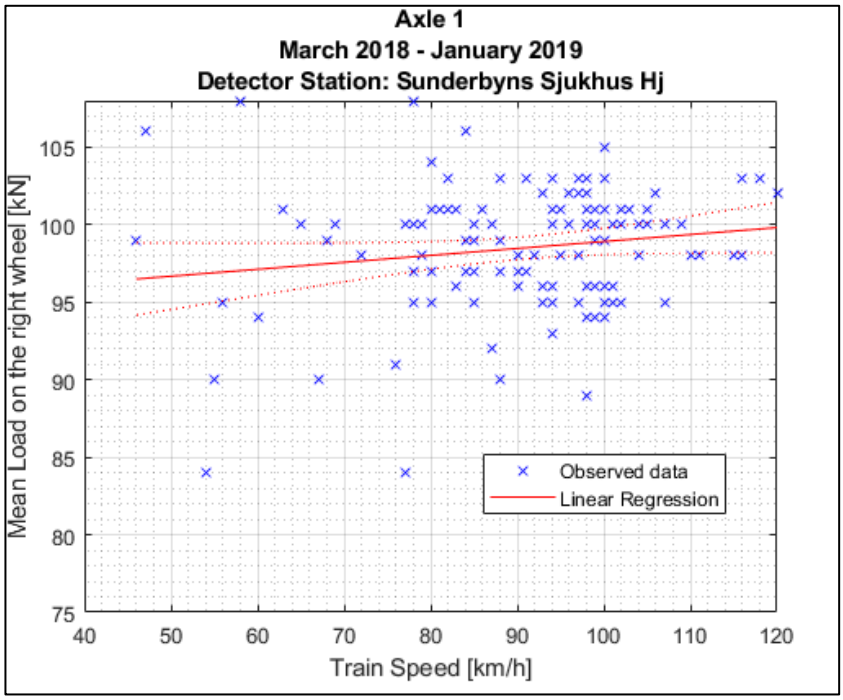

*Figure B1.11: Simple linear regression model between train speed and mean wheel loads detected for the **right** wheel of the first axle of locomotive **917400014341** between March 18th 2018 and January 29th 2019 at **Sunderbyns Sjukhus** detector station.*

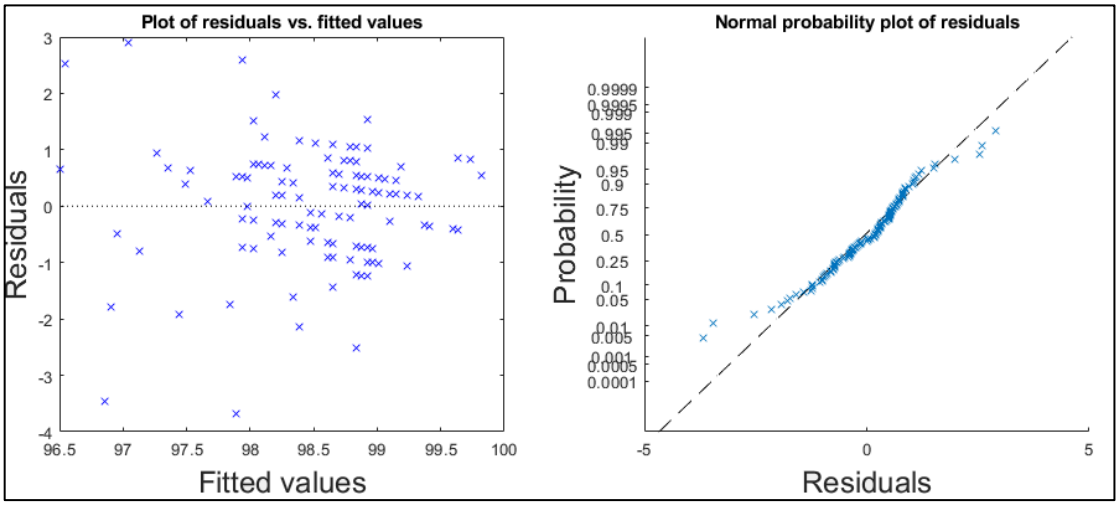

*Figure B1.12: Plot of studentized residuals versus fitted values (on the left) and probability plot (on the right) derived from the simple linear regression model between train speed and mean wheel loads detected for the **right** wheel of the first axle of locomotive **917400014341** between March 18th 2018 and January 29th 2019 at **Sunderbyns Sjukhus** detector station.*

Additional figures helping the readability and the checking of information provided in Table 3.3.

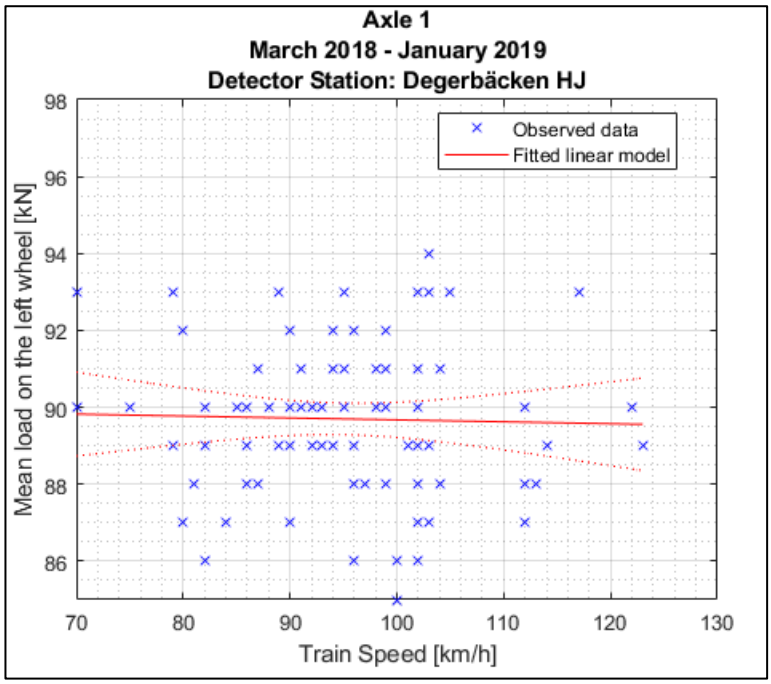

*Figure B1.13: Simple linear regression model between train speed and mean wheel loads detected for the **left** wheel of the first axle of locomotive **917400014234** between March 18th 2018 and January 29th 2019 at **Degerbäcken** detector station.*

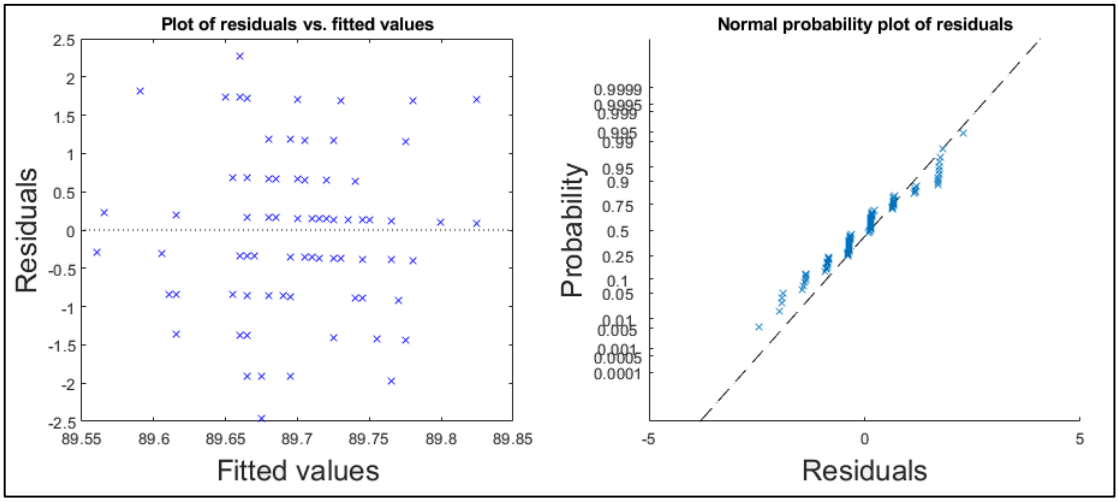

*Figure B1.14: Plot of studentized residuals versus fitted values (on the left) and probability plot (on the right) derived from the simple linear regression model between train speed and mean wheel loads detected for the **left** wheel of the first axle of locomotive **917400014234** between March 18th 2018 and January 29th 2019 at **Degerbäcken** detector station.*

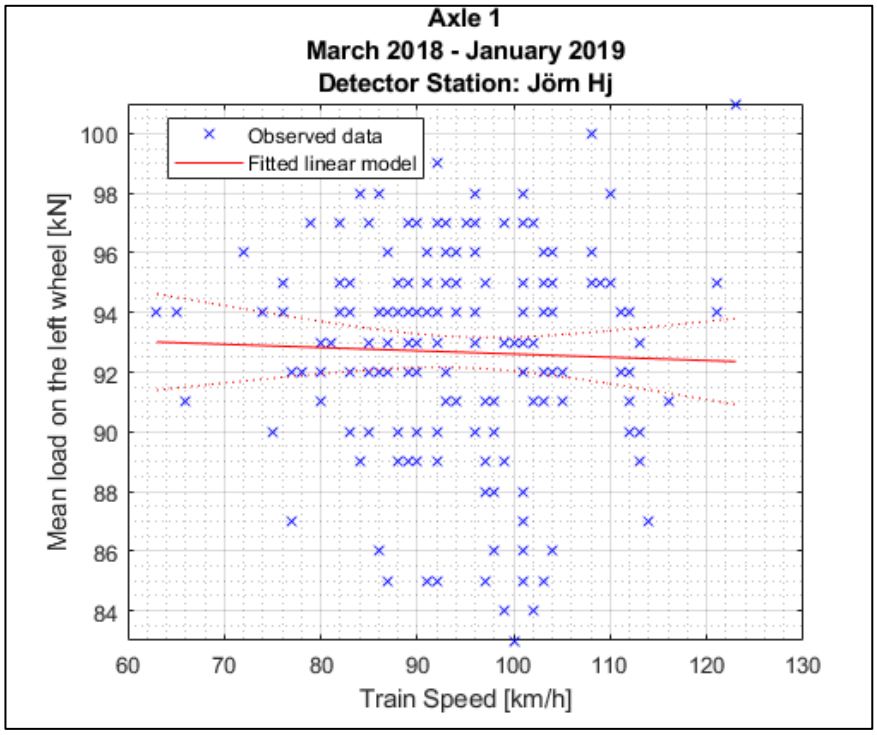

*Figure B1.15: Simple linear regression model between train speed and mean wheel loads detected for the **left** wheel of the first axle of locomotive **917400014234** between March 18th 2018 and January 29th 2019 at **Jörn** detector station.*

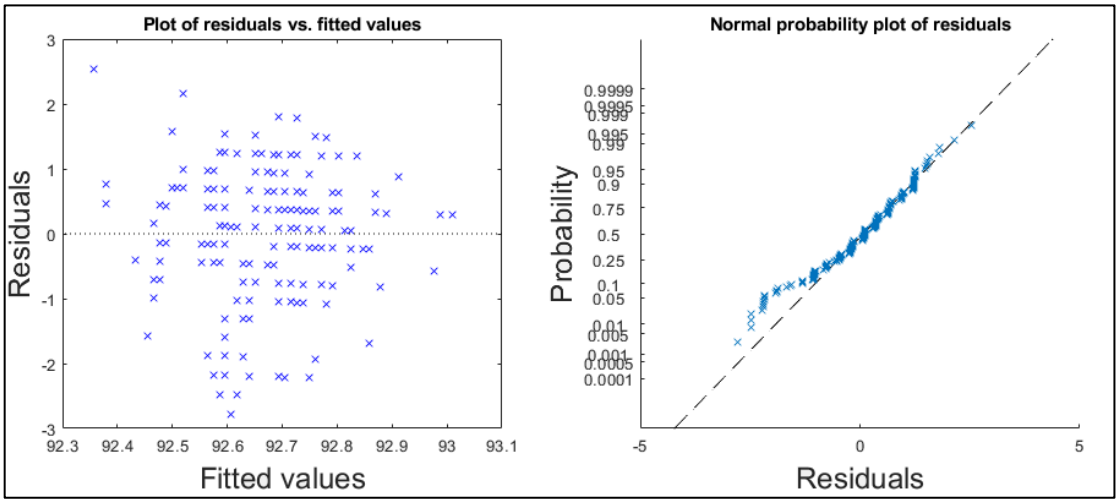

*Figure B1.16: Plot of studentized residuals versus fitted values (on the left) and probability plot (on the right) derived from the simple linear regression model between train speed and mean wheel loads detected for the **left** wheel of the first axle of locomotive **917400014234** between March 18th 2018 and January 29th 2019 at **Jörn** detector station.*

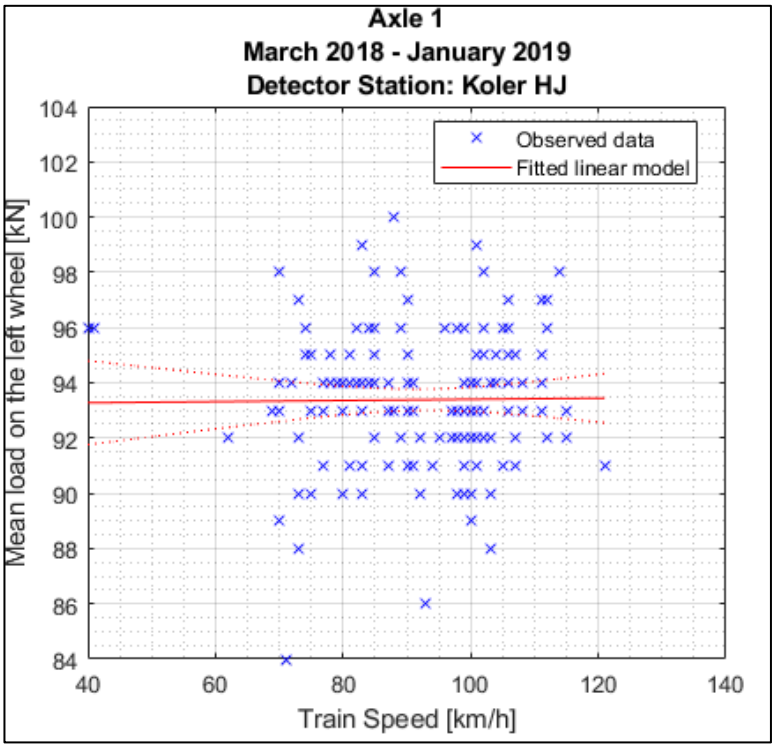

*Figure B1.17: Simple linear regression model between train speed and mean wheel loads detected for the **left** wheel of the first axle of locomotive **917400014234** between March 18th 2018 and January 29th 2019 at **Koler** detector station.*

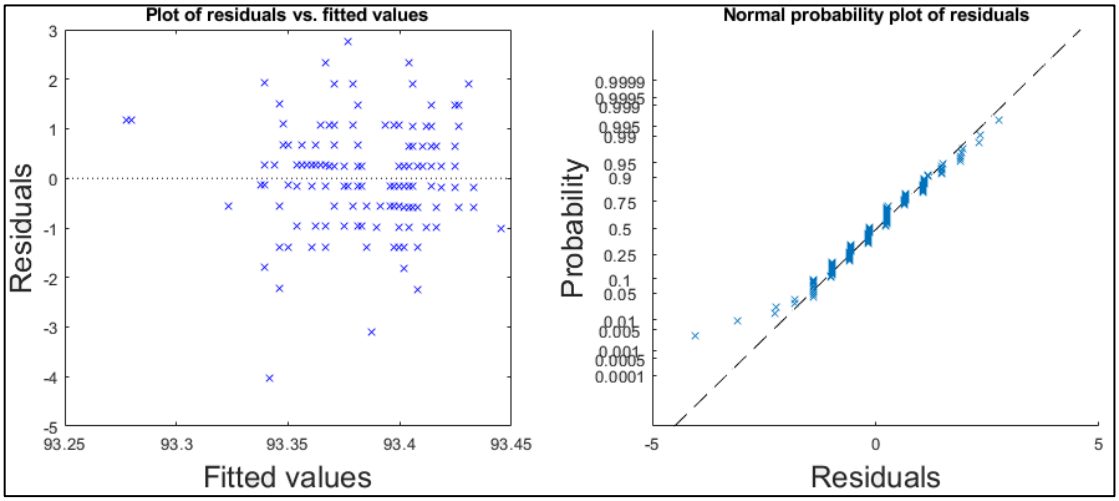

*Figure B1.18: Plot of studentized residuals versus fitted values (on the left) and probability plot (on the right) derived from the simple linear regression model between train speed and mean wheel loads detected for the **left** wheel of the first axle of locomotive **917400014234** between March 18th 2018 and January 29th 2019 at **Koler** detector station.*

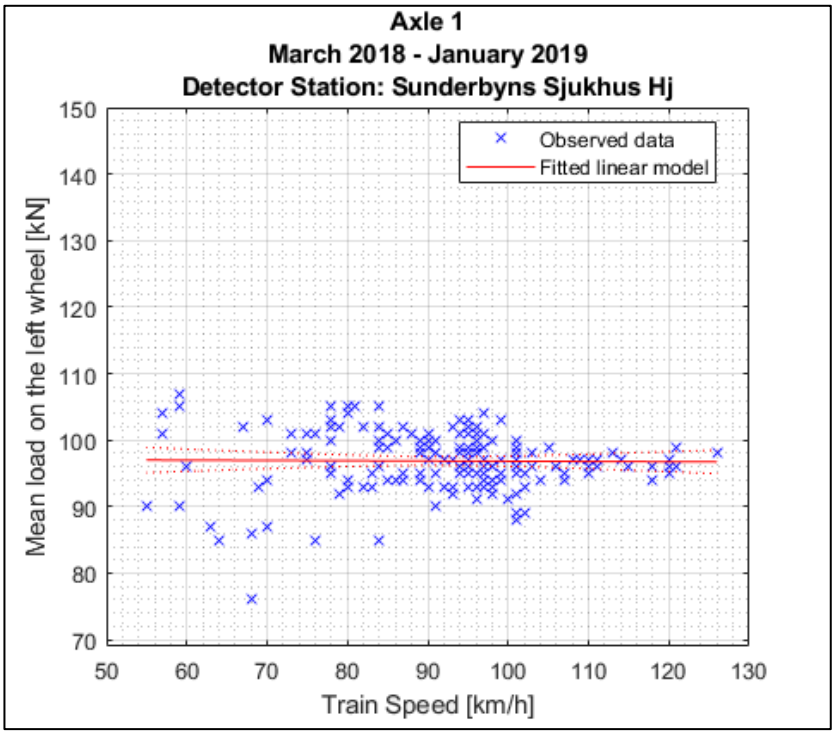

*Figure B1.19: Simple linear regression model between train speed and mean wheel loads detected for the **left** wheel of the first axle of locomotive **917400014234** between March 18th 2018 and January 29th 2019 at **Sunderbyns Sjukhus** detector station.*

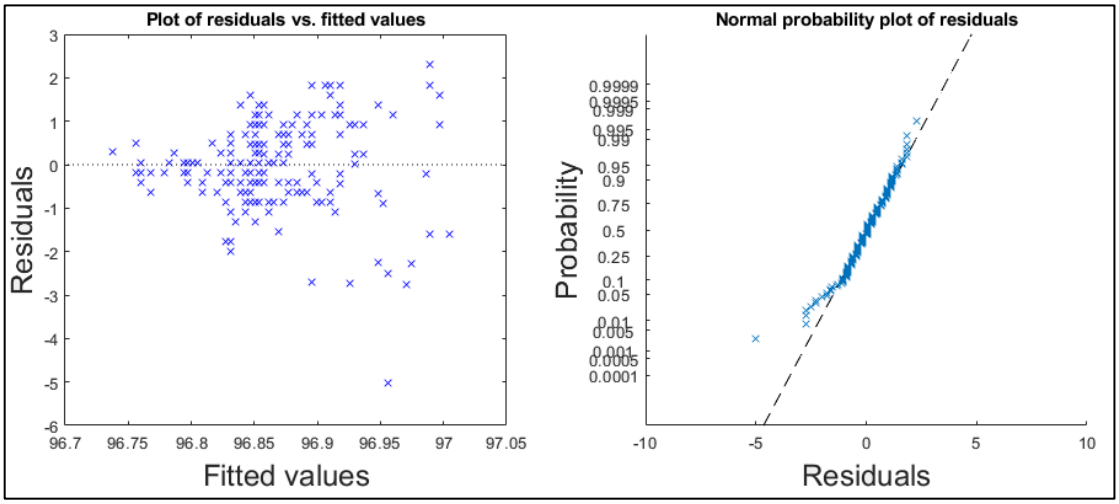

*Figure B1.20: Plot of studentized residuals versus fitted values (on the left) and probability plot (on the right) derived from the simple linear regression model between train speed and mean wheel loads detected for the **left** wheel of the first axle of locomotive **917400014234** between March 18th 2018 and January 29th 2019 at **Koler** detector station.*

Additional figures helping the readability and the checking of information provided in Table 3.4.

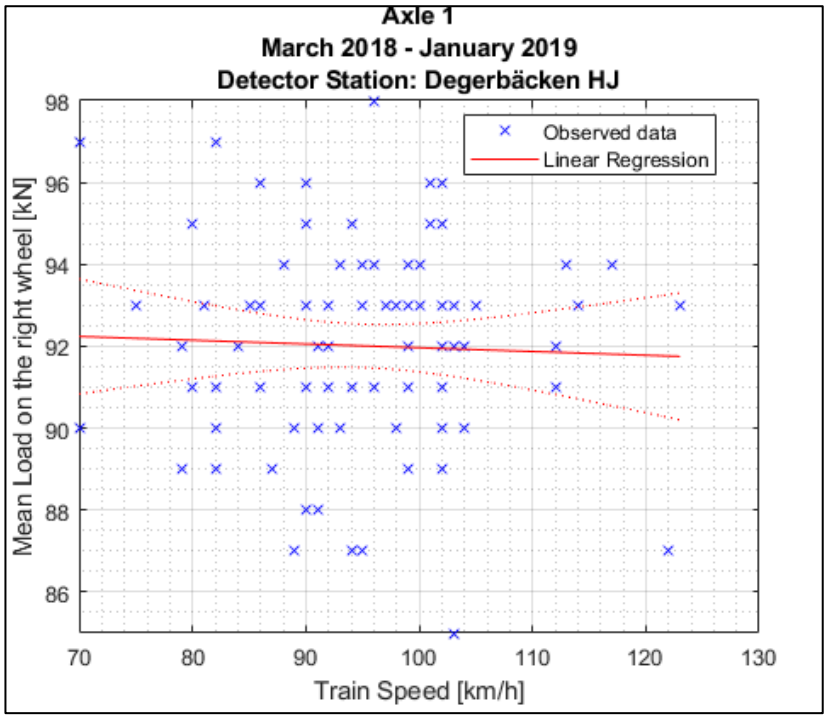

*Figure B1.21: Simple linear regression model between train speed and mean wheel loads detected for the **right** wheel of the first axle of locomotive **917400014234** between March 18th 2018 and January 29th 2019 at **Degerbäcken** detector station.*

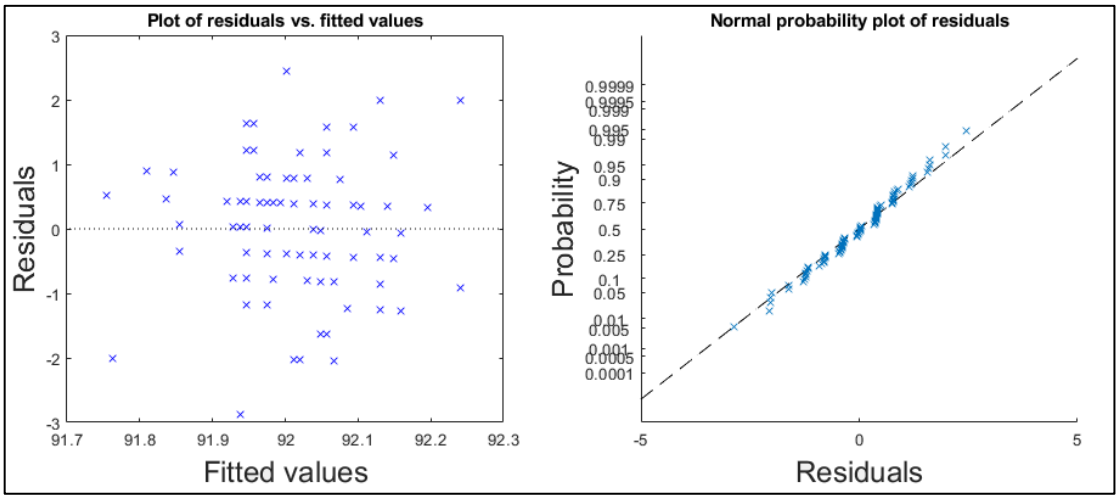

*Figure B1.22: Plot of studentized residuals versus fitted values (on the left) and probability plot (on the right) derived from the simple linear regression model between train speed and mean wheel loads detected for the **right** wheel of the first axle of locomotive **917400014234** between March 18th 2018 and January 29th 2019 at **Degerbäcken** detector station.*

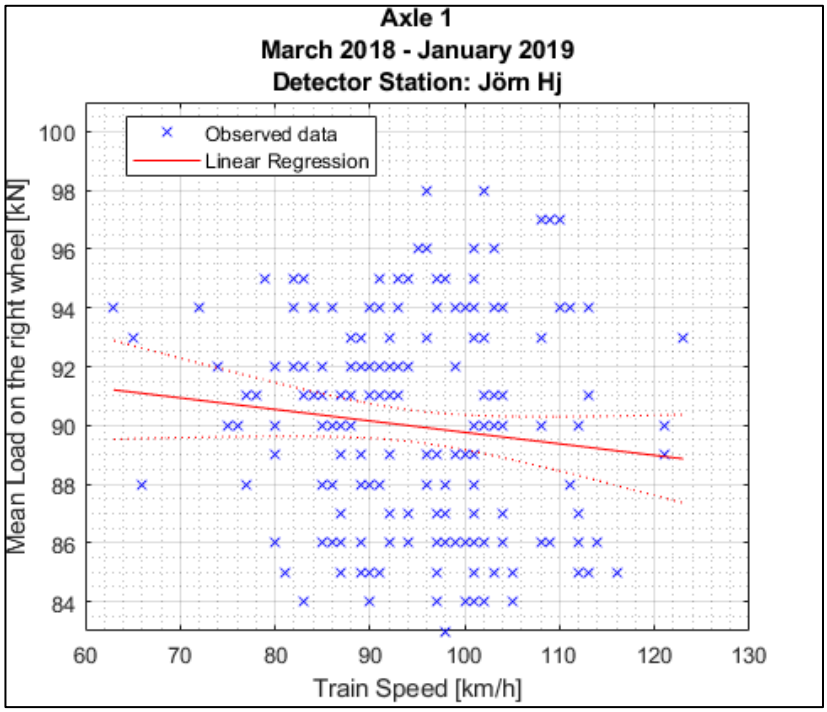

*Figure B1.23: Simple linear regression model between train speed and mean wheel loads detected for the **right** wheel of the first axle of locomotive **917400014234** between March 18th 2018 and January 29th 2019 at **Jörn** detector station.*

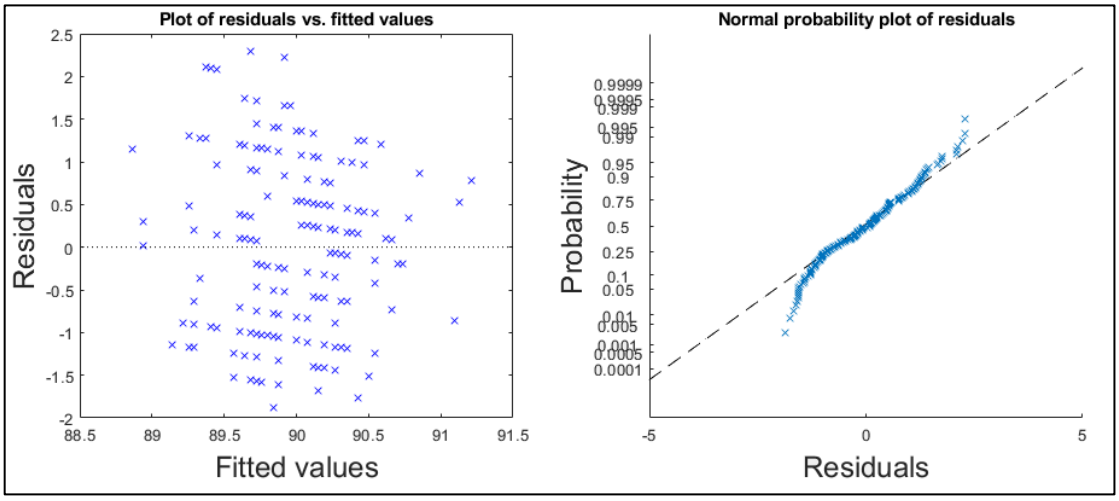

*Figure B1.24: Plot of studentized residuals versus fitted values (on the left) and probability plot (on the right) derived from the simple linear regression model between train speed and mean wheel loads detected for the **right** wheel of the first axle of locomotive **917400014234** between March 18th 2018 and January 29th 2019 at **Jörn** detector station.*

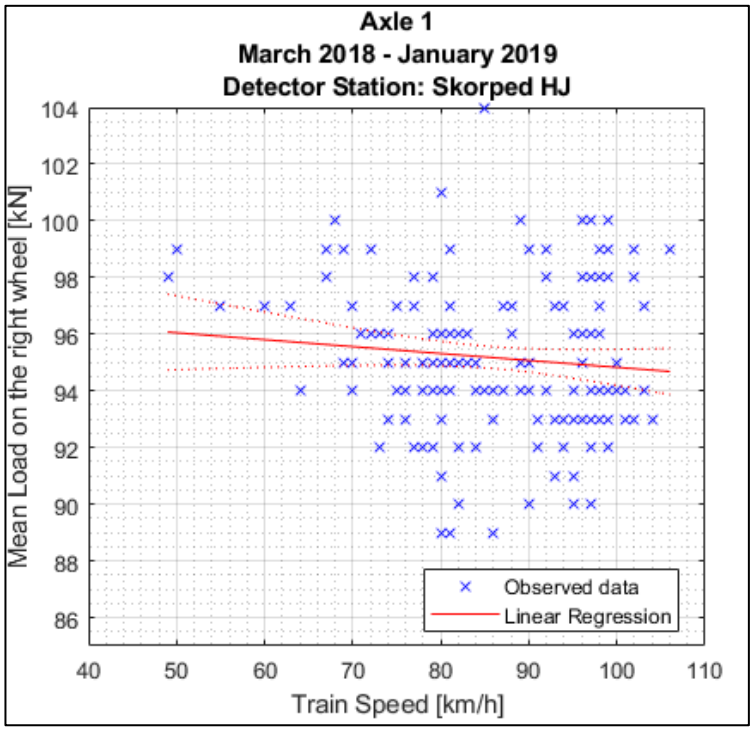

*Figure B1.25: Simple linear regression model between train speed and mean wheel loads detected for the **right** wheel of the first axle of locomotive **917400014234** between March 18th 2018 and January 29th 2019 at **Skorped** detector station.*

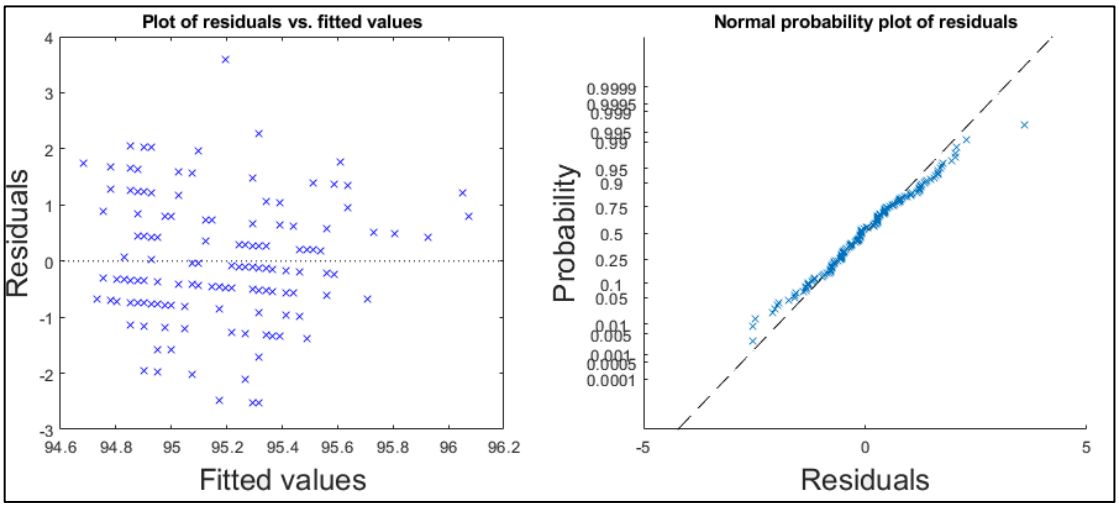

*Figure B1.26: Plot of studentized residuals versus fitted values (on the left) and probability plot (on the right) derived from the simple linear regression model between train speed and mean wheel loads detected for the **right** wheel of the first axle of locomotive **917400014234** between March 18th 2018 and January 29th 2019 at **Skorped** detector station.*

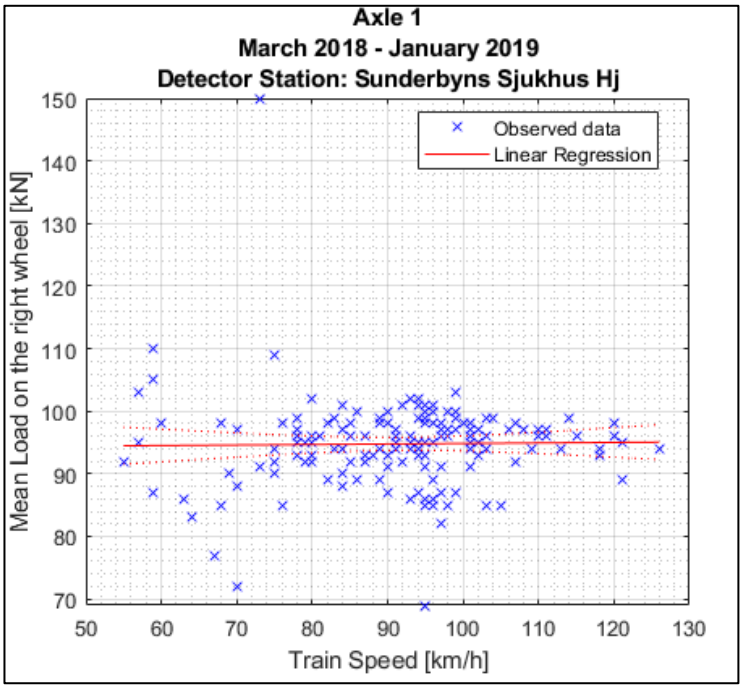

*Figure B1.27: Simple linear regression model between train speed and mean wheel loads detected for the **right** wheel of the first axle of locomotive **917400014234** between March 18th 2018 and January 29th 2019 at **Sunderbyns Sjukhus** detector station.*

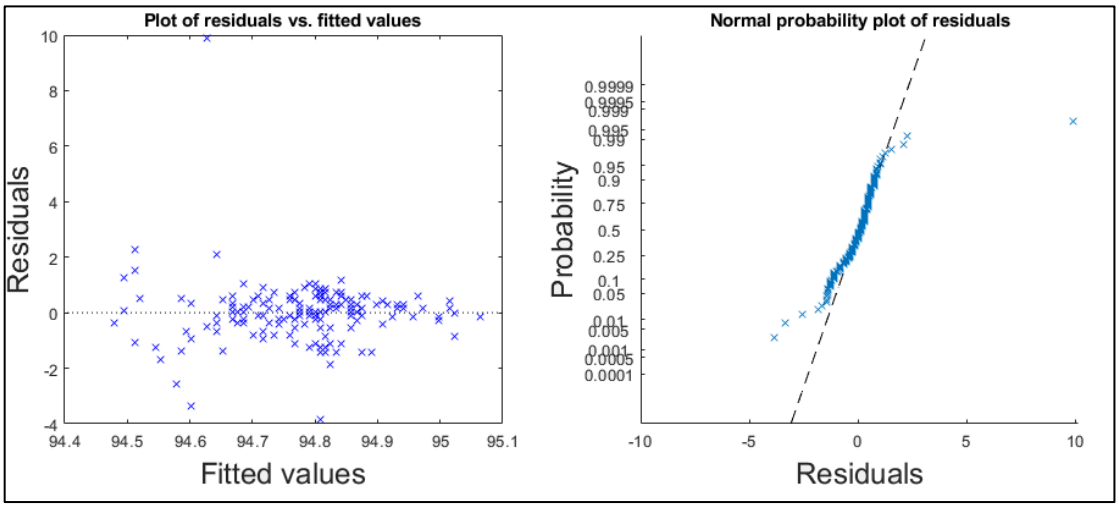

*Figure B1.28: Plot of studentized residuals versus fitted values (on the left) and probability plot (on the right) derived from the simple linear regression model between train speed and mean wheel loads detected for the **right** wheel of the first axle of locomotive **917400014234** between March 18th 2018 and January 29th 2019 at **Sunderbyns Sjukhus** detector station.*

Additional figures helping the readability and the checking of information provided in Table 3.5.

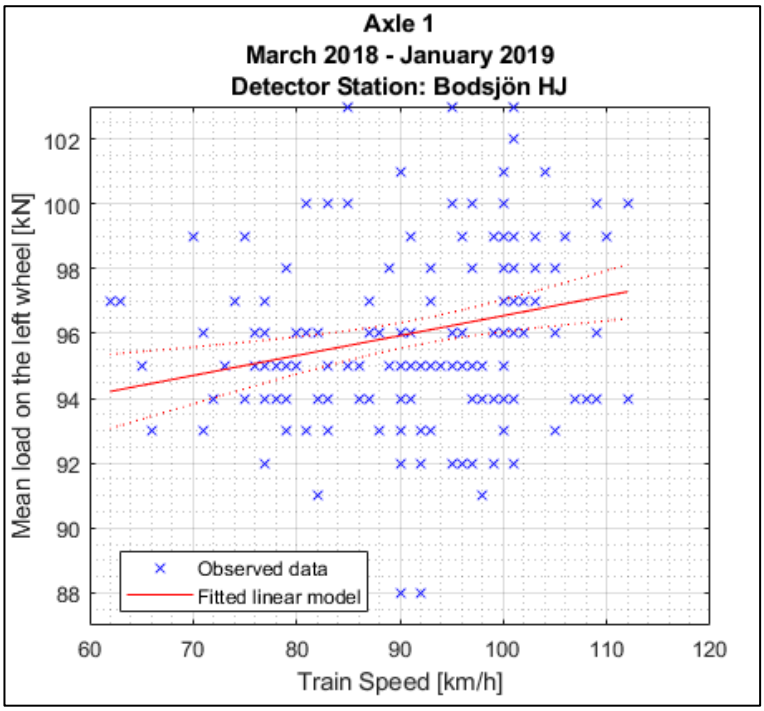

*Figure B1.29: Simple linear regression model between train speed and mean wheel loads detected for the **left** wheel of the first axle of locomotive **917400014235** between March 18th 2018 and January 29th 2019 at **Degerbäcken** detector station.*

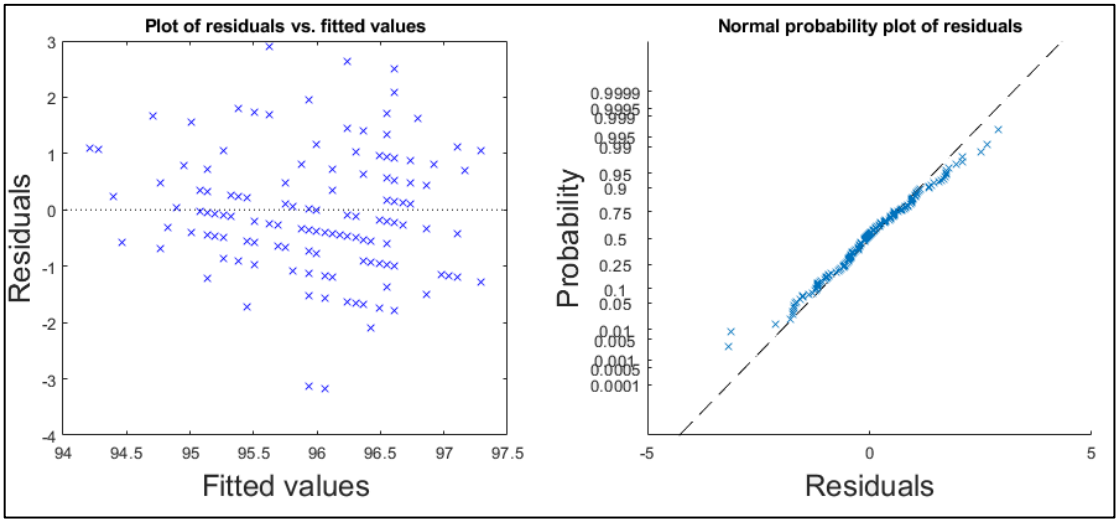

*Figure B1.30: Plot of studentized residuals versus fitted values (on the left) and probability plot (on the right) derived from the simple linear regression model between train speed and mean wheel loads detected for the **left** wheel of the first axle of locomotive **917400014235** between March 18th 2018 and January 29th 2019 at **Degerbacken** detector station.*

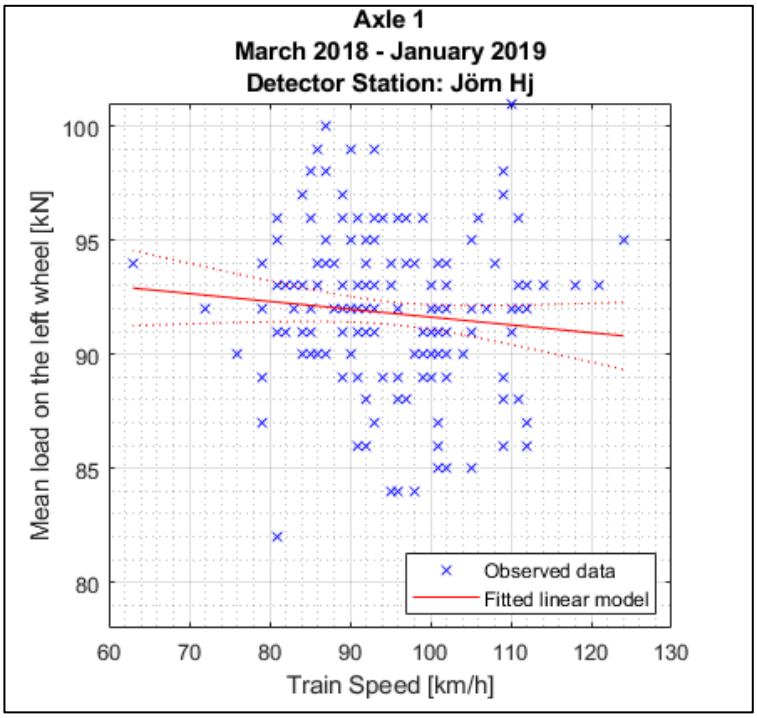

*Figure B1.31: Simple linear regression model between train speed and mean wheel loads detected for the **left** wheel of the first axle of locomotive **917400014235** between March 18th 2018 and January 29th 2019 at **Jörn** detector station.*

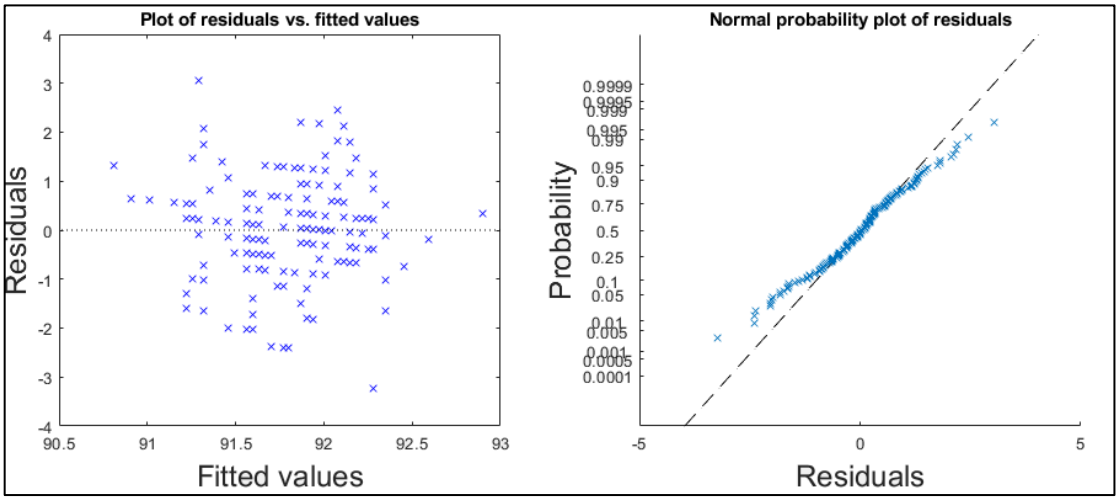

*Figure B1.32: Plot of studentized residuals versus fitted values (on the left) and probability plot (on the right) derived from the simple linear regression model between train speed and mean wheel loads detected for the **left** wheel of the first axle of locomotive **917400014235** between March 18th 2018 and January 29th 2019 at **Jörn** detector station.*

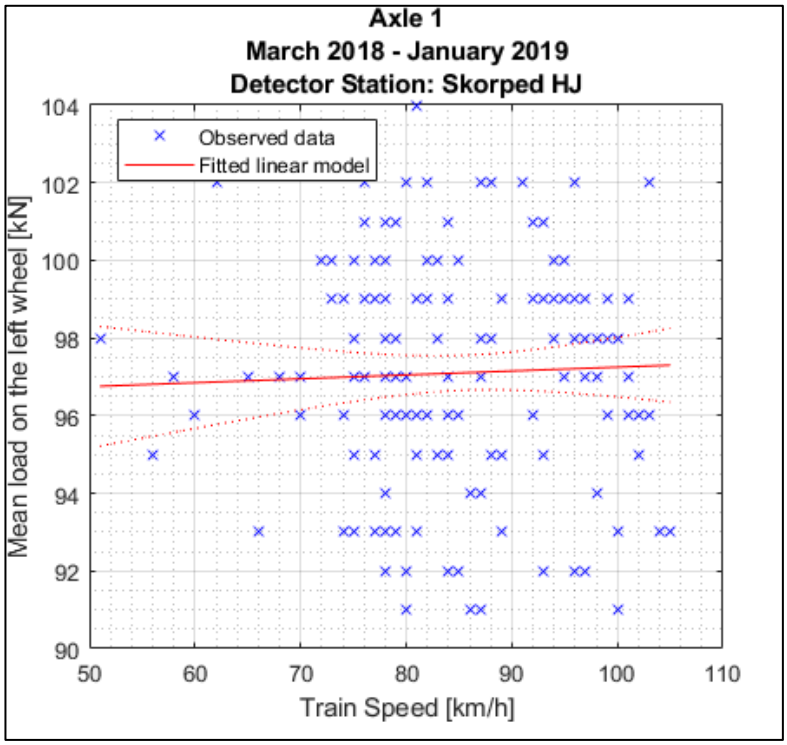

*Figure B1.33: Simple linear regression model between train speed and mean wheel loads detected for the **left** wheel of the first axle of locomotive **917400014235** between March 18th 2018 and January 29th 2019 at **Skorped** detector station.*

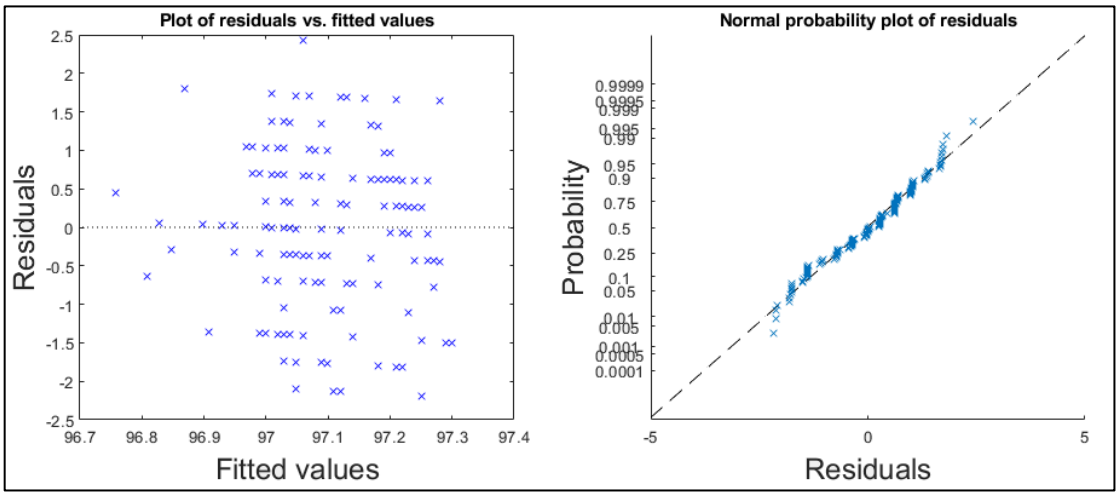

*Figure B1.34: Plot of studentized residuals versus fitted values (on the left) and probability plot (on the right) derived from the simple linear regression model between train speed and mean wheel loads detected for the **left** wheel of the first axle of locomotive **917400014235** between March 18th 2018 and January 29th 2019 at **Skorped** detector station.*

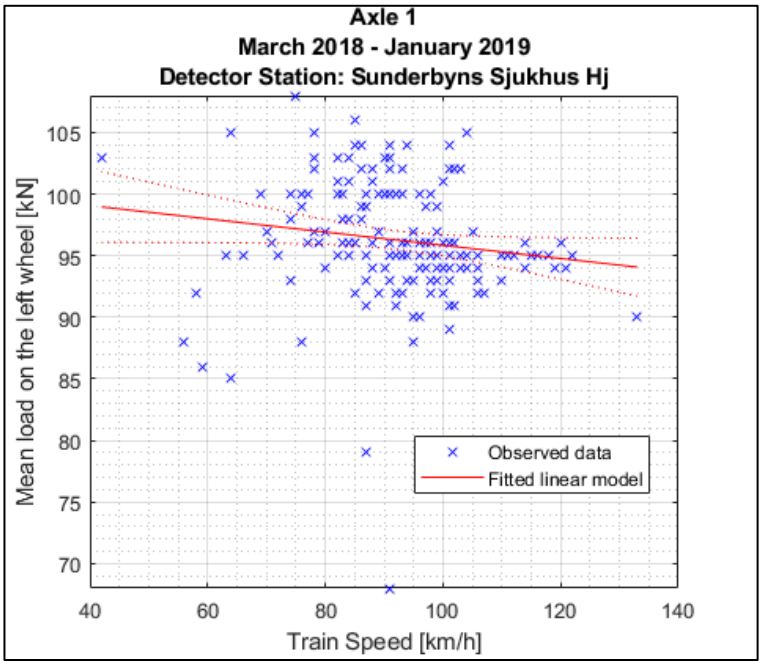

*Figure B1.35: Simple linear regression model between train speed and mean wheel loads detected for the **left** wheel of the first axle of locomotive **917400014235** between March 18th 2018 and January 29th 2019 at **Sunderbyns Sjukhus** detector station.*

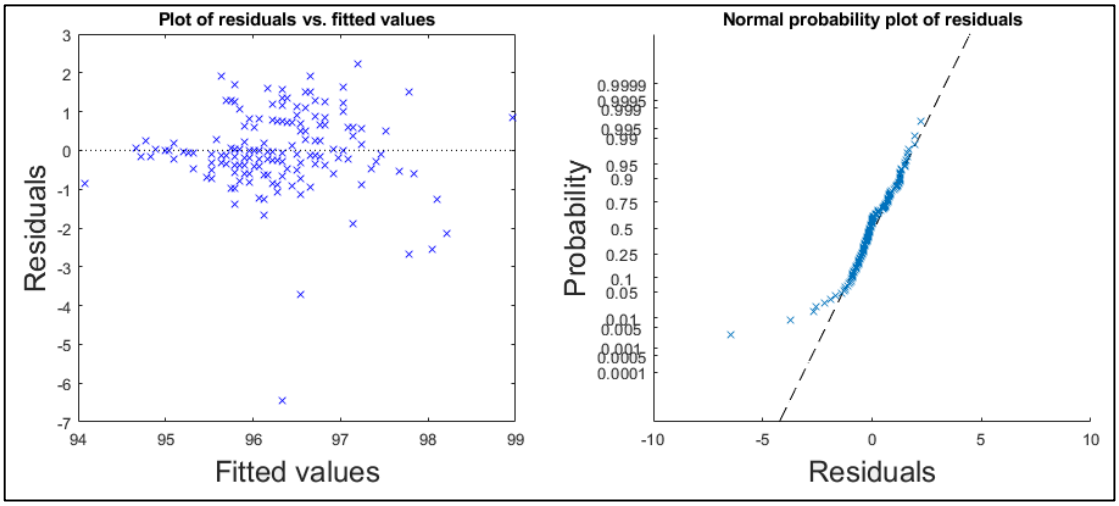

*Figure B1.36: Plot of studentized residuals versus fitted values (on the left) and probability plot (on the right) derived from the simple linear regression model between train speed and mean wheel loads detected for the **left** wheel of the first axle of locomotive **917400014235** between March 18th 2018 and January 29th 2019 at **Sunderbyns Sjukhus** detector station.*

Additional figures helping the readability and the checking of information provided in Table 3.6.

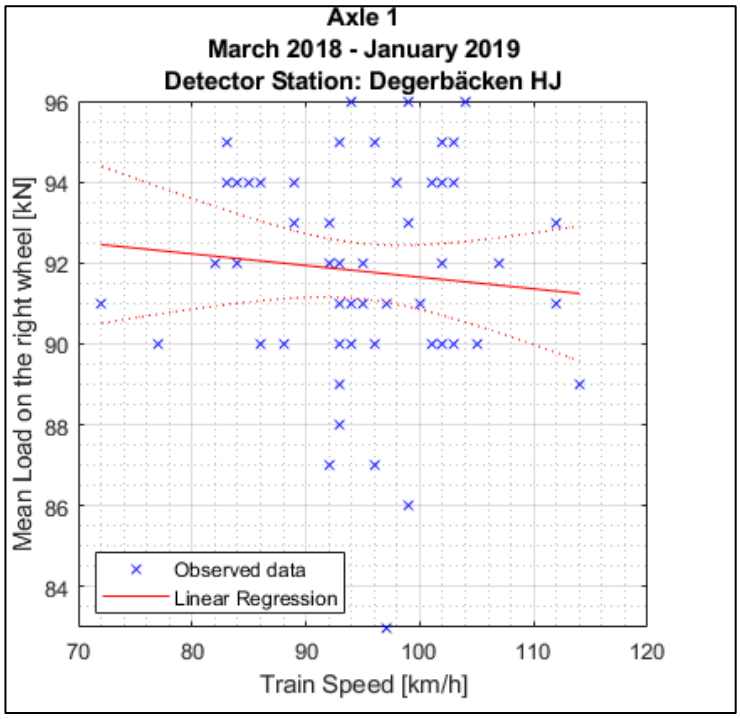

*Figure B1.37: Simple linear regression model between train speed and mean wheel loads detected for the **right** wheel of the first axle of locomotive **917400014235** between March 18th 2018 and January 29th 2019 at **Degerbäcken** detector station.*

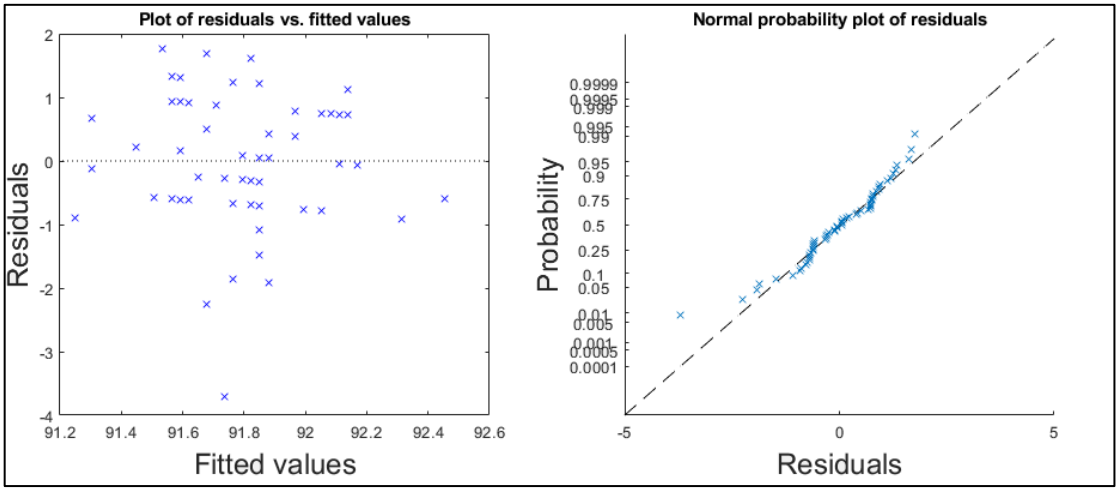

*Figure B1.38: Plot of studentized residuals versus fitted values (on the left) and probability plot (on the right) derived from the simple linear regression model between train speed and mean wheel loads detected for the **left** wheel of the first axle of locomotive **917400014235** between March 18th 2018 and January 29th 2019 at **Degerbäcken** detector station.*

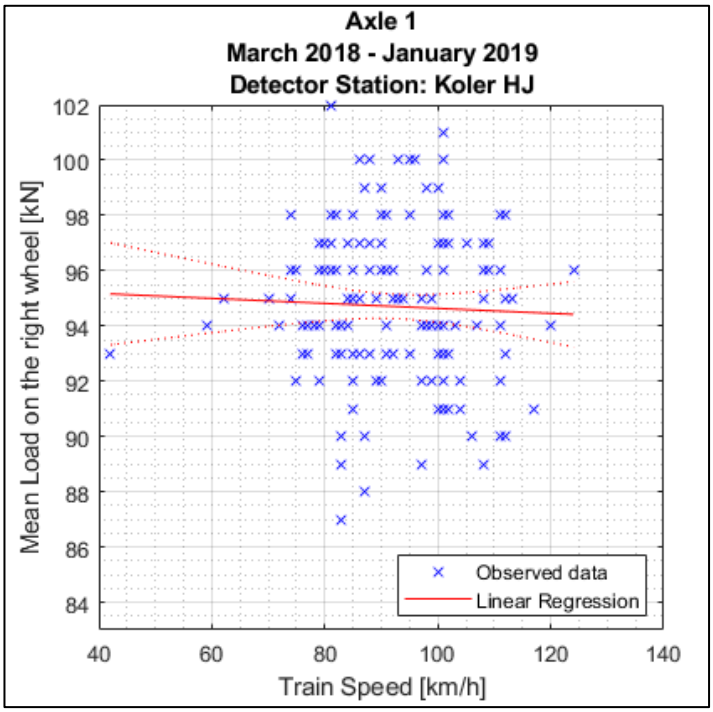

*Figure B1.39: Simple linear regression model between train speed and mean wheel loads detected for the **right** wheel of the first axle of locomotive **917400014235** between March 18th 2018 and January 29th 2019 at **Koler** detector station.*

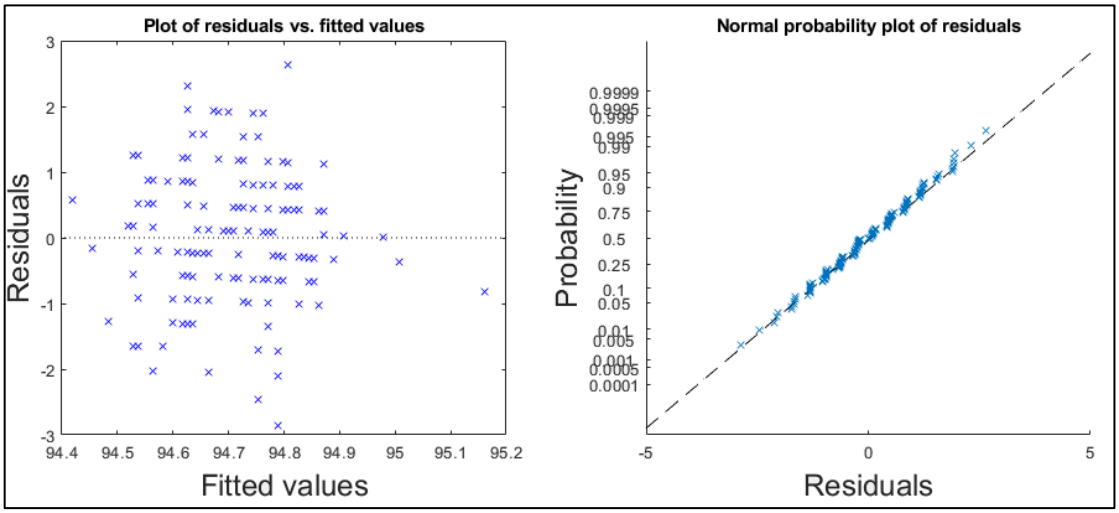

*Figure B1.40: Plot of studentized residuals versus fitted values (on the left) and probability plot (on the right) derived from the simple linear regression model between train speed and mean wheel loads detected for the **left** wheel of the first axle of locomotive **917400014235** between March 18th 2018 and January 29th 2019 at **Koler** detector station.*

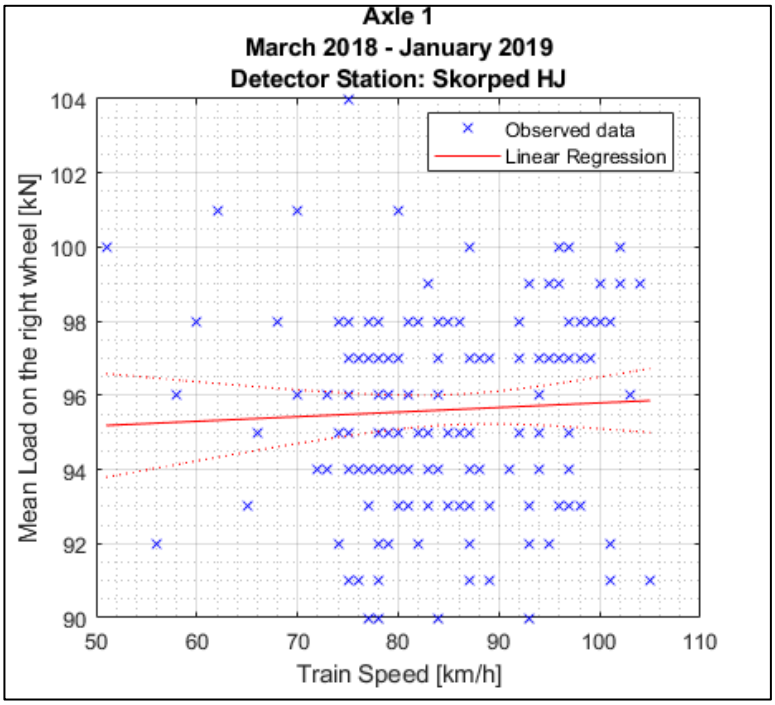

*Figure B1.41: Simple linear regression model between train speed and mean wheel loads detected for the **right** wheel of the first axle of locomotive **917400014235** between March 18th 2018 and January 29th 2019 at **Skorped** detector station.*

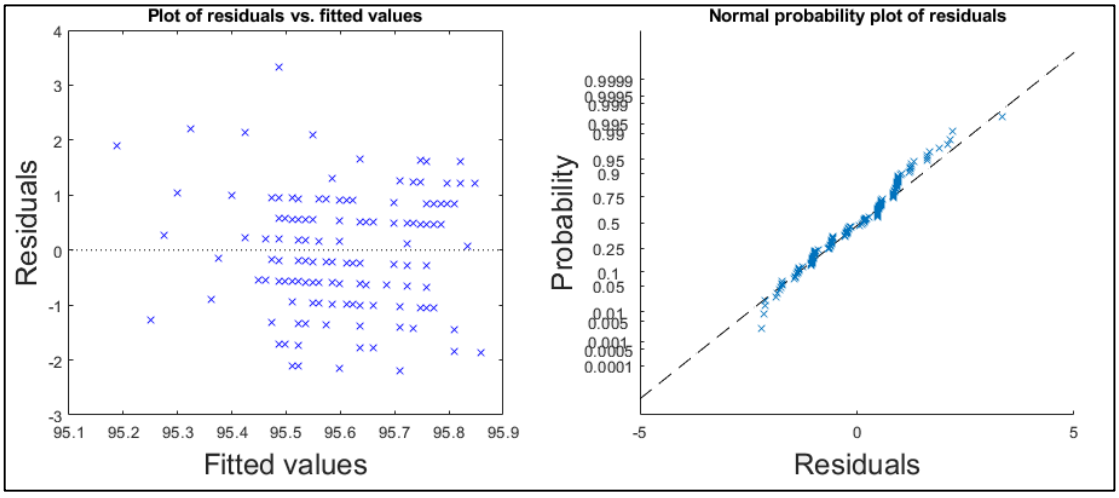

*Figure B1.42: Plot of studentized residuals versus fitted values (on the left) and probability plot (on the right) derived from the simple linear regression model between train speed and mean wheel loads detected for the **left** wheel of the first axle of locomotive **917400014235** between March 18th 2018 and January 29th 2019 at **Skorped** detector station.*

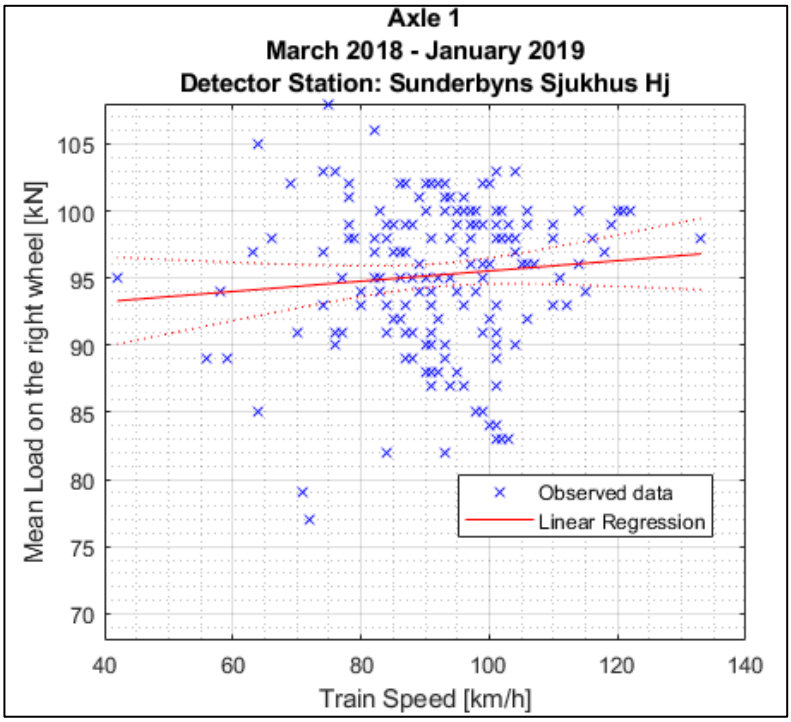

*Figure B1.43: Simple linear regression model between train speed and mean wheel loads detected for the **right** wheel of the first axle of locomotive **917400014235** between March 18th 2018 and January 29th 2019 at **Sunderbyns Sjukhus** detector station.*

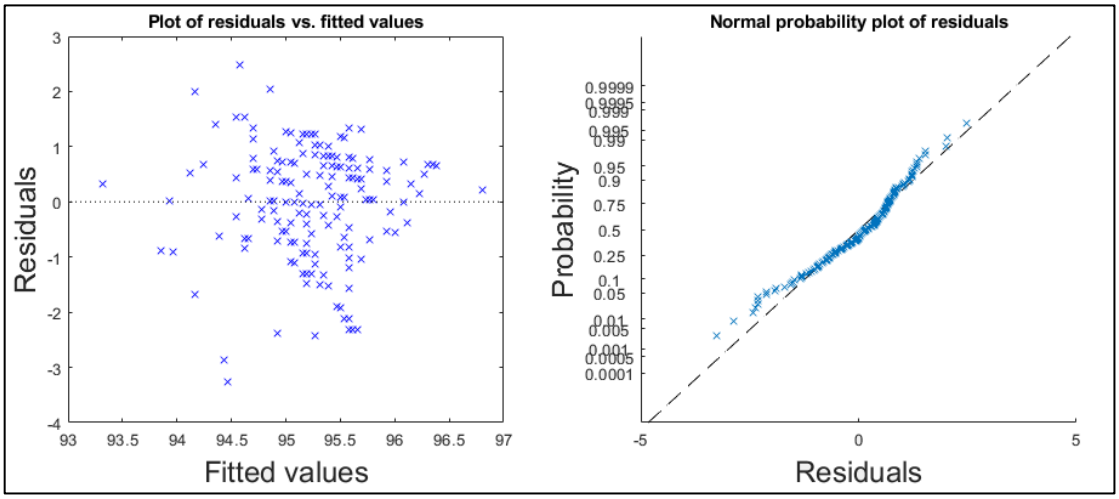

*Figure B1.44: Plot of studentized residuals versus fitted values (on the left) and probability plot (on the right) derived from the simple linear regression model between train speed and mean wheel loads detected for the **left** wheel of the first axle of locomotive **917400014235** between March 18th 2018 and January 29th 2019 at **Sunderbyns Sjukhus** detector station.*

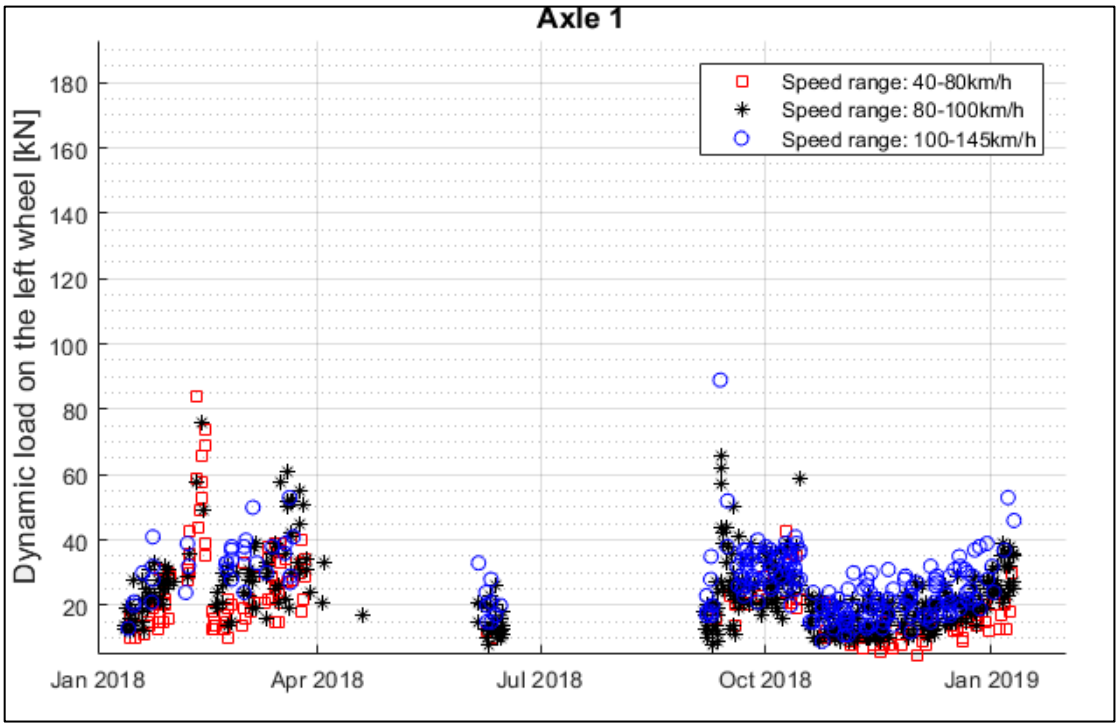

*Figure B1.45: Scattered data of dynamic impact loads acting for the **left** wheel of the first axle of locomotive **917400014341** registered by WILDs over one year period. The data have been plotted for three different train speed ranges.*

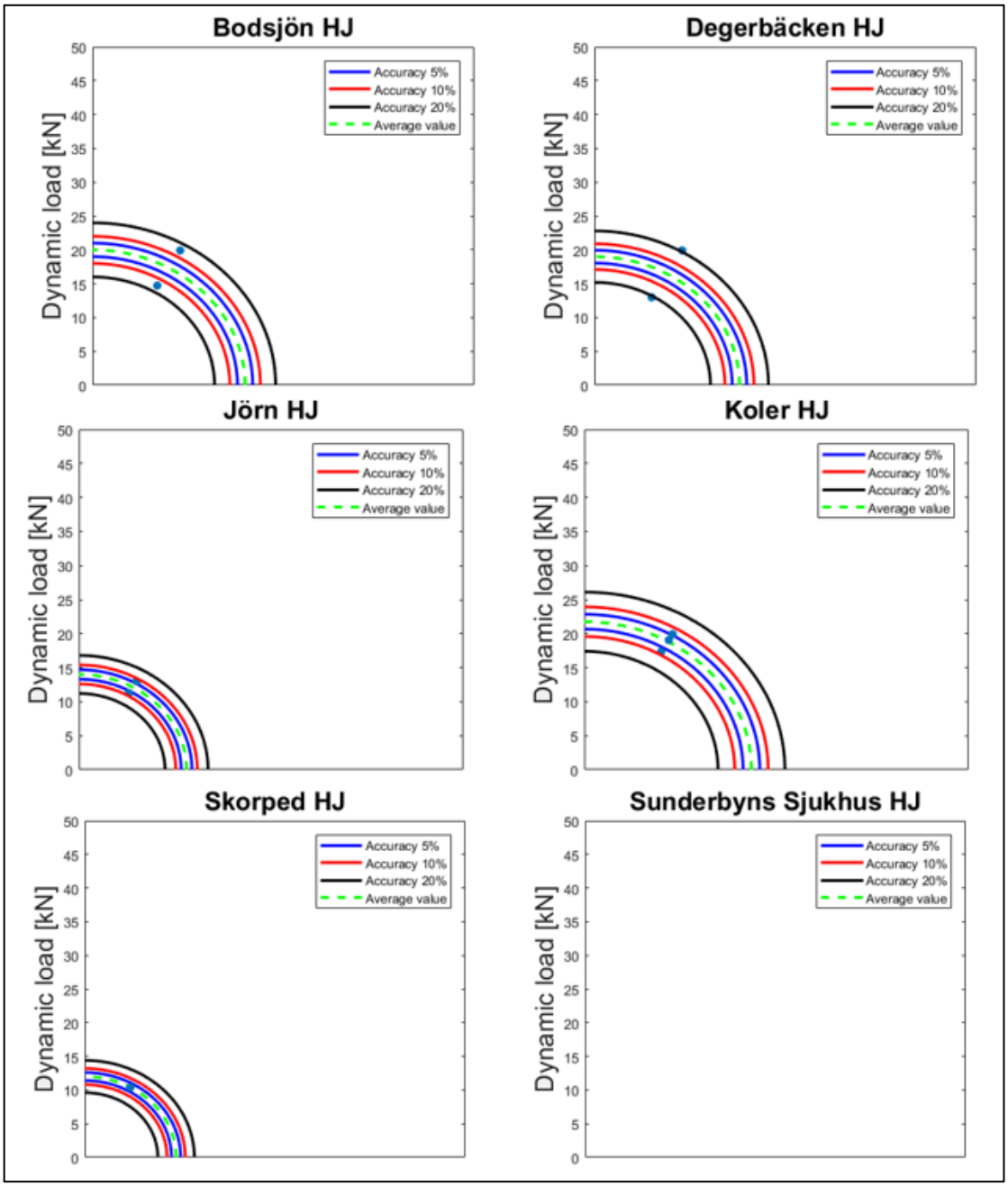

*Figure B1.46: Target diagrams involving dynamic impact loads registered at each detector station and referring to the **right** wheel of the first axle of the locomotive identified by the vehicle number **917400014341**. Data were measured between **October 18th and October 30th 2018** and correspond to a measured train speed ranging between **98 km/h and 102 km/h**. The green dashed line indicates the mean value of dynamic loads. The blue solid lines represent an accuracy of 5%, the red solid lines an accuracy of 10% whereas the black solid lines an accuracy of 20% computed with respect to the mean value.*

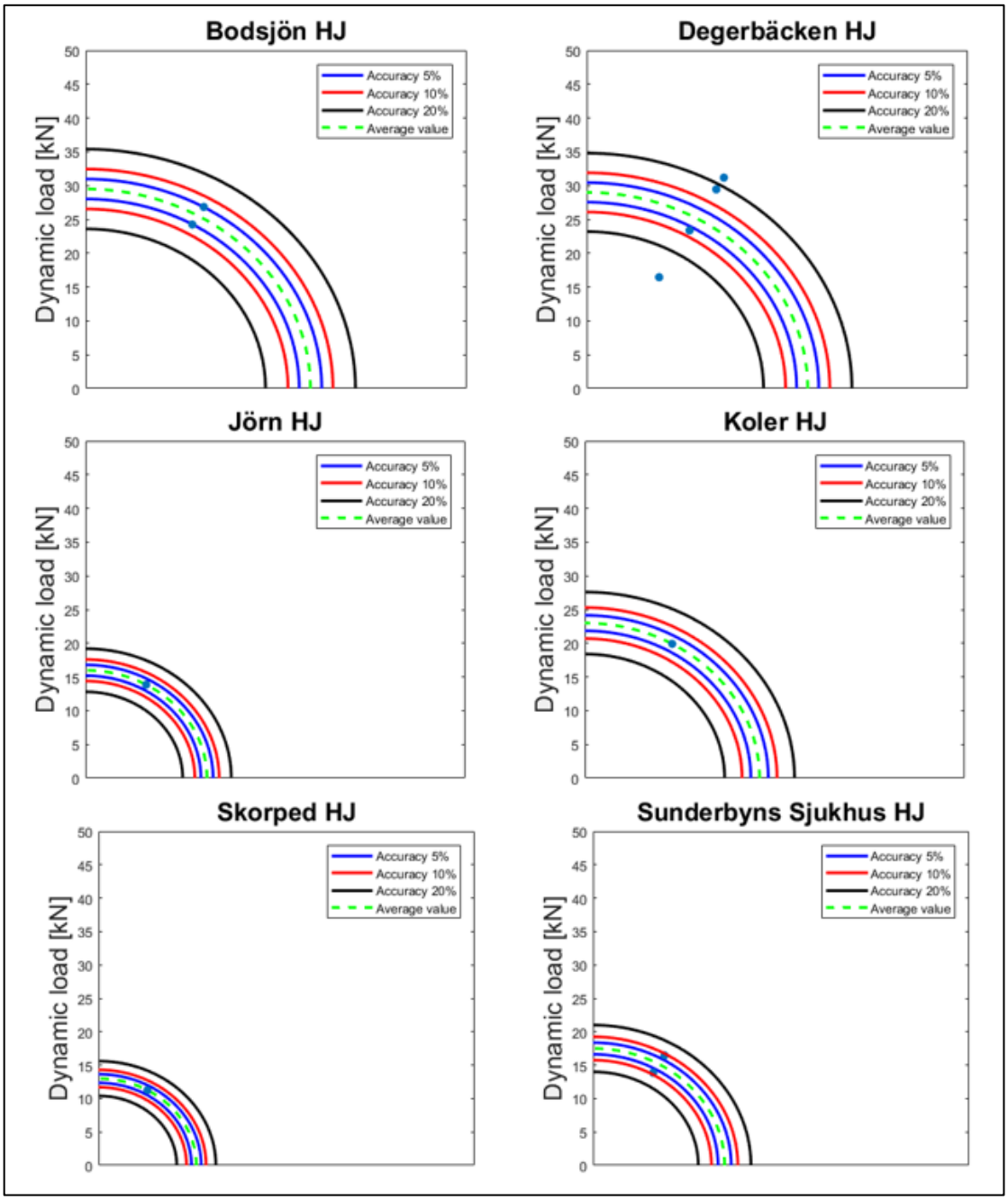

*Figure B1.47: Target diagrams involving dynamic impact loads registered at each detector station and referring to the **right** wheel of the first axle of the locomotive identified by the vehicle number **917400014341**. Data were measured between **October 31st and November 11th 2018** and correspond to a measured train speed ranging between **98 km/h and 102 km/h**. The green dashed line indicates the mean value of dynamic loads. The blue solid lines represent an accuracy of 5%, the red solid lines an accuracy of 10% whereas the black solid lines an accuracy of 20% computed with respect to the mean value.*

B2 Complementary information to Section 3.4

Further results related to the analysis proposed in Section 3.4 may be found in this section.

*Table 3. 1:Results in terms of PRESS statistics, R^2_{Adj} and MS_{res} deriving by the adoption of different regression models involving respectively the regressor variables indicated in the rightmost cells of the table. Analysis involved dynamic impact loads measured for the **right** wheel of the first axle of locomotive **917400014341** at the Bodsjön detector station between **October 18th** and **December 18th**.*

LOCOMOTIVE 917400014341 Bodsjön								
N° of regressor variables	PRESS	R^2_{Adj}	MS_{res}	t	v	t^2	v^2	v^3
1	54.43	0.061	29.67	x				
1	56.30	0.583	13.12		x			
2	57.67	0.598	12.67	x	x			
2	56.31	0.583	13.12		x	x		
2	55.78	0.650	11.03		x		x	
3	57.21	0.650	10.97	x	x		x	
4	60.77	0.640	11.1	x	x		x	x

*Table 3. 2: Results in terms of PRESS statistics, R^2_{Adj} and MS_{res} deriving by the adoption of different regression models involving respectively the regressor variables indicated in the rightmost cells of the table. Analysis involved dynamic impact loads measured for the **left** wheel of the first axle of locomotive **917400014341** at the Bodsjön detector station between **October 18th** and **December 18th**.*

LOCOMOTIVE 917400014341 Bodsjön								
N° of regressor variables	PRESS	R^2_{Adj}	MS_{res}	t	v	t^2	v^2	v^3
1	54.46	-0.015	47.91	x				
1	56.89	0.593	19.26		x			
2	59.03	0.594	19.54	x	x			
2	56.895	0.592	19.25		x	x		
2	61.79	0.620	17.82		x		x	
3	62.92	0.622	17.83	x	x		x	
4	61.82	0.640	16.72	x	x		x	x

*Table 3. 3: Results in terms of PRESS statistics, R^2_{Adj} and MS_{res} deriving by the adoption of different regression models involving respectively the regressor variables indicated in the rightmost cells of the table. Analysis involved dynamic impact loads measured for the **right** wheel of the first axle of locomotive **917400014234** at the Bodsjön detector station between **October 18th** and **December 18th**.*

LOCOMOTIVE 917400014234 Bodsjön								
Number of regressor variables	PRESS	R^2_{Adj}	MS_{res}	t	v	t^2	v^2	v^3
1	54.69	0.205	67.22	x				
1	55.28	0.265	62.12		x			
2	60.11	0.480	43.97	x	x			
2	55.28	0.265	62.12		x	x		
2	58.37	0.357	54.32		x		x	
3	63.39	0.537	39.14	x	x		x	
4	77.72	0.530	39.70	x	x		x	x

*Table 3. 4: Results in terms of PRESS statistics, R^2_{Adj} and MS_{res} deriving by the adoption of different regression models involving respectively the regressor variables indicated in the rightmost cells of the table. Analysis involved dynamic impact loads measured for the **left** wheel of the first axle of locomotive **917400014234** at the Bodsjön detector station between **October 18th** and **December 18th**.*

LOCOMOTIVE 917400014234 Bodsjön								
Number of regressor variables	PRESS	R^2_{Adj}	MS_{res}	t	v	t^2	v^2	v^3
1	65.99	0.292	39.56	x				
1	65.23	0.142	47.98		x			
2	74.07	0.444	31,09	x	x			
2	65.23	0.142	47.98		x	x		
2	70.98	0.163	46.80		x		x	
3	83.90	0.444	31.08	x	x		x	
4	148.09	0.429	31.89	x	x		x	x